Investigation of the use of Dynamic Resistance in Adaptive Welding and Statistical Relation to Quality

by

Kyu Won Choi

A thesis
presented to the University of Waterloo
in fulfillment of the
thesis requirement for the degree of
Master of Applied Science
in
Mechanical and Mechatronics Engineering

Waterloo, Ontario, Canada, 2019

AUTHOR'S DECLARATION

I hereby declare that I am the sole author of this thesis. This is a true copy of the thesis, including any required final revisions, as accepted by my examiners.

I understand that my thesis may be made electronically available to the public.

Abstract

The pursuit of real time quality detection of a resistance spot weld (RSW) in the automotive industry has progressed alongside technology. With the capability of modern controllers to collect real-time data from the welding procedure on a millisecond scale, the use of the dynamic resistance curves has become feasible. The controller used in this study was a Bosch Rexroth PSI63C0.120L1 with adaptive welding capabilities. The adaptive welding method used by Bosch is based on a reference dynamic resistance curve upon which the controller bases all of the adjustments to the welding current and/or time.

In this study the dynamic resistance curves of a simple 2 high stack up of USIBOR$^{®}$ was welded under possible unideal process conditions such as shunting, edge welding, and shim/gap welding. It was found that under extreme cases for shunt and edge welds, the dynamic resistance curve changes significantly. For the particular set up in this thesis, it was found that at a center to center weld shunting distance of 10 mm and an edge distance of approximately half the electrode face is statistically detectable. For shim/gap welding, the change in the dynamic resistance curve was present at a 1mm gap and less at the 2mm gap due to the set-up of the robot arm. When performing the welds under the same process conditions with adaptive welding, there was little change to the adaptive dynamic resistance curves. In the shunted condition, the adaptive welding extended the time and was able to overcome the shunting effect to produce an ideal nugget size. During edge welding it resulted in expulsion when it would otherwise not occur, producing undersized nuggets.

In an analysis of the quality indicators of the weld controller, it was discovered that the Stabilization Factor is based on the average values of the weld, while the UIP values are based on the deviation of the dynamic resistance of the weld to the reference. Both the quality indicator variables the controller output were found to have no correlation to either the nugget diameter or the tensile strength of the welds. Thus, an alternative to make use of the data the controller collects was explored through a statistical approach of large data and regression modelling. A model with a fit of 40% was made for the similar stack up and validated with production parts, but it lacked the robustness to capture all the data. When attempting to replicate the study on a dissimilar weld situation, the laboratory data and the data from the production part resulted in an unacceptable fit. This was due to the strong effect of different robot welders on the dynamic resistance curve, the lack of robustness in creating the model, and lack of logic found in the model parameters and coefficients.

Acknowledgements

I would like to take this moment to thank my supervisors, Dr. Adrian Gerlich and Dr. Norman Zhou. Their patience and guidance were crucial in progressing my research. Their knowledge and expertise in the field of welding and materials was vital in building this thesis.

Thank you to Darren Baigent from Honda of Canada Manufacturing and his team for supplying materials, and feedback on the direction of application of results. Their knowledge of real-life applications in the automotive world guided the experimental objectives.

Also, a huge thanks to the members of center for advanced materials and joining (CAMJ). Special thanks to the resistance spot-welding group: Chris DiGiovanni, Erica Wintjes, Xu Han, and Josh He. Their perspective o my research and lunch time discussions was crucial for my time during my masters.

Special thanks to my parents, for their sacrifice in pursuit of a better future for me. Your perseverance, strength, and love pushed me to be who I am today. Lastly thank you to my girlfriend, Grace, for putting everything into perspective and not letting me lose sight of what is ahead.

Table of Contents

List of Figures

List of Tables

Chapter 1
Introduction

Resistance spot welding (RSW) is a popular choice in joining sheet metals in any high-volume manufacturing setting. Due to its ease of automation, relatively low capital cost, and quick production speed, the automotive industry has accepted it as the main form of joining vehicle bodies. The average vehicle will be composed of various sheets of metal joined together with upwards of 5000 spot welds [1]. The automotive industry's desire to move forward with more lightweight materials led to the introduction of stronger and thinner sheets of steel, referred to as advanced high strength steels (AHSS), with their grades and properties comparted in Figure 1.1. Most vehicles in production are composed of these AHSS, such as dual-phase (DP), transformation-induced plasticity (TRIP), and press hardened steels (PHS) [2]. The material used in this study is classified as a 3rd generation AHSS, commonly referred to as USIBOR$^{®}$ 1500 by ArcelorMittal.
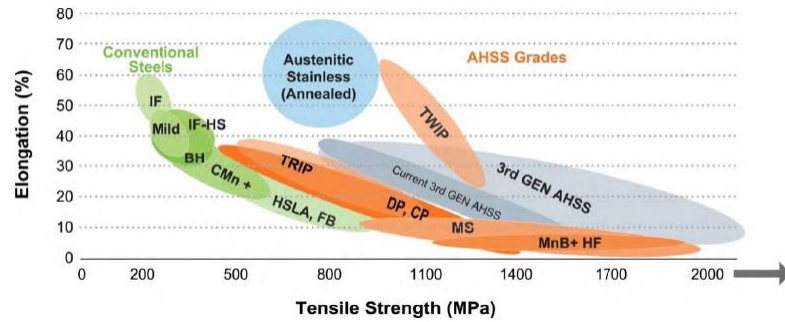
Figure 1.1. Steel Strength Ductility Diagram of Today's AHSS Grades [2]

1.1 Quality of Resistance Spot Welds

Based on the sheer volume of spot welds on a vehicle and limited time allotted to production, each weld cannot be inspected for faults or defects. Instead, during the design and mechanical testing process for a vehicle, specifically chosen welds, often referred to as "critical spots", are deemed to represent the integrity of the vehicle as they greatly impact strength/fatigue [3], [4]. During production, there are scheduled non-destructive tests, the most common being chisel checks, to determine if there are any issues. Further explained in section 2.3.2, the chisel check verifies if a weld nugget is present if the workpieces do not separate when the chisel is inserted. In the case of a detection of defect, all of the parts between the detection and previous test are required to be individually checked and possibly rewelded. This method is common practice in the automotive industry which is inefficient as the cause

1

and occurrence of the issue is difficult to identify and requires downtime to inspect and perform the required repairs.

The main quality indicators of the resistance spot weld in the automotive industry are the weld nugget size, the tensile/cross-tension strength, and presence of defects [5], [6]. The most common forms of defects in spot welds are: undersized welds, stuck welds, expulsion, cracks, voids, and mislocated/edge welds [5]–[9]. All of the listed defects directly affect the performance of the joint, leading to loss of strength or change in failure modes [8]. The two extremes of a weld fracture mode are the complete button pull out and interfacial fracture (as seen in Figure 1.2). In conventional steels, the button pull out is the preferred failure method as it is known to absorb more energy in comparison to interfacial failure [10]. AHSS have a higher fracture toughness which encourage interfacial failure but exhibit low to no loss of load bearing strength [11].
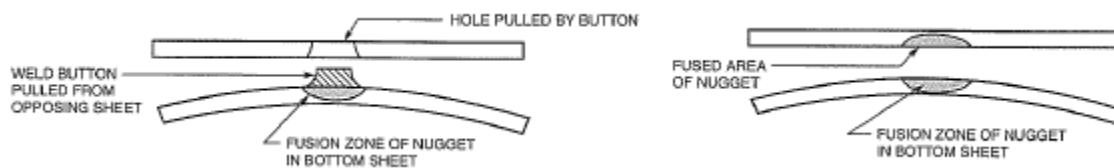
Figure 1.2. Diagram of Button Pull Out Failure (Left) and Interfacial Failure (Right) [6]

1.2 Current Quality Detection Process

As briefly mentioned, the current process utilizes chisel checking specified critical welds as the main non-destructive method at a designated interval to prevent batches of defects. From a control perspective, the same welding parameters are applied to each weld using an automated process allowing for low variability in the repetition of the welds. Unfortunately, there are unaccountable variables or circumstances such as poor set up, wrong material, electrode misalignment, etc. which cause unideal welding conditions [12]–[15]. While an error in the process will be detected by the periodic quality tests it may miss the outliers or the one-off weld defect which occurs between the quality checks. Thus, the need for online quality monitoring arose to detect the one-off defect and ultimately avoid the periodic quality tests that occur during fabrication.

Multiple methods over the years have been proposed to detect the quality of a weld in real-time. They can be categorized as either a secondary process or utilizing the in-situ signals. The chisel check falls under the secondary process category as it requires an additional step in inspecting the weld quality and may incur an increase in production time and cost. The use of in-situ signals is the preferred

2

method as it allows for instantaneous interpretation of values. The primary signal used in this study is the dynamic resistance, the resistance curve recorded between the electrodes during the weld.

1.3 Statistical Tools

To perform online monitoring of weld quality, the data the controller can collect and export to the network needs to be analyzed against the quality indicators to define a correlation and ultimately link causation. The three main statistical analysis performed was hypothesis testing, linear regression, and analysis of variance (ANOVA). The hypothesis testing was performed using the student's t-distribution:

$$\left| \frac{\bar{X}_{sample} - \mu_0}{S/\sqrt{n}} \right| \leq t_{n-1,\frac{\alpha}{2}} \tag{Eq. 1}$$

Where, $\bar{X}$ is the sample mean, μ_0 is the null hypothesis of population mean, t is the t-distribution variable, S is the variance, α is the significance level, and n is the number of data points. Application of hypothesis testing allows for determining outliers, means comparisons of different conditions, and paired testing. The linear regression method was performed using Minitab, an external software, but the regression modeling followed this matrix calculation:

$$Given\ model\text{: } y_i = \beta_1^* + \beta_2^* x_i + \cdots + \varepsilon_i$$

$$\hat{\beta} = (X'X)^{-1}X'y \tag{Eq. 2}$$

Where for a given data set of n trials and p parameters, the X is a n by $p+1$ matrix, and y is a n by 1 vector, resulting in a $p+1$ by 1 vector corresponding to the coefficients of best fit to the linear model. This level of regression is the basis for any modelling or neural network fitting.

The analysis of variance is a popular method to breakdown the analysis of regressions (as seen in Table 1.1). From left of the table to the right, the sum of squares of the regression (SSR) and error (SSE) can be calculated using the experimental values of Y (Y), the mean of Y ($\bar{Y}$) and estimate of Y ($\hat{Y}$). The mean square/variance (MSR & MSE) can be found with the degree of freedom (DoF), where p is the number of parameters and n is the number of observations. The final column is compared to the F-test where if the value of MSR/MSE is greater than F(p-1, n-p) then the regression is significant, and the model explains a majority of the variability in the data. A low MSE indicates a strong regression model. Another indicator of the model is the coefficient of determination (R^2=SSR/SST), where the

ratio indicates the percentage of variation the model accounts for (ranging from 1 accounting for all, and 0 accounting for none).

Table 1.1. Basic Summary of the ANOVA Table of a Regression

Source	Sum of Squares	Degree of Freedom	Mean Square	F
Regression	$\Sigma(\hat{Y} - \bar{Y})^2$	p-1	SSR/(p-1)	MSR/MSE
Error	$\Sigma(Y - \hat{Y})^2$	n-p	SSE/(n-p)	
Total	$\Sigma(Y - \hat{Y})^2$	n-1		

Another measure of the data's fit to the regression model/equation is the R^2 or R-sq value which explains how well the input variables explain the variation of the output variable. On a curve, it relays how effective the line of best fit is. When performing regressions with multiple variables an adjusted value of R-sq (adj), calculated by (Eq. 3), to counter the superficial increase of R-sq with additional variables. In either case, the close the value is to 100%, the better the model explains the values.

$$R^2_{adj} = 1 = \left(\frac{(1 - R^2)(n - 1)}{n - k - 1} \right) \qquad \text{(Eq. 3)}$$

1.4 Objectives

The main objective of this thesis is to fully investigate the quality detection ability of the resistance spot welding process using the dynamic resistance curve and identifying the capability of the adaptive welding controls. Correlating the dynamic resistance to quality such as microstructure, and tensile tests along with the implementation of adaptive welding allows for a stronger understanding of this technology. The specific objectives are:

1. Investigate how the dynamic resistance of USIBOR® during resistance spot welding changes according to external variability (such as edge proximity, shunting, shims)

2. Understand the adaptivity feature of the weld controller along with the quality indicators (StabilizationFactor and UIP) output by the controller

3. Determine if quality indicators provide any insight or correlation to the weld quality

4. Investigate the adaptive welding controls and outputs to determine feasibility of better weld quality detection

1.5 Criteria and Constraints

The welding parameters used in this study were based on the industry partner's current welding set-up. The parameters of the welding schedule was verified based on existing literature and the American Welding Society standards for spot welding (AWS 8.1 and 8.9) [5], [6], [16]. The nugget size evaluated was deemed acceptable. All other testing or experimentation was based on the AWS standards if not specified. The experiments were all limited to the material USIBOR® as the experiment process was not material dependent and was the most commonly used material in the specified process under investigation by the industry partner.

1.6 Thesis Outline

The following thesis report has been organized in the following 7 chapters:

Chapter 1: *Introduction* to the report covering the background, problem, objectives and further insight to the field.

Chapter 2: *Literature Review* of the resistance spot welding process, the fundamental parameters of spot welding, the representation of the dynamic resistance curve, and material used.

Chapter 3: *Experimental Methods* undertaken to gather results presented in the latter sections of the thesis. Inclusion of specimen specifications, equipment, and experimental design.

Chapter 4: *Effect of Process Conditions on the Dynamic Resistance Curve of USIBOR®* investigates the effect of shunting, edge proximity and shim/alignment of the welds on the dynamic resistance curves.

Chapter 5: *Analysis of Adaptive Welding Capabilities of Bosch Rexroth PSI63C0.120L1 Controller* explores the effect of adaptive welding on the dynamic resistance curve and determines the main variables making up the quality indicators.

Chapter 6: *Identification of Potential Variables to Correlate the Nugget Size of USIBOR® and Dissimilar Stack Up* provides insight into utilizing the quality indicators to derive a stronger regression model for relating nugget diameter.

Chapter 7: *Conclusion and Final Remarks* are the final statements, summarizing all of the major findings of each chapter and recommendations.

Chapter 2

Literature Review

To best approach the issues involved in detecting quality of the resistance spot welding process, the basic concepts and theory behind it must first be reviewed. Throughout this chapter, the principles of resistance spot welding are explained, and the corresponding signals are explored. Current literature attempting to solve the same issues are also compiled to determine the feasibility or see if a unifying theory is present.

2.1 Resistance Spot Welding

Resistance spot welding (RSW) utilizes the contact surface resistance between sheets of metal to localize heat generation with a high current. Two copper electrodes are required to apply pressure while conducting the current to a small diameter area [17]–[19]. The invention of the RSW process was accredited to Elihu Thomson, who submitted a patent for an electrical welding apparatus in 1891 that modern resistance welders (spot, seam, and flash butt welding) are based upon [20]. The welding heat is based on Joule heating, where Q is the amount of heat (joules), I is the current (amperes), R is the resistance (ohms), and t is the time (seconds):

$$Q = I^2 R t \qquad \text{(Eq. 4)}$$

The RSW process equipment consists of a step-down transformer to produce currents on the scale of thousands of amperes (at low voltages), a clamping/pressurizing mechanism, electrodes, a water-cooling system, and a welding controller. Concerning the power sources used for RSW, direct current (DC) is preferred over alternating current (AC) in the automotive industry due to its robust weld lobes, larger nuggets at lower current inputs, and efficient melting heat [21], [22].
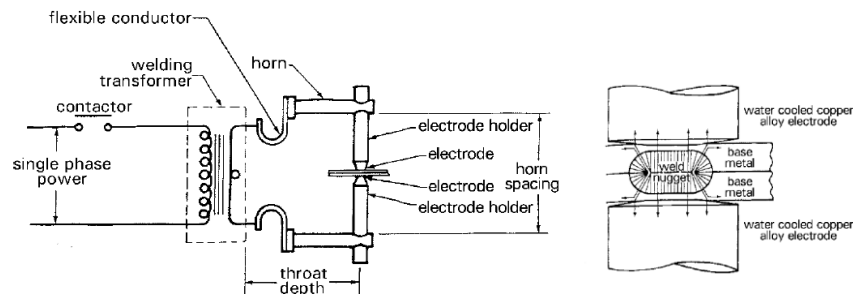
Figure 2.1. Schematic Breakdown of RSW Components [17]

2.1.1 Basics of RSW

1. Clamp   2. Squeeze   3. Current   4. Hold
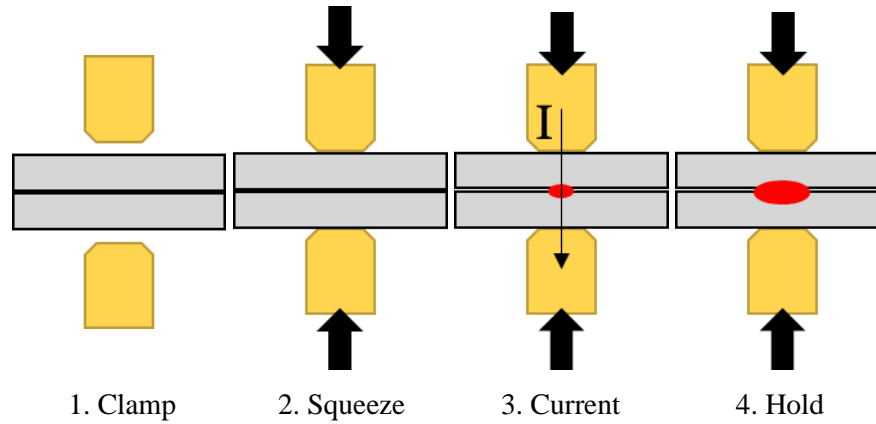
Figure 2.2. Stages of a Resistance Spot Weld

The RSW process is broken down into 4 stages: clamping, squeeze, current, hold as summarized in Figure 2.2. The purpose of the clamping stage is to ensure proper positioning of the electrodes before high forces (on the scale of kN) are applied to the surface. When using a manual or pedestal welder, this step is important for precise welding locations and to avoid any irreversible mistakes. With the rise of automated resistance spot welders, the first step is less crucial as electronics ensures repeatable positioning [23]–[26]. During the squeeze stage, a high force is applied through the electrodes. The current is then passed through the material form one electrode to the other allowing for Joule heating to occur at the metal to metal interface. After the designated welding time, the nugget is held between the electrodes to help cool the nugget and finalize the solidification process. The workpiece is then released by the electrodes signaling a completed weld. This entire procedure occurs on the scale of hundreds of milliseconds.

2.1.2 RSW Parameters

To produce an ideal weld in production, the parameters are required to be optimized through offline studies. Determining the boundaries of acceptable welding conditions is often referred to as the weld lobe curve or process window (see Figure 2.3). The upper bounds of the weld lobe are defined by the presence of expulsion (undesired ejection of metal from weld, seen as sparks/spatter) but not limited to failure method, indentation, etc. The lower bounds is most commonly defined by a minimum nugget size, which follows the AWS standard or the rule of thumb $4\sqrt{t}$ [6].
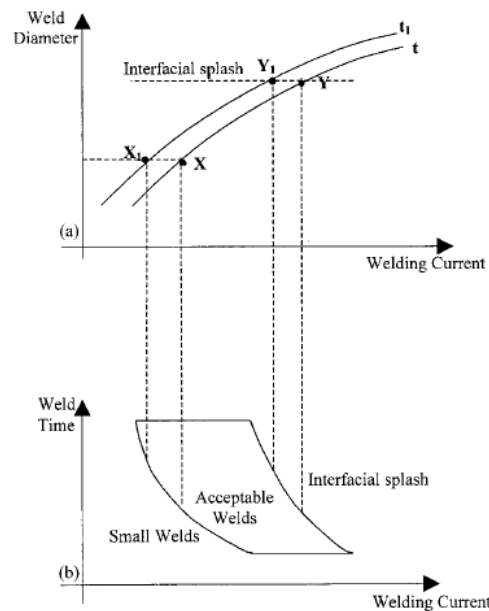
Figure 2.3. Representation of a Standard Weld lobe Curve [17]

The variables that can be optimized in creating a welding schedule are the electrode cooling rate, electrode force, current, and time. As a guideline all of the parameters are generalized in the AWS standard based on the strength of the material [5], [6]. The reason these generalized parameters may not be universal is due to the multiple interactions that occur in the process based on the material stack up.

2.1.2.1 Electrode Cooling Rate

The electrode flow of cooling water through the electrodes prevents any expulsion or sticking at the electrode-workpiece surface [27]. The cooling rate of the nugget is recorded to be on the magnitude of thousands of degrees Celsius per second, thus the temperature of the cooling water is widely neglected [27]–[29]. It is recommended to increase the cooling water flow rate for thicker materials to help dissipate the relative increase in heat required to weld.

2.1.2.2 Electrode Force

The applied electrode force has two main purposes. The first is that it allows for improved localization for the current path due to the breakdown of surface asperities. The reduction of surface asperities decreases the resistance in the pressurized area promoting the current to be concentrated in the area under the electrodes. The second purpose is that it helps to contain the molten nugget during

the weld resisting expulsion [17], [18], [30]. As the nugget expands due to thermal expansion and melting, the pressure exerted by the electrodes contain the nugget with the assistance of the corona bonds which form a ring around the nugget. The corona bonds are the results of solid-state diffusion between the workpieces in the HAZ area due to the indirect heat and pressure from the weld nugget, as shown in Figure 2.4 [19]. At higher electrode forces, more current can be applied to the material as it resists expulsion but risks excessive indentation. Excessive indentation creates a stress concentration during tensile or fatigue tests and is predominant in thicker sheets (>2mm) [8], [31]–[33]. The presence of the stress concentration changes the failure location and risks a loss in strength.
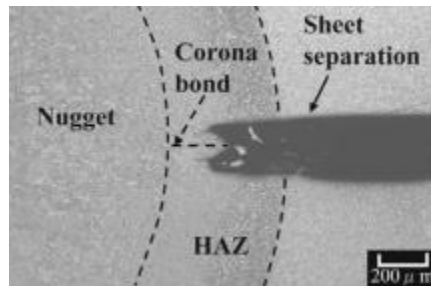
Figure 2.4. Identifying Corona Bond in a Spot Weld [34]

2.1.2.3 Current

      As previously mentioned, the more popular current applied during spot welding in the automotive industry is a direct current (DC). Referring to Joule's heating (Eq. 4), the heat is a function of the current squared making the current the greatest contributor to the heat inputted to create the weld. At higher currents the risk of expulsion is much greater and a minor change in the current has a greater impact to the process compared to the welding time. Studies have found that the polarity of the current can cause electrodes to degrade quicker on the supplying side and even affect weld nugget sizes [35], [36].

9
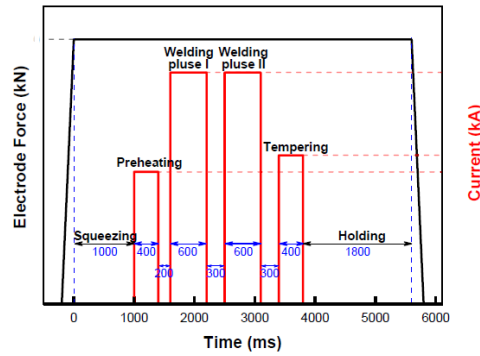
Figure 2.5. Example of a Welding Current Schedule [37]

The current profile in any schedule can be changed to have a pre-current, pulses, or a tempering current. The purpose of the pre-current/pre-pulse is to apply heat into the weld to help with fusion and has been shown to displace surface coating and lubricant between interfaces allowing for a more homogenous fusion [37]–[40]. The main welding current can be applied as a pulse to apply cooling time in between for heat balance or manipulate the nugget growth [41]. The tempering current applies heat to a pre-existing nugget to temper the microstructure and improve mechanical properties [42]–[44].

2.1.2.4 Welding Time

Within the variable of welding time, it can be broken down into three categories of time: squeeze, weld, cooling, and hold. The squeeze time correlated with stage 2 seen in Figure 2.2 and explained in section 2.1.1. The welding time is the duration the current is passed through the material. When pulsing the current, the time between each pulse is referred to as the cooling time and can be increased to allow for more heat dissipation for further weld control. The hold time is correlated with stage 4 explained in section 2.1.1.

2.1.2.5 Electrode Geometry

The electrode geometry affects the application of pressure and current onto the workpiece. The common spot-welding electrodes are either conical or rounded with a flat machined face. These electrode faces can be recut (also referred to as "dressed") to create a new surface and renew the use of the electrodes. The number of welds between each dress is referred to as the wear of the electrodes. Purpose of dressing the electrodes is to remove any surface roughness caused by material build up on the surface or distortion of the electrodes, referred to as mushrooming shown in Figure 2.6. The effects

10

of any geometry change in the electrodes change the pressure distribution or current density which directly affects nugget formation [19], [45].
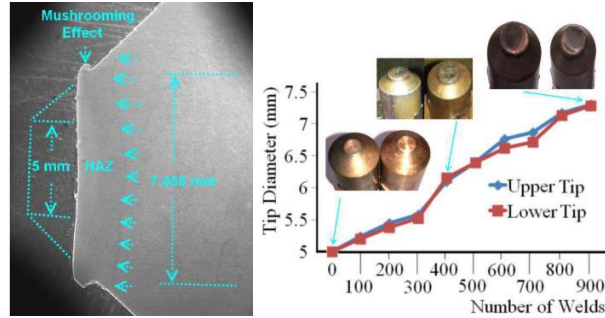
Figure 2.6. Mushrooming Effect (Left) and Effect on Electrode Diameter (Right) [46]

2.2 Resistance in RSW

Resistance is categorized as the combination of a material's resistivity and geometry which the current passes through. Resistivity of a material is the physical property of the material to oppose the flow of the electrical current. The resistance for specific material can be defined by the following equation:

$$R = \frac{\rho l}{A}$$
(Eq. 5)

Where R is the resistance, l is the length travelled, A the area of conductance, and ρ the material's resistivity. The source of all the heat generation in the welded nugget stems from the presence of a resistance for Joule heating to occur. There are five main resistances present in a typical sheet-to-sheet spot weld as shown in Figure 2.7: two electrode-workpiece contact resistances (R1 & R5), the two material bulk resistances (R2 & R4), and the sheet faying interface (R3). Electrode-workpiece contact resistances are low due to the copper electrode's high conductivity and cooling system. The material's bulk resistance plays a vital role in heating of the material allowing for easier melting throughout the sample. The contact resistance between the workpieces (R3) plays the most vital role as it is the initiation of the weld nugget formation. The resistance of the electrodes by themselves are commonly excluded as they are considered a constant in the welding application.
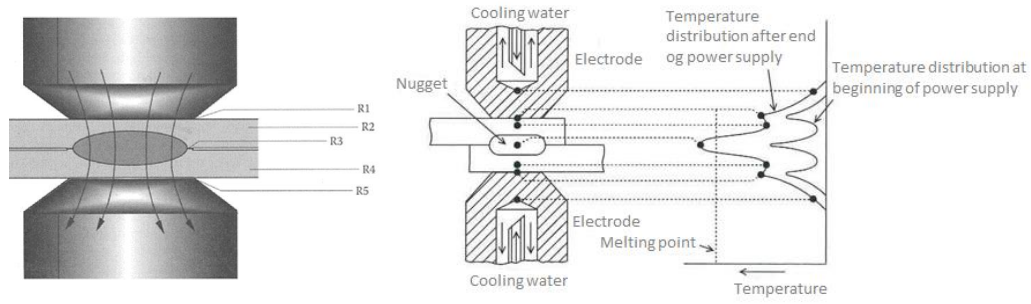
Figure 2.7. Breakdown of Electrical Resistances During RSW [19], [47]

2.2.1 Dynamic Resistance Curve

With the help of current technology, the ability to gather the quantity of voltage and current between the electrodes at every millisecond is possible. Using these two values, the resistance can be simply calculated using Ohm's law:

$$R = \frac{V}{I}$$ (Eq. 6)

where R is the resistance (ohms), V is voltage, and I is current (amperes). By plotting the resistance between the electrodes at every millisecond, a dynamic resistance curve is created. The dynamic resistance curve shown in Figure 2.8 compiled by Dickinson, Franklin, and Stanya is widely accepted as the standard for interpreting the resistance curve [48]. Subsequent study conducted by Cho and Rhee verified the development of the welding nugget and correlation to the dynamic resistance using a truncated electrode and a high speed electrode [49].
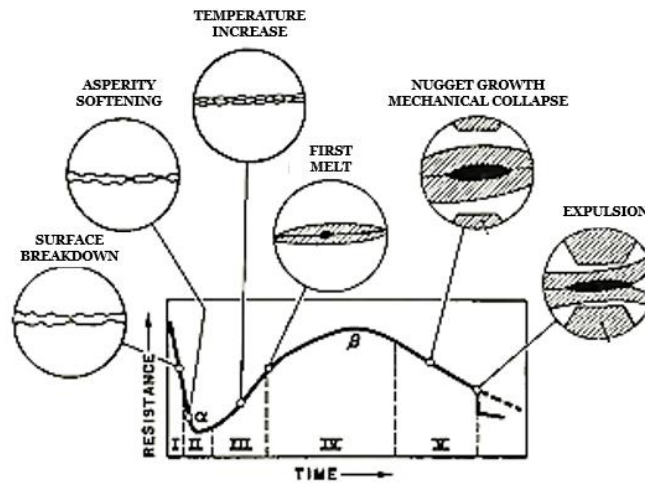
Figure 2.8. Generalized Dynamic Resistance Curve Correlated with Events During RSW Process [48]

The dynamic resistance curve defined by Dickinson et al. of uncoated steel, is broken down into 5 distinct stages. The first stage (I) is when the current first starts to flow through the workpieces where the two surfaces meet. Due to surface asperities and contaminants, there are localized micro-areas of electrical conduction resulting in a high initial resistance. The resistance drops over time as heat is localized at the interface and the surface asperities breakdown increasing the area of contact. At lower electrode forces there is more surface asperities present at the interface resulting in a higher resistance, which is ideal for improving heating to input power (current) efficiency. As previously explained in section 2.1.2.2, the trade-off for lowering the force is the higher risk of expulsion. This is due to the relationship between electrode force and contact resistance explained by Kimchi and Phillips in Figure 2.9. At the lower electrode forces, there is a greater change in the contact resistance in comparison to higher electrode forces, causing instability at the lower forces [50].

13
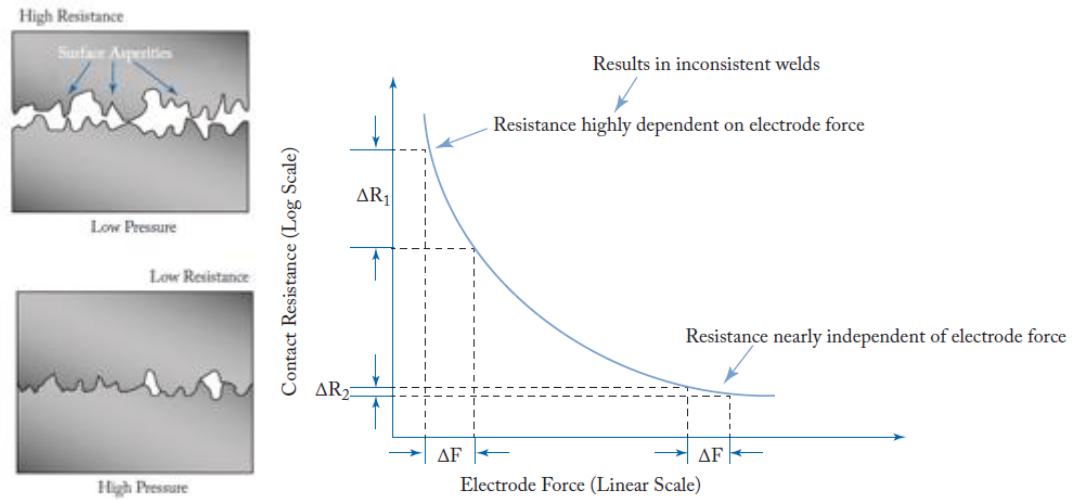
Figure 2.9. Effect of Surface Asperities, and Electrode Force on Contact Resistance [50]

The second stage (II) of the dynamic resistance curve, the surface asperities continue to breakdown and there is direct metal to metal contact. At this stage an equilibrium is formed where the increasing contact area lowers the resistance while the bulk heating of the material increases the resistance. This equilibrium results in a local minimum point often referred to as the alpha point (α) [48]. The third stage (III) is dominated by the change in resistance due to bulk heating which acts as a self-amplifying cycle promoting heating of the material, especially at the fraying interface.
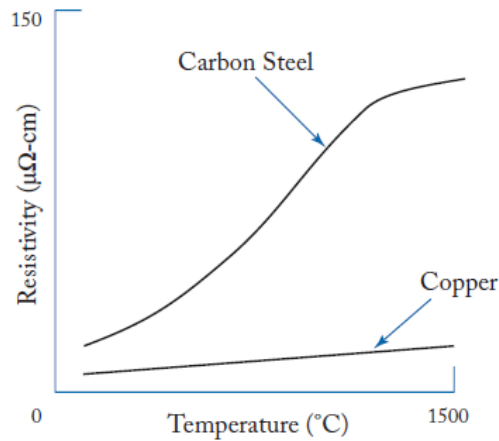
Figure 2.10. Relation Between Resistivity of Steel and Copper as a Function of Copper [50]

Because the influence of temperature on the resistivity of steel is stronger than of copper's, as shown in Figure 2.10, the contribution of coppers resistivity to the dynamic resistance curve is neglected [50]. The fourth stage (IV) begins when the first localized melting occurs. The maximum

resistance is often reached at this stage and is referred to as the beta peak (β). A common misconception is that the beta peak itself is when the weld nugget is formed, but it is another equilibrium point where the presence of a molten nugget, material softening, and indentation cause a decrease in resistance competing against the bulk heating (leading to temperature stabilization). The last stage (V) is a relatively linear decrease in resistance due to the previously mentioned mechanisms overwhelming any bulk heating of the material. At any point in the last stage, if the weld nugget expands to a point where the electrode force and the corona bonds cannot contain the molten metal, expulsion occurs. On a dynamic resistance curve, expulsion is easily distinguishable as a near vertical drop in resistance (caused by a sudden loss of material between the electrodes).

2.2.2 Effect of Coating

Application of a coating to the steel often reduces surface roughness, decreasing the available contact resistance [19]. As a result, the welding lobe curves shift towards higher current ranges to compensate [51]. Due to the need for corrosion resistant components, the majority of all industrial components were and are coated. Gedeon, et al., performed initial experiments in 1987 which suggested the most of the change in the resistance was at the electrode-sheet interface, not at the faying interface [52]. This meant that the breakdown of the resistance curve would not be as representative as Dickinson's model for uncoated metal. Tsai, et al. (1992) conducted a review of the modeling of the nugget growth and found the most accurate models incorporated a dynamic contact resistance at the coated faying surface to match the reported temperature profiles [29]. Thornton, et al. (1996), isolated the change in the bulk resistance and interfaces in attempts to determine the change in resistance due to loading, and found all components played a role in the dynamic resistance [53]. Wang and Wei (2002) created a model of the dynamic resistance of the spot welding using the summation of the bulk resistance of the coated material and contact resistance [54]. The results shown in Figure 2.11 provide strong evidence that the majority of the change in dynamic resistance of coated materials is not solely due to the electrode/workpiece interface but a summation of the entire process. The cause for the two different viewpoints is most likely due to the difference in available measuring equipment.

15
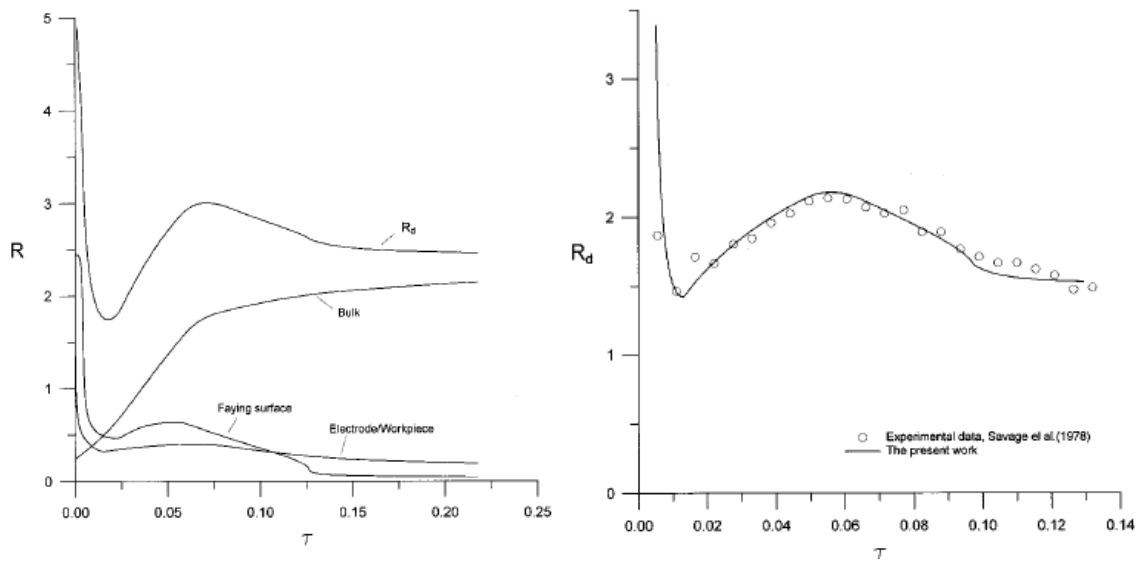
Figure 2.11. Breakdown of Dynamic Changes in Resistances of RSW Process (Left) and Comparison to Experimental Data (Right) [54]

Thus, further studies on coated steels were conducted to understand the impact . The most well-known study was conducted by Savage et al., and Gedeon et al. using a Zn coating, varying with uncoated, hot-dipped, and galvanized [52], [55], [56]. It was found that within each condition, there was consistency in the dynamic resistance curves which indicated that the dynamic resistance curve was reflective of the material condition.
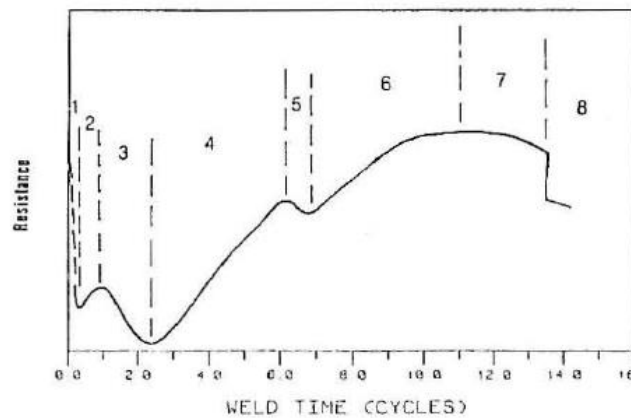
Figure 2.12. Generalized Dynamic Resistance Curve of Coated Steels [52]

Gedeon proposed a new generalized dynamic resistance shown in Figure 2.12, where the uncoated materials exhibits regions 1, 6, 7 and 8 (corresponding well with Dickinson), while the galvannealed coating exhibits all regions excluding 4 and 5 [52]. The hot dipped samples exhibited all

16

8 regions. Regions 2 and 3 are exclusive to the coated samples, in which the rise and fall of resistance is primarily driven by the bulk heating of the coating at the electrode-sheet interface and the change from solid to molten zinc [52]. The decline in resistance to near zero after region 3 is due to the strong presence of the molten zinc between the interface overpowering any bulk heating or possible asperities. Region 4 and 5 are exclusive to the hot dipped samples due to the weaker of Zn-Fe interlayer, allowing for the softer zinc to be melted and pushed around (allowing for the later drop in region 5).
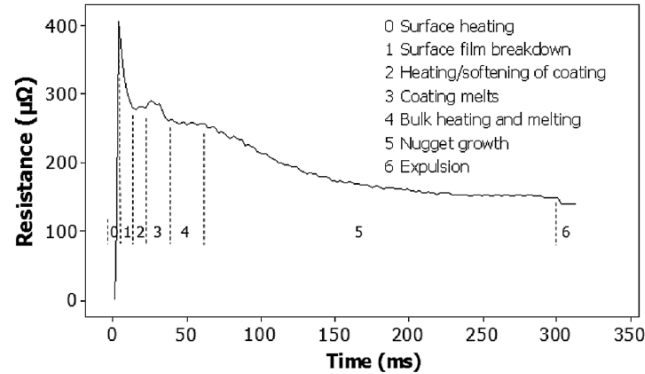
Figure 2.13. Generalized Dynamic Resistance Curve of Recent AHSS [57]

A more recent study of the dynamic resistance curve was conducted with a currently popular AHSS known as USIBOR®. The introduction of AHSS, of different alloying compositions, and coating application methods/compositions all play a role in the resistivity of the material. The study performed on USIBOR® was performed with an Al-Si coating. The results found correspond to the same dynamic resistance stages as Gedeon's galvannealed curve. The main difference is the introduction of stage 0, where the material undergoes surface heating as the voltage builds up before fritting begins (shown in Figure 2.13). It should be noted that the beta-peak is present in region 2 to 3 which corresponds to the heating/softening and melting of the coating. According to Gedeon's model, the resistance in region 4 should rise again due to bulk heating of the material but the increase in the heat resulted in softening of the coating at the electrodes. The softening at the electrodes lead to indentation which in turn resulted in a reduction of current path and increased current area countering the increase in resistance [52], [57].

2.3 Quality of RSW

The quality of a resistance spot weld is critical as it is the dominating form of joining for all automotive applications. Because the structure and integrity of a vehicle depends on the quality of the welds, industry standards are monitored and updated as steels and technology advances. The most

common standard in North America is American Welding Society's (AWS) specification for automotive weld quality & testing methods (D8.1 & D8.9) [5], [6]. The standard defines four major methods of determining the quality of the weld: surface inspection, peel/chisel test, shear/cross tension test, metallographic analysis [6]. Of the four major methods, they can be classified as destructive (DT) or non-destructive (NDT) tests. The most accurate measure of the weld will be the use of a DT but is not applicable outside of the laboratory setting, thus there is more attention being directed to other NDT. The results of the test provide if there are defects present, weld nugget size, or weld ultimate tensile strength.

2.3.1 Surface Inspection

The inspection of the surface typically involves NDT, ranging from a quick glance at the weld to the use of a macroscope. A general surface inspection can detect a misplaced/missing weld, expulsion flash/marks, surface cracks, holes, excessive indentation, etc. With the help of automation technology, the problem of misplaced or missing welds is significantly decreased. When a weld experiences expulsion, it is visible as sparks during the welding process. The two locations for expulsion are at the faying surface or at the electrode interface. The impact of expulsion at the electrode interface is insignificant in comparison to expulsion at the fraying surface where material loss of the molten nugget occurs [33], [45]. Surface cracking is a phenomenon which occurs due the microstructural changes that allow for weakening of grain boundaries or solidification mechanics. Materials such as magnesium [58] and aluminum [59] have a high cracking susceptibility at higher welding currents due to hot cracking. Steels with higher austinite content, such as stainless steels, are also more susceptible to cracking [37], [60]–[62]. The more relevant 3rd generation AHSS such as dual phase and TRIP steels are currently under investigation as they exhibit liquid metal embrittlement (LME) when coated with zinc [63]–[66]. The main mechanism of LME is the zinc melting prior to the physical and thermal stressed steel, allowing it to penetrate into the grain structure creating intergranular failure.
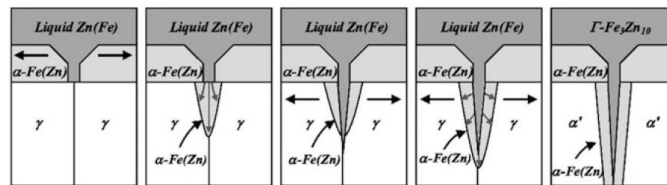
Figure 2.14. Mechanism of Liquid Metal Embrittlement within the Zn-Fe Binary System [66]

2.3.2 Peel/Chisel Test
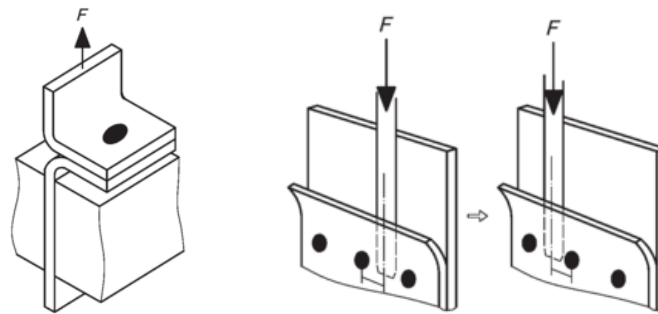
Figure 2.15. Generic Peel Test (Left) and Chisel Test (Right) [67]

Peel testing is the quickest destructive test that can be performed to determine the quality of the weld. By welding at one end of the strip of the workpiece, the other end can be pulled apart to reveal a weld button to measure. The peel test is the most convenient method but is limited to only providing the weld nugget size and fracture surface. The chisel test is a destructive test that allows the operator to apply a normal force by wedging open the space between the welds. A well-known deviation of this test is the chisel check where the test is conducted to an acceptable limit and not to failure. A chisel designed to separate the workpieces to a specified distance is inserted in between two workpieces with force (often with a hammer or mechanical assistance). If the welds separate upon insertion of the chisel, it is categorized as inadequate nugget formation and needs to be rewelded. This process induces plastic deformation upon testing the strength and is repaired to its prior appearance.

2.3.3 Shear/Cross-Tension Test

Shear and cross tension testing are the quantitative testing of the weld by performing the tests with a tensile machine (setups shown in Figure 2.16). As the names suggest the shear test evaluates the strength of the weld parallel to the workpiece, and the cross-tension test evaluates the strength perpendicular to the workpiece. The main benefit of this method is the ability to gather the extension and applied force on the sample allowing for a calculation and plotting of an engineering stress-strain curve for further analysis.
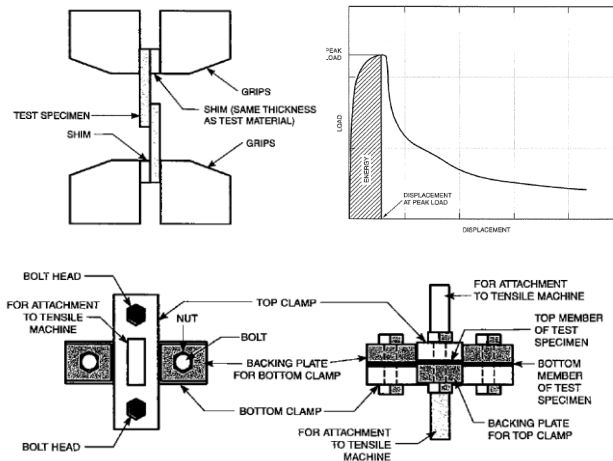
Figure 2.16. Shear Tensile Test (Top Left), Resulting Load-Displacement Graph (Top Right), Cross Tension Test (Bottom)

2.3.4 Metallographic Evaluation

Metallographic analysis of the weld is the preferred quality testing method in a laboratory setting. The benefits of the metallographic method allow for the analysis of the weld nugget diameter, microstructure, measurement of indentation or possible flaws. Possible flaws that can be found by conducting the cross-sectioning are solidification voids, internal cracks, or incomplete fusion due to an interlayer/coating.
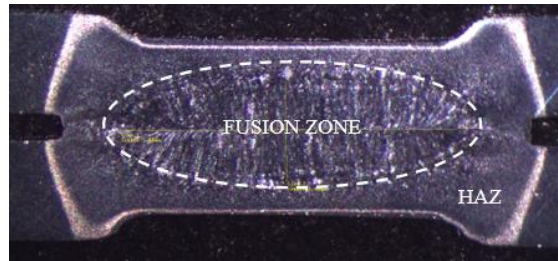
Figure 2.17. Polished and Etched Cross Section of a Spot Weld

2.4 Quality Monitoring

Real time quality resistance spot welding monitoring is the next step in research and application for the automotive industry. The term real time monitoring refers to the ability to interpret or be notified the moment a defect is detected. The main reasons for this shift is the traditional methods for inspection of spot welds are not an efficient use of time and materials, potential batch repair or scrapping of components, and cannot guarantee every weld is inspected [68]. With the advancements in technology,

20

various alternative methods to determine the quality of the weld had become available. The two major categories which all of the real-time quality monitoring fall under is either an automated secondary process or analysis using in-situ signals. Processes that fall under the automated secondary process category occur after the welding procedure in the same cell or in a separate testing cell along the production line. The in-situ processes occur simultaneously or instantly after the weld and requires minimal or no additional equipment.

2.4.1 Secondary Process

The most common secondary process is an ultrasonic inspection of the resistance spot weld, often performed manually but newer technology allows the test to be automated [69]–[71]. As the name suggests, ultrasonic inspection utilizes high frequency waves to detect any geometric or material defects. The waves are transferred to the weld surface and at any boundary created from a change in material (microstructure, gap/gas, air from cracks, etc.), a proportional reflection of the wave occurs and is picked up by the sensor [72]. The results of an ultrasonic inspection is often a graph of peaks representing reflections and impedances as shown in Figure 2.18 [73]. Proper interpretation and operation of the ultrasonic testing device requires a certified operator which is an additional use of resources. In addition to this, ultrasonic inspections of the weld require surface preparation by either flattening or applying a conductive gel.
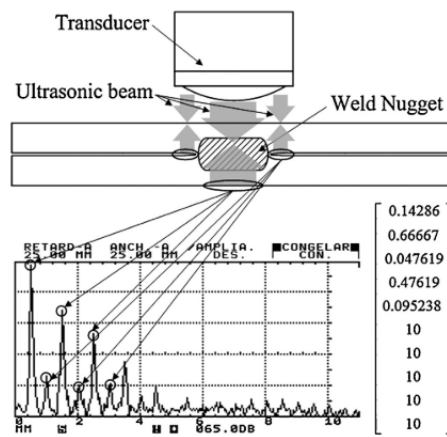
Figure 2.18. Results from Ultrasonic Inspection Detecting Undersized Nuggets [73]

Acoustic microscopy is the use of ultrasonic inspection to create an image on a monitor to make it a more robust user-friendly method to inspect the weld. This method allows the user to visually inspect the size and shape of the nugget as well as the presence of any defects [74]. The data collected

from the acoustic microscopy are now analyzed using neural networks or image analysis programs to quickly inspect the weld without the need for an operator [75]–[77]. The trade-off for the easy to interpret visual of acoustic microscopy is the high capital cost of the machine. The development of 2D array transducers and optimization of algorithms introduced a cheaper and quicker method of interpreting the ultrasonic waves into an image [78]–[81]. The difference in the image can be shown in Figure 2.19.
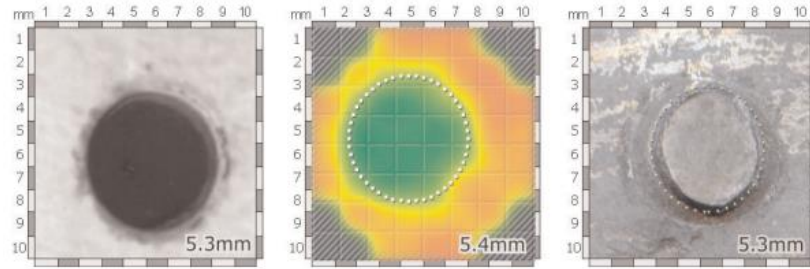
Figure 2.19. Results from Acoustic Microscopy, Ultrasonic 2D Array, and Destructive (Left to Right) [79]

Visual analysis of the weld using surface image taken from a camera is also a potential solution to analyzing the weld quality. By applying filters to the surface image of a weld and determining an appropriate distance function, the weld nugget size and shape can be found [82].
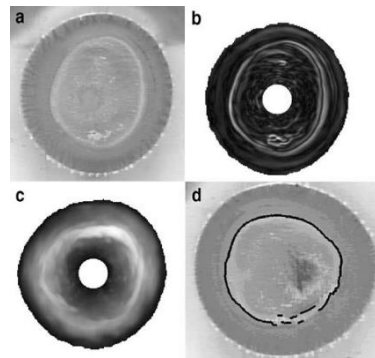
Figure 2.20. Image Filtering and Application of Functions (From a to d) [82]

Another imaging method is the use of an infrared camera and a flashlamp. The theory is to apply a short burst of heat through a flashlamp or equivalent tool to heat the weld and surrounding area and take an image of the heated weld to inspect. This method follows the same idea as the previously mentioned surface imaging but has the potential to capture internal errors in addition to the weld nugget

diameter. Studies have found the brighter and uniform images indicate a good weld, where welds with defects do not have a uniform intensity, as shown in Figure 2.21 [83]–[85].
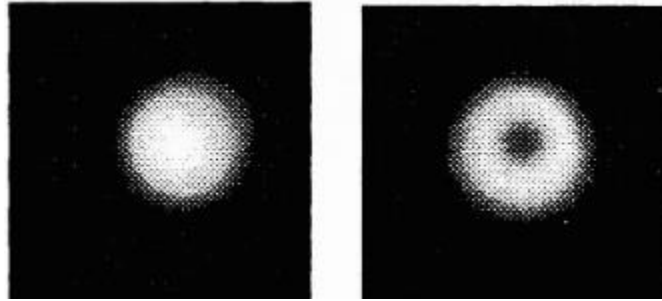
Figure 2.21. Example of a Good Weld (Left) and Bad Weld (Right) Using Infrared Camera [83]

The use of a secondary process to detect quality was proven to have a strong ability to conclusively determine the quality of the weld using the ultrasonic method. Even with cheaper alternatives such as using regular or infrared cameras, inspection of the quality of the weld has demonstrated effectiveness in detection of quality. The issues with a secondary process is the additional step which increases the production time of a part, which is not ideal when production of parts are measured on the scale of seconds. Another issue is the additional maintenance required to maintain and calibrate the equipment to have reliability. Possibly on a small production scale, these methods would be ideal but with a large production requirement, it is less feasible in the automotive industry.

2.4.2 In-Situ Signals

The next step in monitoring the quality of the process is to analyze the already available signals that are collected by the welding/robot controller. The signals that have been analyzed by current literature are the electrode force/displacement, acoustic emission, and dynamic resistance.

2.4.2.1 Electrode Force/Displacement

Studies of the electrode during the welding process provided strong relation to the presence of a defect or undesirable weld. Upon investigation, the instantaneous (millisecond) displacement and force of the weld was not constant and displayed dynamic behavior that correlated to the changes with the weld, shown in Figure 2.22 [86].
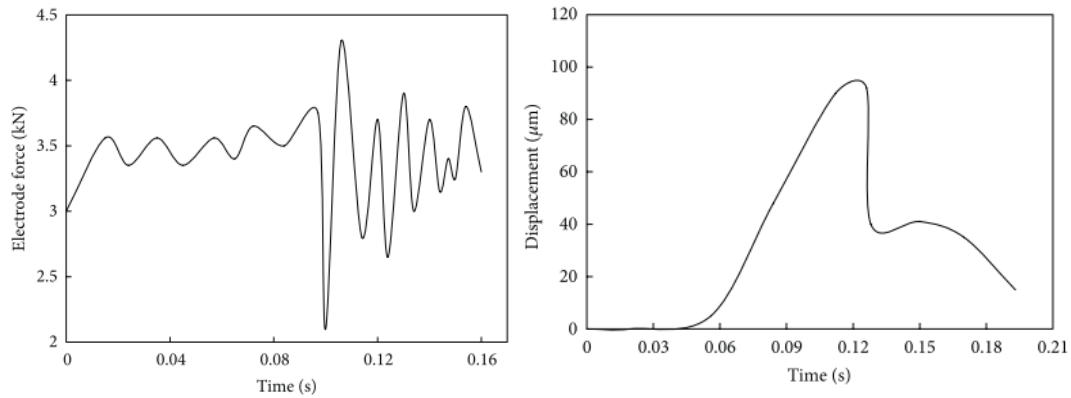
Figure 2.22. Dynamic Electrode Force (Left), Displacement (Right) Curve with Expulsion [87], [88]

During the spot-welding process, the electrode force displays a tendency to increase greater than the preset welding force due to the thermal expansion. As the material is heated through Joule heating, it undergoes a thermal expansion acting against the electrodes creating an instantaneous opposing force against the electrodes [68], [87]. As the material continues to heat and a welding nugget has formed, the material begins to soften and provides less resistance to the electrodes. In the case of detection, when expulsion at the faying interface occurs, there is a loss of materials and a sudden loss of volume results in a sharp drop in the force shown in Figure 2.22.

The electrode displacement was found to react in the same manner as the electrode force. The thermal expansion experienced by the work pieces are measured during the welding process and the peak thermal expansion was found to represent the amount of weld growth [68]. Thus, undersized nuggets could be detected when the peak displacement of the electrodes are less than the standard. Expulsion could also be identified by a sudden drop in the displacement due to the loss of material, shown in Figure 2.22. Current automated welding machine operate using a servo motor robot to perform the welds. The servo motors operate using an encoder to measure travel as well as applied force. A study using the indentation measurement from the encoder found that at a select welding parameter, there exists a range of acceptable indentation depths which meet the required strength of the weld [89].

The main drawbacks of utilizing the electrodes as an in-situ monitoring signal is the electro-magnetic forces that are created during the process of welding (since magnetic fields are a function of currents). These magnetic fields create noise in the data collection of the electrode displacement and

24

electrode force allowing for poor confidence when collecting data. With the measurements of the forces and displacement, rigid structures are recommended for data acquisition which is not applicable for welding guns in automotive settings. Without the rigid structures, precise measuring tools or systems are required to perform these measurements which is a cost factor.

2.4.2.2 Acoustic Emissions

Acoustic emissions during welding is not a common signal that can be gathered during the welding procedure. A piezoelectric sensor is attached to either one or both of the electrodes and the emissions from the electrodes are measured. Studies have found, the acoustic emissions of a weld can detect plastic deformation, cracking, melting, and martensite transformation [68], [86], [90].
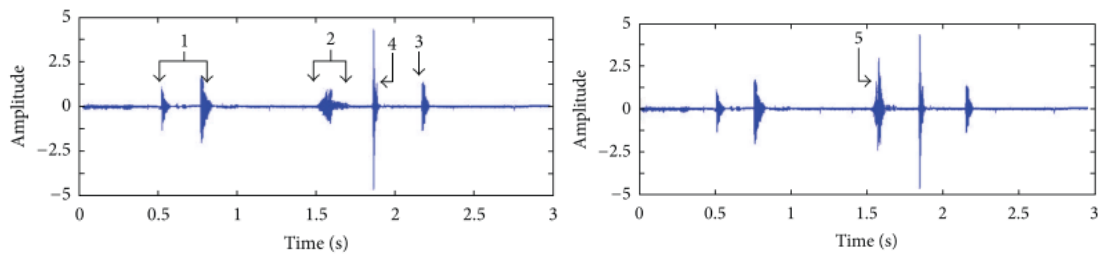
Figure 2.23. Acoustic Emission of Weld with Crack (Left) and Expulsion (Right) [68], [86]

Section 1, 2 and 3 in Figure 2.23 are the acoustic emissions of the closing and clamping of the electrodes, the nugget nucleation, and the electrodes opening (respectively). Event 4 was the detection of a crack while event 5 during the nucleation of the nugget was the detection of expulsion [68], [86]. While all of these events can be detected, in an industrial setting, the level of noise which is introduced to the system significantly increases (due to ambient noise/vibrations, heavy operating machinery, etc.) which will require complicated noise reduction systems.

2.4.2.3 Dynamic Resistance

The most common signal used to determine the stability or quality of the welding process is the dynamic resistance. The use of dynamic resistance is closely tied with the use of voltage as most systems used constant current controllers which meant if resistance changes, the voltage would directly change (based on Ohm's law). Thus, multiple welding controllers with quality detectors in the 1970s and 1980s would track the voltage fluctuations [52]. As technology advanced, the values could be recorded cycle by cycle, down to milliseconds, and the use of dynamic curves explained by Dickinson could be employed [48]. As previously explained in Section 2.2.1, the stages of the weld nugget

formation and completion were correlated to the segments of a dynamic resistance curve. The idea of using the dynamic resistance curve as a quality indicator was pursued in the late 1980s to the early 2000s and various methods were investigated. Prior to the 2000s, most research focused on following Kamat and Lagoo's [91] logic of comparing the entire dynamic resistance curve against a known curve to determine if the weld experienced any abnormalities [52], [91]–[93]. Livshits [94] calculated an optimal resistance using the minimum and maximum resistance to use as a quality indicator, shown in (Eq. 7), where X, Y, and Z are electrode dimension, current density, and joint geometry correction factors (respectively) [94].

$$R_{opt} = \frac{YR_{min}}{2Z\left(1 - \sqrt{1 - \frac{R_{min}}{XR_{max}}}\right)} \qquad \text{(Eq. 7)}$$

Starting in the 1990s, most investigations focused on breaking down the dynamic resistance curves into qualitative values to use as inputs to regressions or neural networks. The breakdown of the dynamic resistance curve was either into segments based on time/cycles, material phenomena, or graphical. Wen, et al., investigated the relationship between the final resistance of the curve to the weld nugget size of a stainless steel weld [14]. The main issue with using only one variable to find correlation to a quality indicator is that it does not prove a robust solution and still required a separate analysis of the curve. To create a more robust model, the dynamic resistance curve was broken down based on the curve's features. Cho and Rhee [95], [96] were the vanguard in breaking down the curve to use for analysis through neural networks, as shown in Figure 2.24, which are still implemented in 2017 by Zaharuddin et al [97].
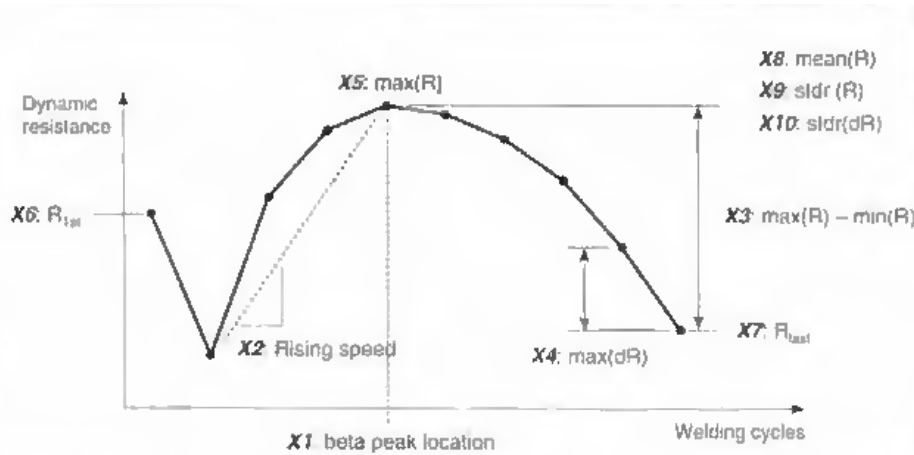
Figure 2.24. Breakdown of a Dynamic Resistance Curve for Analysis [95]

26

The alternative method to obtain the inputs is to segment the curve into time-intervals and calculate a significant value from the interval (max, min, or average) [98]–[100]. The premise of either analysis was to obtain a singular quantitative input from a feature or segment of the dynamic resistance curve to input into a neural network or regression model to provide a quality indicator output. Figure 2.25 is an example of a resistance curve transformed into a binary array to input into a neural network. This method of analysis is purely based on experimental data and is repeatable under the same conditions, but the downside is the lack of theory applied to the results as the neural network acts as a black box.
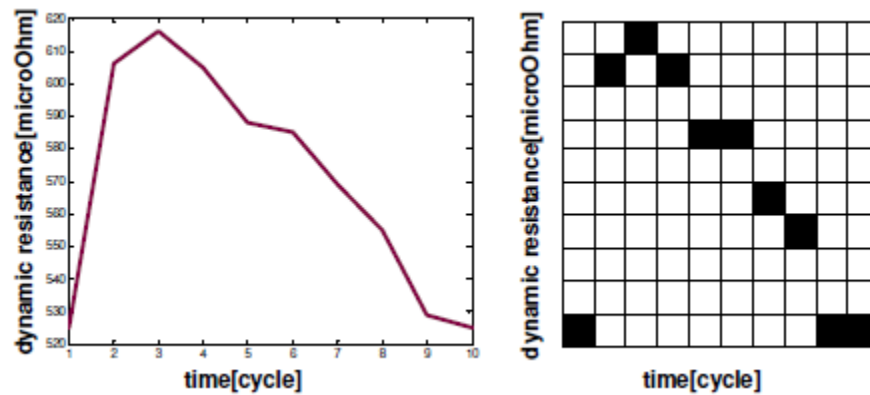
Figure 2.25. Example of Time-Interval Segmentation of a Curve [98]

2.5 USIBOR® Steel Sheet

USIBOR® 1500 is classified as a press hardened AHSS alloyed with boron, named by Arcelor Mittal. The composition of the material is found in Table 2.1. According to Arcelor Mittal, USIBOR® is best used for complex geometry components, uniform mechanical properties, high strength, and weldability. Recommended high-strength applications are structural beams or reinforcements for doors, windows, floors, etc. [101].

Table 2.1. Elemental Composition of USIBOR® 1500 [101]

C (%)	Si (%)	Mn (%)	P (%)	S (%)	Al (%)	B (%)	Ti+Nb (%)	Cr+Mo (%)
0.25	0.4	1.4	0.03	0.01	0.01-0.1	0.005	0.12	1

The uniqueness of USIBOR® is the ability to undergo forming and pressing process for manufacturing applications. There are two methods in which the material could be stamped, directly

where the material is austenized, then formed and quenched in the same step. The indirect method involves a cold pre-forming before the austenization where the last step is to calibrate and quench the part.
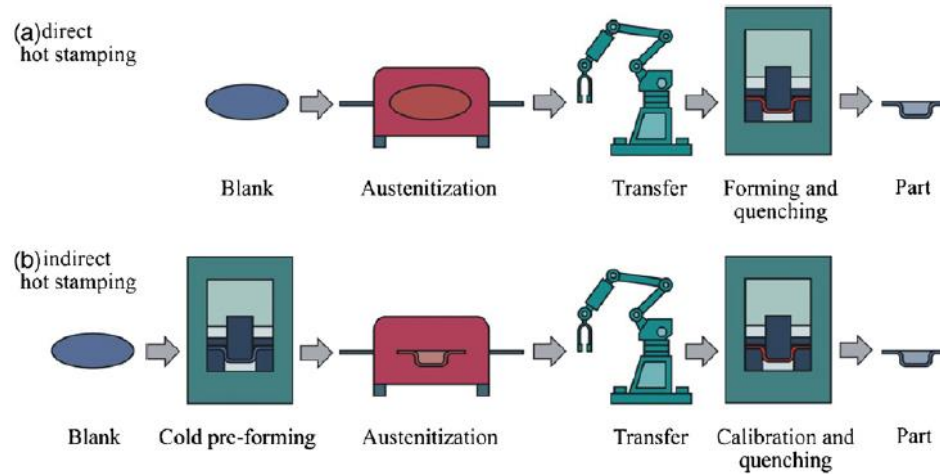
Figure 2.26. Standard Hot Stamping Process Chain [102]

During the austenization step in the hot stamping process, the steel is at risk of oxide scale formation (surface oxidation) and decarburization [102]. To prevent any change to the steels during the austenization stage, they are coated with a protective layer of Al-Si. The melting point of the Al-Si coating of 600°C is lower than the general austenizing temperature of steel (727°C) but when heated, the diffusion of Fe into the Al-Si coating is activated, with the most stable form Fe_2Al_5 melting at 1171°C [103].
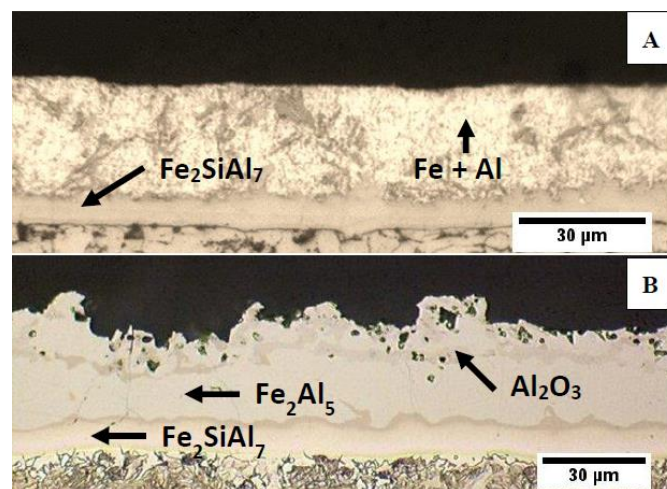
Figure 2.27. Metallography of Al-Si Coating: A) As-Delivered B) Hot-Stamped [101]

28

Compared to a zinc coating, the Al-Si does not provide any cathodic protection but performs better as a barrier. Due to the low forming limits of Al-Si it cannot undergo indirect hot stamping as the cold forming will cause discontinuity in the coating surface [102].

2.5.1 Challenges Welding USIBOR®

Investigating the weldability of the newer AHSS, it was discovered that the metal behaved differently in comparison to the lower strength steels. Firstly, AHSS have narrower weld lobes resulting in stricter welding conditions [2]. The strengthening elements in the steels increase the electrical resistance providing a higher heat generation which in turn lowers the expulsion current limits. The presence of the coating and the formation of an intermetallic between the coating and base metal during hot stamping also contribute to the change in resistance. Due to the higher strength of the AHSS, higher electrode forces are required to weld the steels. The increase in the electrode forces result in faster electrode deformation and increased surface asperity breakdown. All of these factors influence the weld lobe curves indicating AHSS weldability is stricter than weaker metals.

Another challenge in welding USIBOR® metal is the softening of material that occurs in the heat affected zone (HAZ). Previously discovered in spot welded dual-phase (DP) steels, the hardness profile of the weld showed a drop between the base metal and the weld nugget due to martensite tempering [104]. During weld, the heat affected zones reach temperatures that do not reach melting temperatures; thus, the microstructures are dependent on diffusion mechanics. During this time, the martensite of the base metal will experience heating and cooling which leads to decomposition of martensite and formation of cementite or ferrites which are lower in hardness. Lu et al. modelled the HAZ softening of USIBOR® based on the same mechanics found in DP steels and found evidence the primary mechanics of soften are the same as that of DP [105]. HAZ softening is attributed to lowering the strength of the weld and increase in elongation of the material which is not desired in a stiff structural component.
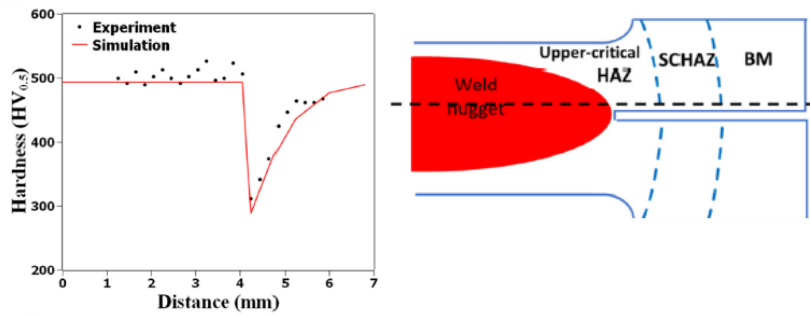
Figure 2.28. Results of Modelling the HAZ Softening in USIBOR® [105]

The weld and base metal of USIBOR® is composed fully of martensite, providing high strength and low ductility AHSS is known for. Due to the high hardness and brittle nature of martensite the weld nuggets are susceptible to interfacial failure. Interfacial failure in USIBOR® spot welds are linked to the notch effect (Figure 2.29) present in spot welds and the brittleness of the nugget, leading to susceptibility to crack propagation [106]. In terms of fatigue, this is an undesired property as the presence of a notch lowers fatigue life significantly. In non-AHSS, interfacial failure of a spot weld is correlated to lower energy absorption (lower strength) but due to AHSS microstructure, there is insignificant correlation between the strength of a weld and the failure method [107].
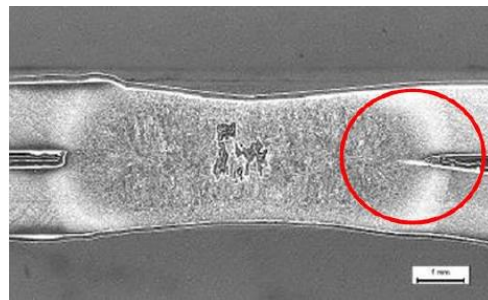
Figure 2.29. Example of a Notched Spot Weld Nugget

Chapter 3
Experimental Design

3.1 Welding Equipment

The testing performed in this thesis was all performed using either a pedestal welder or an automated servo-robot spot welder. Results in Chapter 4 were gathered using a medium frequency direct current (MFDC) 144/180 kVA pedestal welder manufactured by Centerline Ltd. A Rexroth PSI63C0.120L1 controller was retrofitted to operate with the pedestal welder. The electrodes used to weld were RWMA Group A, Class 2, domed-flat nose with a 6mm diameter flat face.
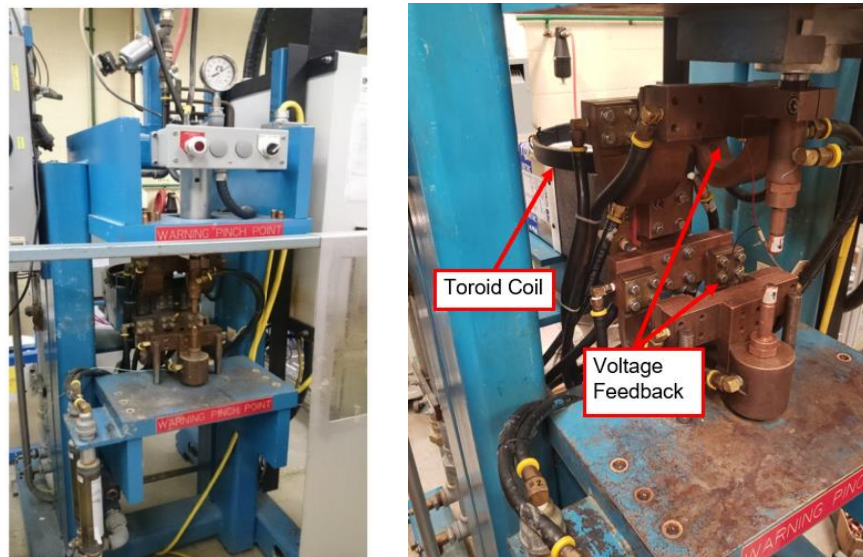
Figure 3.1. MFDC Pedestal Welder (Left) and Data Collectors (Right)

The current was measured using a toroid coil on the secondary pick up of the transformer, and voltage on the copper electrode mounts. Measured values were recorded every millisecond and the resistance was calculated. The adaptive feature of the controller was used to extract the current, voltage, and resistance curves.
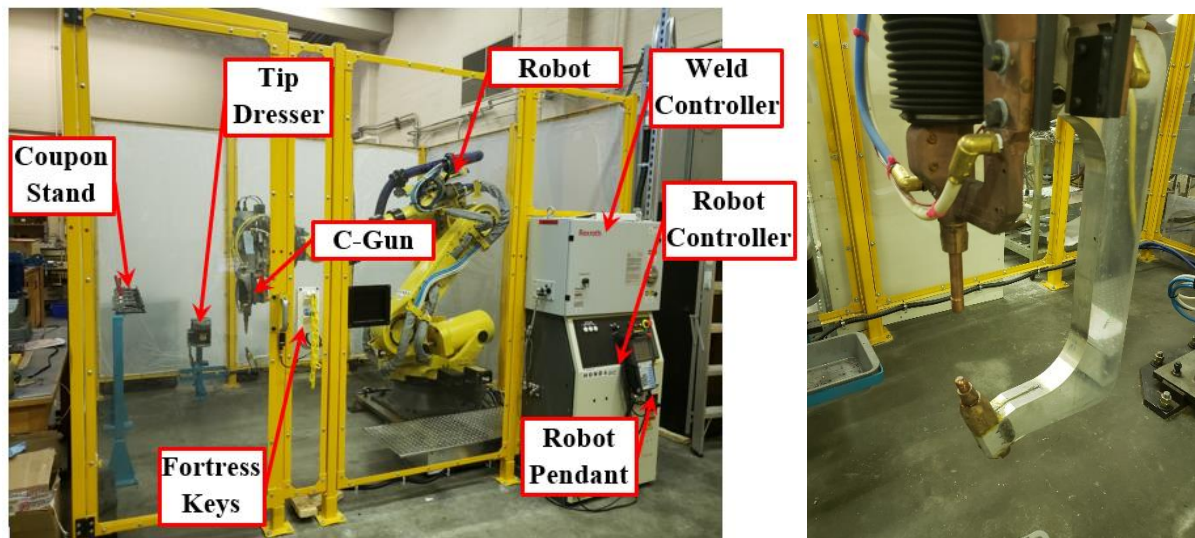
Figure 3.2. Robot Spot Welding Cell (Left) and C-Gun (Right)

The automated servo motor robot used was a Fanuc 2000ic (210F) with an industry designed c-gun resistance spot welder attached at the end. This set up was performed for all later results in Chapter 5 and Chapter 6. The top electrode of the c-gun used the same as the pedestal, where the bottom is angled at 20 degrees. The same welding controller on the pedestal welder was used on the robot welder. A G&T tip dresser with 6mm cutter blades was used to maintain fresh electrode tips and mimic production conditions. The welding cell, fixtures, and safety features were designed by Honda of Canada Manufacturing.

3.2 Welding Process

3.2.1 Chapter 4

The welding schedule used for the tests in Chapter 4 were based on industry provided welding schedule and modified based on a previous weld lobe curve study. The chosen weld schedule was set to 7kA for 500ms and AWS D8.9M recommendations of 5.5kN and cooling rate of 6L/min for 1.6mm thick group 4 steels were followed [5]. Ten welds using the weld settings previously described were conducted to create a reference dynamic curve

. The set up for the experiments was simplified and shown in Figure 3.3. The centerline of the weld was measured to the center of the closest weld to investigate the effect of shunting and measured to the edge for edge proximity. Shunts were welded at distances of 10, 20, 30, and 40mm apart. The

edge welds started at the center of a 40mm wide coupon (chosen as the reference point) and moved closer to the edge in increments of 5mm. Eight welds were made per shunt distance, five welds were made per edge weld distance, and five welds nuggets of each parameter were measured. Shims were placed on one side to mimic a bent part or debris between the workpiece. This interference was replicated with a 2mm and 4mm shim placed 40mm away from the weld location to allow the material bend under the electrode force. The effective gap between the electrodes was calculated to be 1mm and 2mm (at approximately 2.8º and 5.7º respectively).
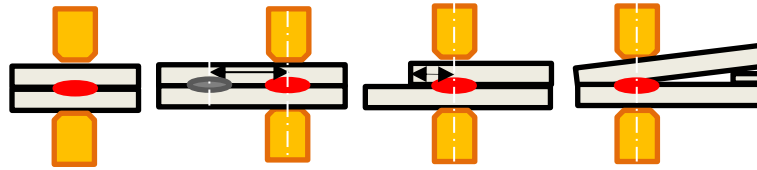
Figure 3.3. Representation of a Standard, Shunted, and Edge Weld (from Left to Right)

Using a similar approach as outlined by Cho, Rhee, and Zaharuddin [95]–[97] the dynamic resistance curves were broken down into the following six measures: average resistance, maximum resistance (beta-peak), final resistance, formation slop, and growth slope. Linear slopes between the start to beta peak, and beta peak to final resistance are used to take into consideration the relation between the beta peak times and the beta peak/final resistance. Contrary to previous literature, the initial surface heating (i.e., 'fritting') stage, where the resistance experiences a rapid steep increase and decrease due to breakdown of films, scales, or asperities, was not captured [55].

3.2.2 Chapter 5-6

The welding schedule used for the latter chapters were based on an industry recommended schedule. The initial pre-weld was set to 12kA for 30ms to apply a burst of heat to reduce the effect of the coating. The main current was set to a constant 7.8kA for 450ms with a 20ms cooling time in between the pre and main current. The maximum applicable force by the servo motor of 550kgf (or approximately 5.5kN) was used to weld the samples.

To set up the adaptive welding feature for the Bosch Rexroth controller, ten welds of a specified welding schedule were recorded and inspected to be an acceptable size and free of defects. The recorded dynamic curves were then averaged and set as the reference curve for adaptive welding to be active. When the adaptive welding feature was on, none of the settings could be changed.

The welding schedule for the dissimilar stack-up welding in section 6.2.2 was also provided by the industry. The main current was set to 7.5kA for 417ms (25 cycles) at a force of 350kgf. The same procedure for setting up the adaptive welding was used.

3.3 Specimen Dimensions

The specimen dimensions were recommended and provided by the industry partner to use 125x40mm for welding and tensile testing. Smaller samples of 25x25mm for the pedestal welder were made for isolated welding testing.

3.4 Metallography

Welds were cross sectioned using Struers Accutom-50 precision cutter machine with a 50A15 blade. The machine was set to 0.015mm/s feed rate, 2800 rpm wheel speed, and applied low force. The surface is cleaned with ethanol and air dried. The samples were finished with a 3-micron diamond polisher then etched with a 5% nital solution, composed of 5% nitric acid and 95% ethanol. Images were captured with a macroscopic stereoscope and electron microscope. Weld nuggets were measured using image analysis software ImageJ.

3.5 Tensile Testing

The tensile test was performed using Instron Model 4206 at 10mm/min according to AWS 8.9m [5]. According to the tendency for USIBOR® to undergo interfacial failure vs button pullout, any nugget measurements are done on the fracture surfaces.

Figure 3.4 Instron Tensile Testing Machine with Tightening Grips

Chapter 4

Effect of Process Conditions on the Dynamic Resistance Curve of USIBOR®

Throughout this chapter, the influence of the common process faults or errors on the dynamic resistance curve of USIBOR® is investigated. The main purpose of this chapter is to determine the strength of the correlation between the dynamic resistance curve to the quality of the welding process itself. Based on previously established analysis of the dynamic resistance curve, it can provide a strong indicator of the stages of the weld nugget formation for steels. Most faults or welding defects occur due to poor welding conditions such as poor weld placement. By proving detection is possible through observation of curves, one can support the application of adaptive welding controllers which base their systems on the dynamic resistance curve to monitor weld quality.

4.1 Effect of Shunting

Shunting occurs when a pre-existing weld in close proximity to the intended weld site diverts a portion of the current away. The diverted current reduces the amount of heat in the weld area and risks formation of undersized nuggets. A shunted weld may occur through incorrect weld placement, which is a critical fault in production and will require repair or result in scrap. Xing et al., characterized the shunted welds into a simplified electrical circuit of resistors in parallel shown in Figure 4.1[108]. According to (Eq. 5), the overall resistance would depend on the path of travel, material property and inversely on the area. Assuming the material property is uniform, it can either be calculated as an increase in path length and area of the current due to shunting, or two resistances in parallel with same area but difference path lengths. Either calculation resulted in a decrease in the overall resistance due to the presence of a shunting weld.
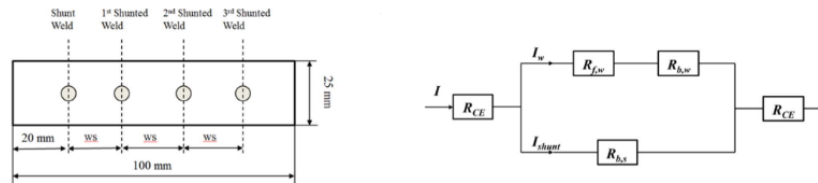
Figure 4.1. Electrical Circuit Equivalent of a Shunted Weld

The subtle difference in the initial transient of the dynamic resistance from 0 to 40ms reflects the initial heat generation at the interface. This has been shown to be highly dependent on the rate at which heating occurs and when the first melting initiates [95]. As the spacing of the welds decreases, the rate of this heating progressively decreased due to the shunted current flow hampering the heat generation. This is reflected by the shallower slope in current shown in Figure 4.2b. Figure 4.2c.
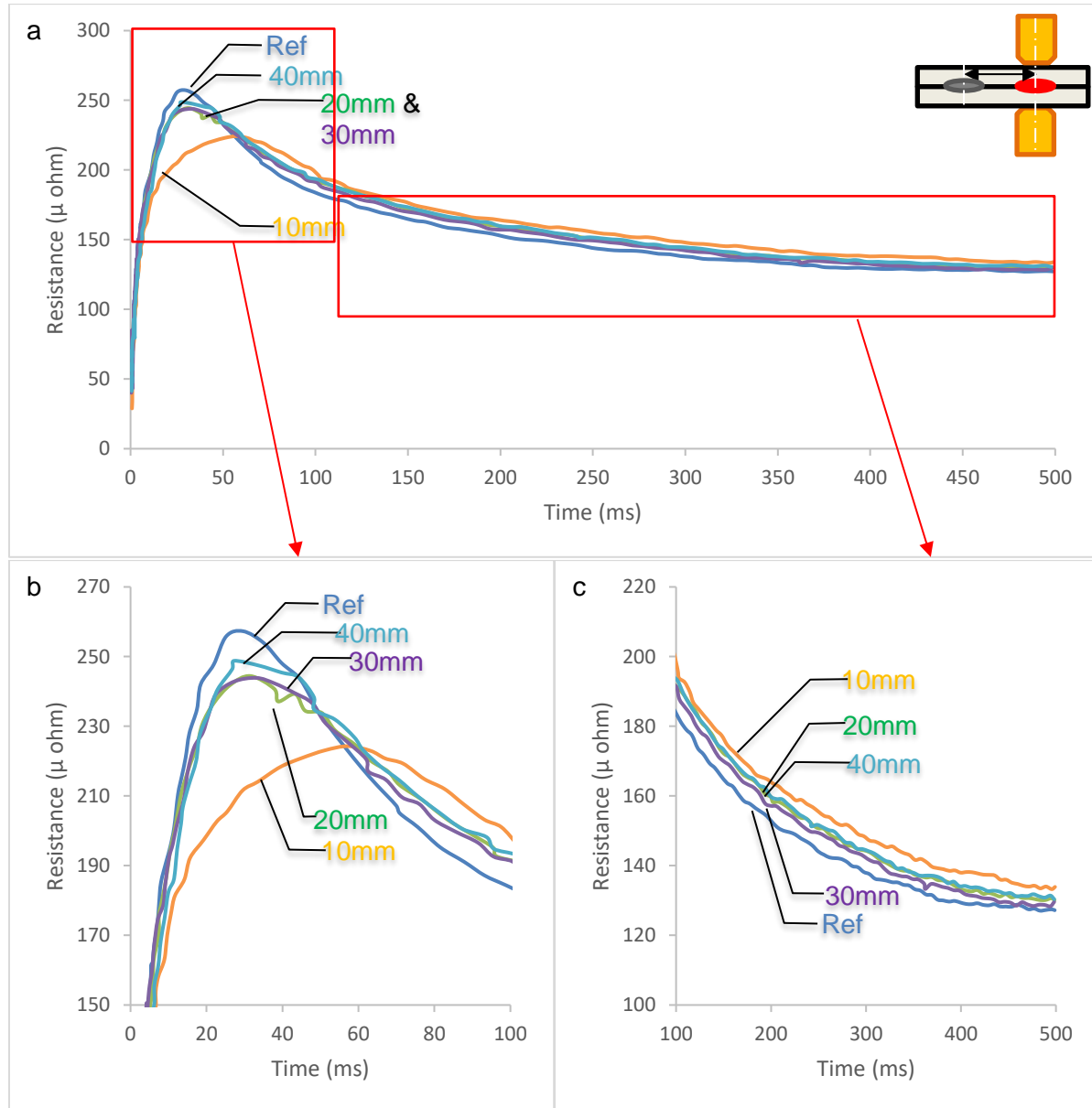
Figure 4.2. a) Overall Effect of Shunting Distance on Average Dynamic Resistance Curves b) Maximum Resistance Peaks c) Tails of Resistance Curves

36
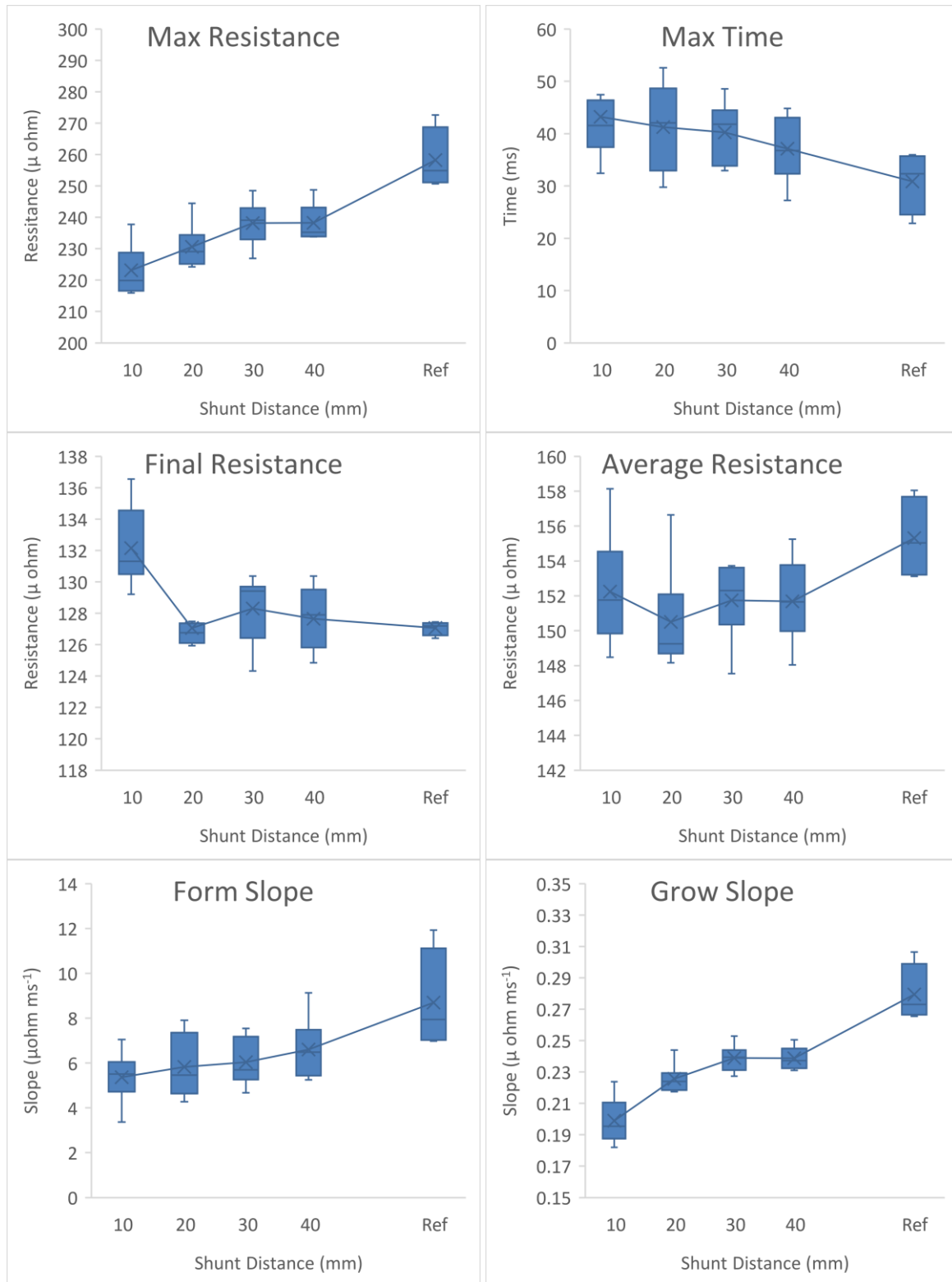
Figure 4.3. Breakdown of 6 Variable of a Dynamic Resistance Curve in Shunted Welds

By comparing the box-whisker plots of all six variables, the trends in Figure 4.3 revealed that shunted welds exhibit a lower maximum and average resistance, which leads to lower heat input (based on Joule heating laws), and a reduced time for nugget growth. The general patterns suggested that as the shunting distance is increased, the maximum resistance increased, and the time to reach max resistance was reduced while the average and final resistances did not appear to be affected. As observed in the curves, the final resistance of the 10mm shunted weld was much higher than all the other welds due to the greater loss of current to the shunt. The relation is less visible in the slope plots, but the general trend remains that with an increase in the shunting distance, the maximum resistance, grow slope, and formation slope increases.

To determine the significance of the results, a hypothesis test comparison between the means of the reference curve and the shunted welds using the t-distribution was conducted, in which:

$$t_{probe} = \frac{\bar{x} - \bar{\mu}}{S_p \sqrt{1/n_1 + 1/n_2}} \text{ , where } S_p = \frac{(n_1-1)S_1{}^2 + (n_2-1)S_2{}^2}{n_1 + n_2 - 2}$$

where $\bar{x}$ and $\bar{\mu}$ are the difference in the means of the desired parameter and the reference, S_P the pooled standard deviation and n is the number of data points. Bonferroni correction for multiple t-tests was taken into consideration and a significant alpha value of 0.01 was used. The calculated t_{probe} values can be found in Table 4.1 and the values found to be greater than the critical t value ($t_{\alpha/2=0.005,16} = 2.921$) were highlighted to identify the most sensitive parameters for monitoring the shunt distance.

Table 4.1. Calculated Mean Parameter tprobe Values for Shunted Welds

Shunt distance t_{probe} values						
Shunt Distance (mm)	Max Resist	Max Time	Final Resist	Form Slope	Grow Slope	Avg Resist
10mm	-7.450	2.338	5.505	-3.517	-49.918	-1.683
20mm	-6.522	2.225	-0.00255	-2.751	-65.799	-2.884
30mm	-4.532	2.644	1.577	-2.846	-69.127	-2.619
40mm	-5.149	1.659	0.156	-2.033	-54.442	-2.503

In comparing t_{probe} values, the most significant variable based on the dynamic resistance curve was the maximum resistance and growth slope, followed by the formation slope, and final resistance. This implies that analyzing only one of the variables may not provide a reliable method for detecting

shunting. The combination of the maximum resistance value and the maximum resistance time represented by the growth slope have the greatest detectability based on a statistically significant difference from the reference curves.

To verify the correlation between weld nugget formation, dynamic resistance curves and the six parameters, the nugget diameter of five randomly selected welds were measured per parameter (Table 4.2). All the shunted welds below 30 mm measured to be smaller than the reference weld by approximately 0.2mm and displayed slight increase in size with an increase of the shunting distance corresponding to Chang's [109] and Wang's [110] findings. Based on a one-tail t-test comparing the reference weld size to each parameter, the nugget sizes were found to be statistically smaller using an overall confidence interval of 95% ($t_{critical\ \alpha=0.01,13} = 2.650$). The increase in nugget diameter correlated to the longer growth time (earlier max resistance times) and growth slopes. The 20mm and 30mm weld diameters were similar in size which reflects the similarity in the observed dynamic resistances as well as the 6 curve variables.

Table 4.2. Measured Nugget Sizes of Shunted Spot Welds

Shunt Distance (mm)	Ref	10	20	30	40
Average Nugget Diameter (mm)	5.37	5.12	5.13	5.13	5.18
t_{probe} value			5.24	4.08	3.87	3.83

4.2 Effect of Edge Proximity

The weld coupons were initially joined at the center of the sample 20mm away from the edge, while subsequent welds were made closer to the edge. There were no observable differences when welding at edge distances from 20mm to 10mm. At a distance of 5mm small infrequent occurrences of expulsion were visible but no large drops in resistance occurred which could indicate it was due to surface expulsion. At a distance of 3mm, the welding procedure produced consistent expulsion. When welding close to or past half of the electrode face (distances less than 3mm) no expulsions were produced however this led to substantial changes in the dynamic resistance curve (Figure 4.4).
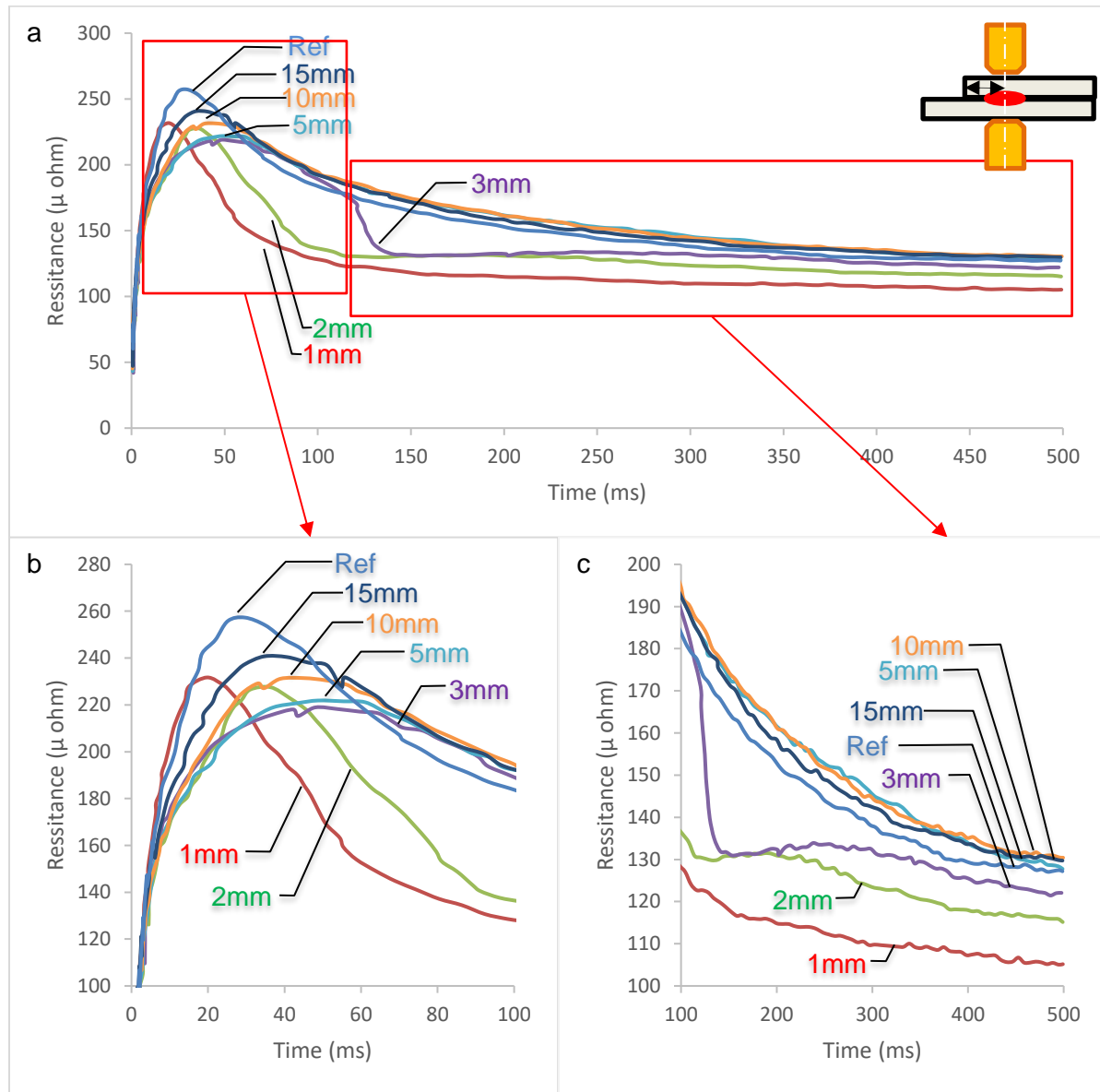
Figure 4.4. a) Overall Effect of Edge Proximity Distance on Average Dynamic Resistance Curves b) Maximum Resistance Peaks c) Tails of Resistance Curves

In comparison to the shunted weld dynamic curves, there is much more variance in the dynamic resistance curves of edge welds. In Figure 4.4b, the curves from 0 to 100 ms gradually moved to the right as the edge proximity distance decreased from 15 to 3mm, and the slopes after the peaks dramatically change at distances of 1 and 2mm. Portrayed in Figure 4.4c, the final resistances of edge welds of 1, 2, and 3 mm remained distinct while the 5, 10, 15, and 20 mm edge welds were indiscernible from one another.
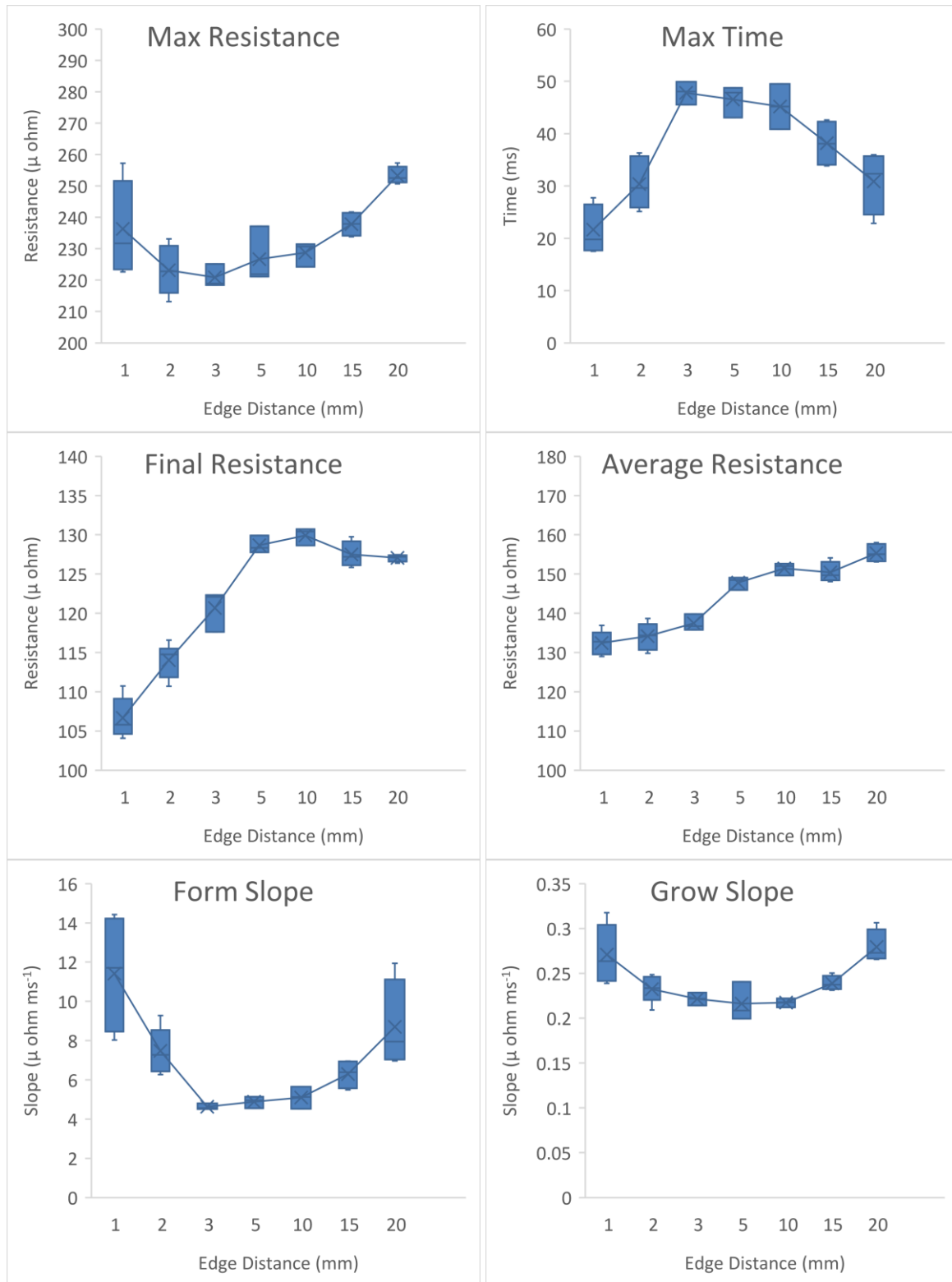
Figure 4.5. Breakdown of 6 Variables of a Dynamic Resistance Curve in Edge Welds

The slight drop in the resistances as the weld approached the edge was also observed in Wen, et al., study with stainless steel, and was explained by cooling rate decreasing as the edge distance decreased resulting in an increase in heating rate [14]. In contrast to the aforementioned study, when the edge distance was at the critical point multiple expulsions were observed whereas in this study, no expulsion was witnessed.

Edge proximity was analyzed in the same fashion as shunting by comparing boxplots of the 6 variables as shown in Figure 4.5. As the edge proximity distance increased, the maximum resistance, final resistance, and average resistance followed a rising trend. The time at maximum resistance generally decreased once past the expulsion region. The formation slope and the growth slope also increased with the edge proximity distance past the expulsion region. To determine the significance between correlating each feature of the dynamic resistance curve with edge proximity, similar values of t_{probe} were calculated for the edge weld variables, tabulated in Table 4.3. Values found to be greater than the critical t value ($t_{\alpha/2=0.005,13} = 3.012$) are highlighted to identify the most significantly different from the reference.

Table 4.3. Calculated Mean Parameter tprobe Values for Edge Welds

Edge proximity t_{probe} values						
Edge Distance (mm)	Max Resist	Max Time	Final Resist	Form Slope	Grow Slope	Avg Resist
1	-2.371	-2.654	-21.588	1.503	-28.798	-12.035
2	-6.962	-0.144	-11.734	-1.135	-47.505	-10.611
3	-10.665	5.864	-6.649	-4.238	-55.809	-10.706
5	-4.688	4.905	2.176	-3.913	-31.346	-5.117
10	-7.958	3.819	3.823	-3.524	-7.419	-2.720
15	-5.308	1.896	0.687	-2.237	-4.337	-2.518

When comparing the t_{probe} of the variables of the edge welds, the growth slope had the greatest significance, which was also observed in the shunted welds, followed by the maximum resistance. It was also noted that the average resistance was significant for all edge distances up to an edge proximity distance of 10 mm. Based on these findings, edge welds could be detected by using the average resistance from 1mm to 10mm away from the edge. Otherwise, the growth slope can be used to detect the presence of edge welding at all distances.

By investigating the weld nugget diameters of the edge welds (Table 4.4) the welds at 3mm or less do not meet the minimum size requirement per AWS D8.1M [6]. The welds at 1 and 2mm were smaller and warped as half or more of the weld was not contained by surrounding base metal (see Figure A.3). All welds below an edge distance of 5mm were found to be statistically smaller using the same t-test conducted for the shunted weld sizes ($t_{critical\ \alpha=0.01,13}$ = 2.650). The welds conducted at 5mm and 10mm were measured on average smaller than the welds at 15 and 20mm due to the lower maximum and average resistance.

Table 4.4. Measured Nugget Sizes of Edge Proximity Spot Welds

Edge Proximity Distance (mm)	1	2	3	5	10	15	20
Average Nugget Diameter (mm)	4.02	3.39	4.36	5.09	5.09	5.27	5.37
t_{probe} value	10.0	20.3	15.5	2.59	4.67	1.18	

4.3 Effect of Shims

With the use of shims, the shim distance was limited to the applied force and relation to the strength of the material. When the top workpiece can no longer contact the bottom workpiece under the applied load of the electrode, no weld will form, and a controller fault for open circuit will appear. Observation of the welding process showed no difference with the use of shims as expulsion did not occur. When comparing the dynamic resistance curve, the beta peak for both the curves are visibly lower than the reference with a higher final resistance.

Study conducted by Shen, Zhang, and Lai, performed with DP steels, discovered that the presence of an initial gap prevented uniform pressure distribution as shown in Figure 4.6 [111]. The increase in the gap distance decreased the contact area along the electrode face while increasing the contact pressure. This results in a net resistance drop as the increase in localized pressure is magnitudes larger than the decrease in contact area for the current to travel.
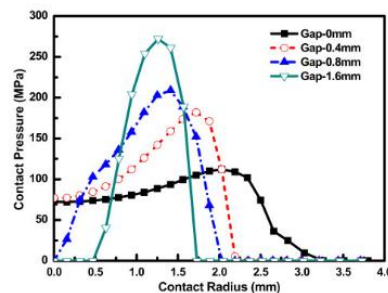
Figure 4.6. Effect of Initial Gaps on the Pressure Distribution on the Workpiece [111]
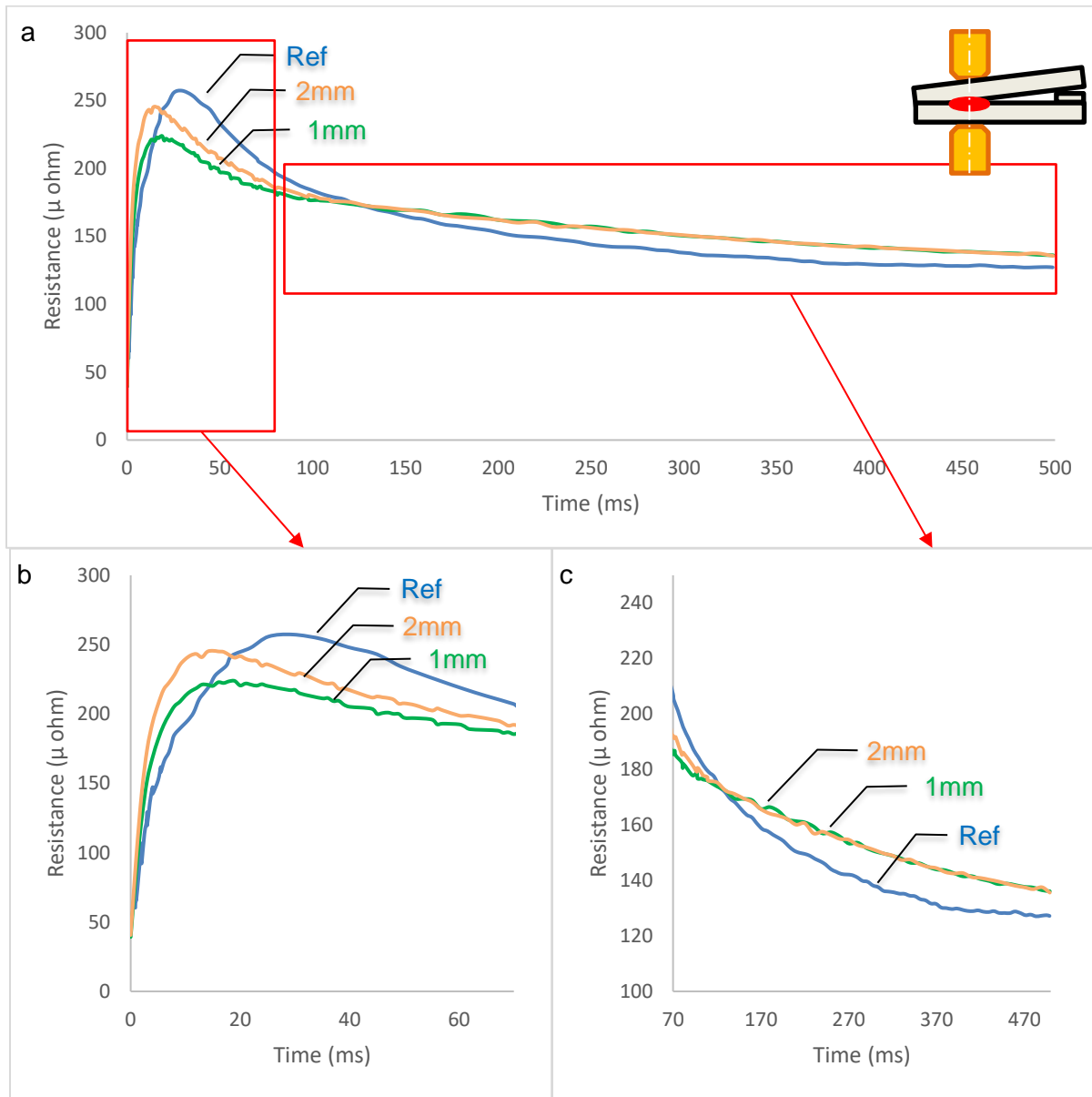
Figure 4.7. a) Overall Effect of Shims on Average Dynamic Resistance Curves b) Maximum Resistance Peaks c) Tails of Resistance Curves

As shown in Figure 4.7b, the beta peak is actually higher with a 2mm effective gap compared to the 1mm but exhibits the same curve. The observed findings with the shims correlate to the findings of Shen et al., as the change in contact area would result in less energy required for the formation of the nugget, resulting in an earlier beta peak.
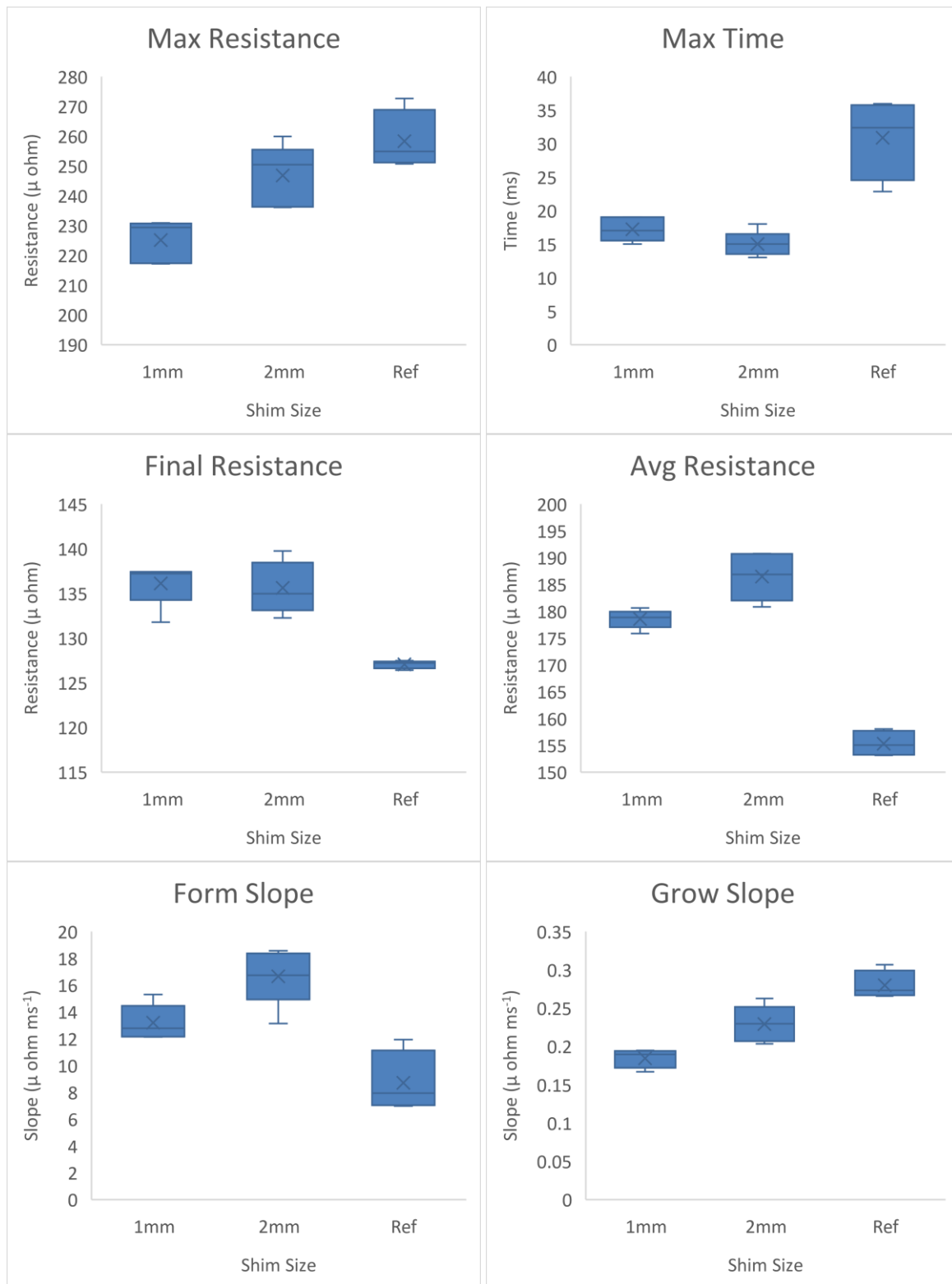
Figure 4.8. Breakdown of 6 Variables of a Dynamic Resistance Curve in Shimmed Welds

45

When analyzing the 6 variables for the introduction of shims, it is evident that they greatly affect the dynamic resistance curve. Interpreting the box-whisker plots in Figure 4.8, the beta peak drops and shifts to an earlier time. The final and average resistance seems to have no strong correlation between the effective gap distances but show a noticeable difference compared to the reference. Similarly, the relational formation slope and growth slope are not greatly different from each other but are different from the reference.

To determine the significance between correlating each feature of the dynamic resistance curve with effective shim gap, t_{probe} values were calculated for the shim weld variables, tabulated in Table 4.5. Values found to be greater than the critical t value ($t_{critical\ \alpha=0.01,9} = 3.25$) are highlighted to identify the most significantly different from the reference. In this case, all variables except the maximum resistance of the 2mm gap were found to be significantly different. This is positive in detecting bent parts or interfering components preventing proper contact between the worksheet.

Table 4.5. Calculated Mean Parameter t_{probe} Values for Shunted Welds

Shim t_{probe} values						
Effective Gap (mm)	Max Resist	Max Time	Final Resist	Form Slope	Grow Slope	Avg Resist
1mm	-7.040	-5.151	6.918	3.836	-9.577	17.189
2mm	-1.533	-5.944	5.510	5.406	-3.421	12.251

The weld nuggets for the shimmed welds are displayed in Table 4.6. The nugget diameter exhibited a decrease in size with the increase in the effective shim distance. Both shimmed welds were found to be statistically smaller using the same t-test ($t_{critical\ \alpha=0.01,13} = 2.650$). In contrast to the previous conditions, the 2mm gap displayed a higher resistance beta peak with a smaller weld nugget. This is due to the higher gap reducing the effective contact area between the workpieces.

Table 4.6. Measured Nugget Sizes of Edge Proximity Spot Welds

Shim Size (mm)	Ref	1	2
Average Nugget Diameter (mm)	5.367	5.122	4.682
t_{probe} value		3.61	6.19

4.4 Summary

The investigation of process changes on the profile of the dynamic resistance curve was reported throughout this chapter. The focus of the process changes was on poor placement of the weld or workpiece, simulated with shunts and edge welding, and workpiece error, simulated with shims. Visual inspection of the dynamic resistance curve may be able to pick up the effect of shunting at 10mm, edge proximity below 3mm, and the presence of a shim or bend. Using the analysis of the 6 variables the dynamic resistance curve was broken down into, the growth slope was found to be the most significant difference for all cases (compared to a reference curve of good welds). It was observed that there existed a critical edge proximity distance of approximately half of the electrode face where expulsion occurs. Below the critical edge distance, a new dynamic resistance curve shape exists. For all scenarios. The weld nuggets correlated with the behavior of the dynamic resistance curve.

Chapter 5

Analysis of Adaptive Welding Capabilities of Bosch Rexroth Controller

The spot weld controller in question for this study was the Bosch Rexroth PSI63C0.120L1. The controller promotes the ability to analyze the dynamic resistance curves based on a set reference dynamic resistance curve (composed of an average of "good" welds). The findings of the previous chapter determined that changes to the process are reflected as a change to the dynamic resistance curve. The solution proposed by Bosch Rexroth was to adapt the welding process in-situ to manipulate the dynamic resistance curve to be similar to the reference. In doing so, they output various quality parameters which they claim to indicate the quality of the weld. The following results throughout this chapter investigate the effectiveness of the adaptive control of the controller and the quality indicators.

5.1 Controller Variables

The controller is capable of outputting various signals of the welding process, the most relevant variables are outlined in Table 5.1. The two main quality variables the controller outputs are labelled uipActualValue and stabilisationFactorActual.

Table 5.1. Summary of Controller Variables

Variable	Description
iActual1, 2, 3	Average current of pre-pulse (1), main weld (2), and tempering (3)
voltageActualValue	Average of voltage throughout weld schedule
currentActualValue	Average of current throughout weld schedule
weldTimeActualValue	Full duration of weld schedule
energyActualValue	Calculation of energy of weld: Power*time
powerActualValue	Calculation of power of weld: $I*V$, $R*I^2$, V^2/R
resistanceActualValue	Average of resistance throughout weld schedule
pulseWidthActualValue	Controller width of the pulse signal
stabilisationFactorActual	Controller defined quality variable
uipActualValue	Controller defined quality variable
uirExpulsionTime	Time which expulsion occurs, 0 if no expulsion

The recommended Bosch Rexroth procedure to monitor the quality of the welding process was to perform multiple verified welds to determine the limits of the UIP values and set alarms for when the controller outputs UIP values outside of the limits. To best understand the capability of this procedure, process conditions performed in chapter 4 known to change the dynamic resistance and affect nugget diameter are applied.

5.2 Effect of Process Condition on Adaptive Welding

For the study conducted in this chapter, the welding was performed with the automated robotic welder equipped with the servo-gun described in Chapter 3, incorporating an initial high pre-pulse to remove the coating layer as requested by the industry partner, schedule shown in Figure 5.1. The study of the effect of pre-pulse on the coating was performed previously by Hou and verified with the pre-pulse current setting of 12kA and 30ms which was outside of the matrix originally presented [112]. Based on the generalized dynamic resistance curve for AHSS evaluated by Ighodaro, the main welding curve would lose the small drop in resistance post-beta peak where the coating breaks down (see Figure 2.13 for reference) [57].
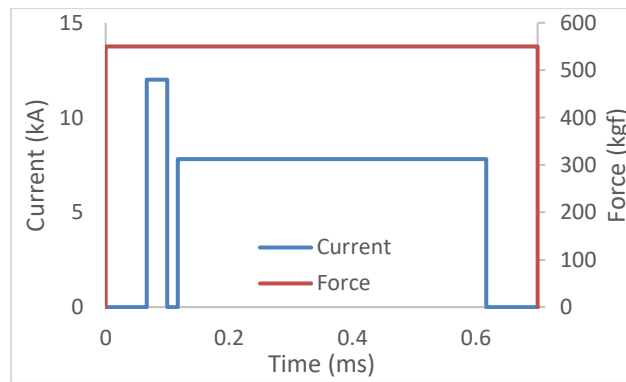
Figure 5.1. Weld Schedule Performed for Study in Chapter 5

5.2.1 Shunting

Only the 10mm and 20mm shunting distances were examined for this analysis as there was a notable change in the curve from the 20mm shunted distance, to the 10mm shunted distance. As seen in Figure 5.2b, the shunted welds displayed similar behavior of a later beta peak. The 10mm displayed the characteristic lower beta peak resistance and higher final resistance as in the previous chapter. The introduction of the pre-pulse did not change the overall effect of the process condition on the resistance

curves but did change the severity as the 20mm and 10mm welds did not decrease as much as it did in Chapter 4. This is due to the presence of heat induced by the pre-pulse changing the heating rates of the material and reducing sensitivity in the main welding pulse.
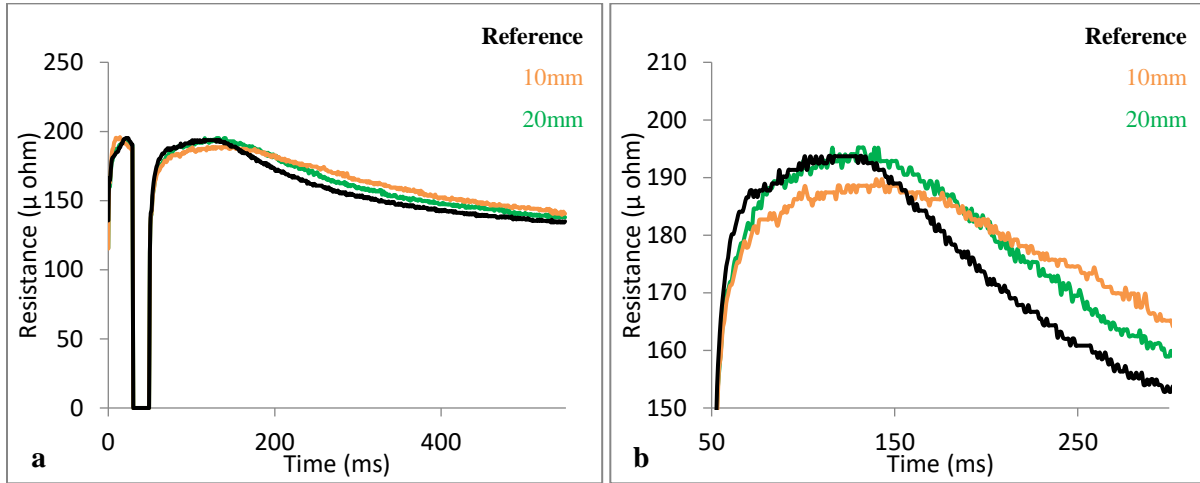
Figure 5.2. Full Schedule (a) and Main Weld (b) Dynamic Resistance Curve of Shunted Welds
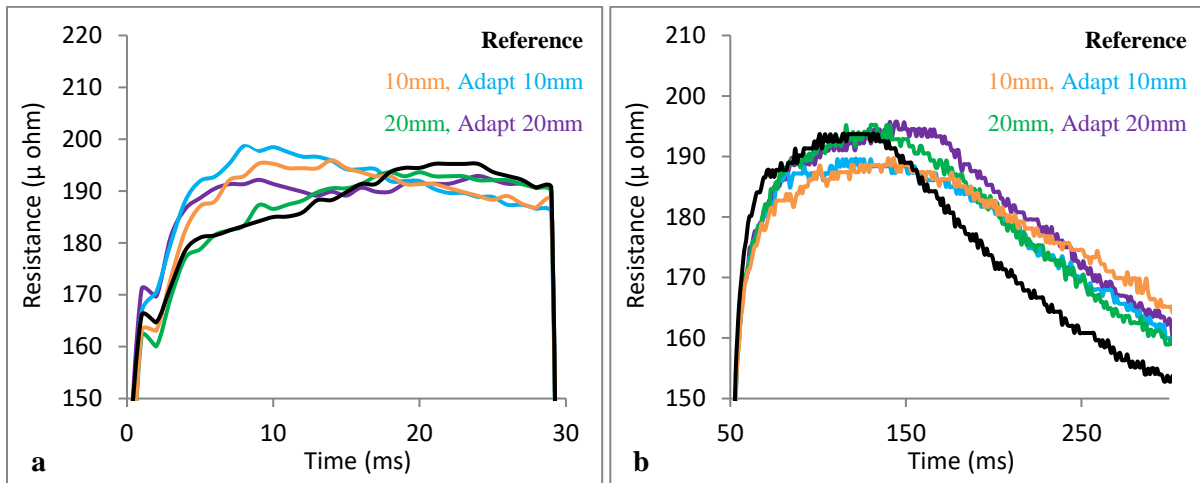
Figure 5.3. Pre-Pulse (a) and Main Weld (b) Dynamic Resistance Curves of Shunted Welds with Adaptive and Constant Current Controls

As noted in Figure 5.3, the dynamic resistance curves of the adaptive and the constant current curves differ slightly due to the control mechanism of the controller. The two most notable cases were in the pre-pulse of the 20mm and main weld of the 10mm. For the pre-pulse of the 20mm weld (Figure 5.3a), the curve starts to increase until 10ms where it drops to fit with the reference curve. In the main current (Figure 5.3b), the adaptive 10mm is much lower than the constant current weld which is

attributed to the weld controller supplying more current to decrease the resistance to better match the reference. In both cases the controller's capabilities do not apply the full 10% current control set for the weld to fit with the set reference curve. This indicates that the function of the controller is not to match the same curve but to meet a set value.

Table 5.2. Controller Values for Shunted Welds with and Without Adaptive Control

Condition	Current (kA)	Resistance (µohm)	Energy (J)	UIP
Reference	7.63	160	5345	-
Shunt 10mm	7.63	166	5538	107
Shunt 20mm	7.63	162	5450	104
Adapt Shunt 10mm	7.84	161	5854	116
Adapt Shunt 20mm	7.77	163	5614	115

Comparing the average values for the shunted welds in Table 5.2, welds with constant current control outputted a higher resistance. The adaptive welds were performed with a higher average current (maximum reaching 8.22kA, ~5% increase). The application of the higher current was able to lower the overall resistance during the weld to resemble the average reference resistance. Performing a means comparison between the UIP values with adaptive welding active versus without, the two UIP values were found to be significantly different. This meant that the UIP values are significantly higher than without the adaptive and possibly more likely to be detected. To determine if the weld controller was limited by the 10% current control setting, the I% was increased to 50% (max) in increments of 10% for a 10mm shunted weld. As shown in Figure 5.4, the current never exceeded 10% and no single variable was found to be significantly different from the initial 10% current control setting.
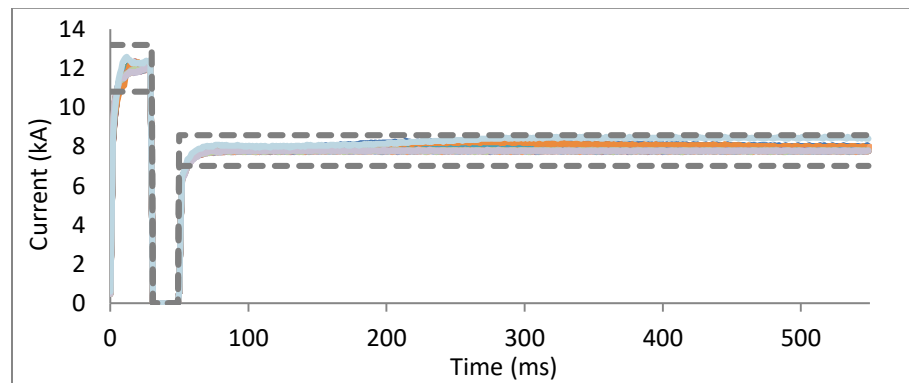
Figure 5.4. Dynamic Current Curves of All Welds Performed with 10 to 50% Current Control

The next setting to investigate on the adaptive welding feature was the time extension of the weld. The feature aimed to correct any welds that experience any source of heat loss (resistance drop)

and require an extension of time to accommodate. In the shunted welds made with a time extension of 50% (Figure 5.5), expulsion occurred when it should not have, and time extension was activated to continue to weld past the set time. The current was not observed to be any different than the other recorded welds and thus was considered an outlier.
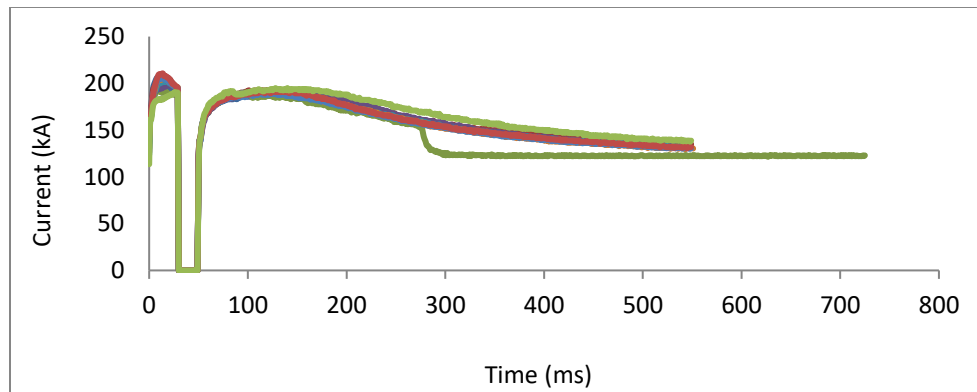
Figure 5.5. Dynamic Current Curve of Shunted Welds with Time Extension Active
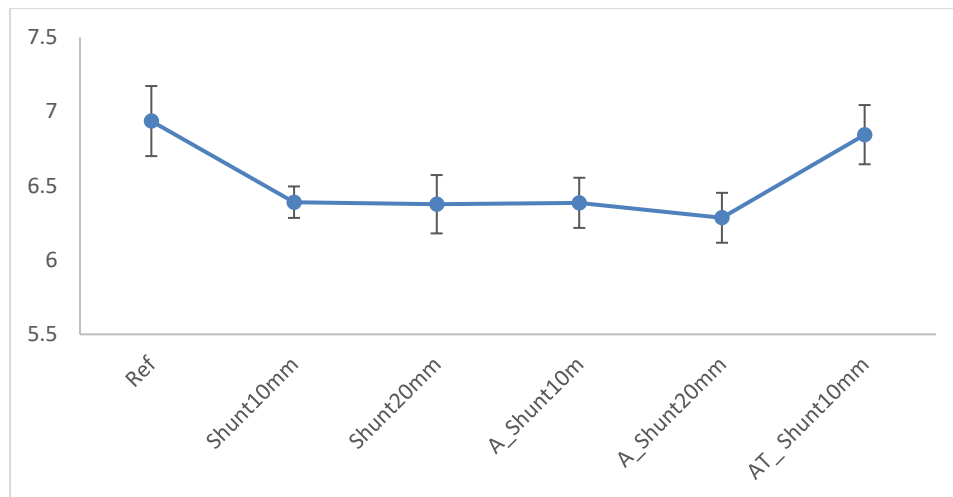
Figure 5.6. Measured Weld Nugget Diameter of Shunted Welds

Figure 5.6 indicates that regardless of whether the adaptive welding was active (A) or not, the shunted welds resulted in a smaller nugget size in comparison to the reference (ideal) welds. Only with time extension active (T) did the nugget diameter no longer significantly differ from the reference. It can be concluded that activating the time extension with welds at risk of shunting may be beneficial.

5.2.2 Edge Proximity

In this study the edge proximity distances were 15 and 10mm as at 10mm and smaller distances, expulsion occurred during adaptive welding until reaching the critical point of half the electrode face.
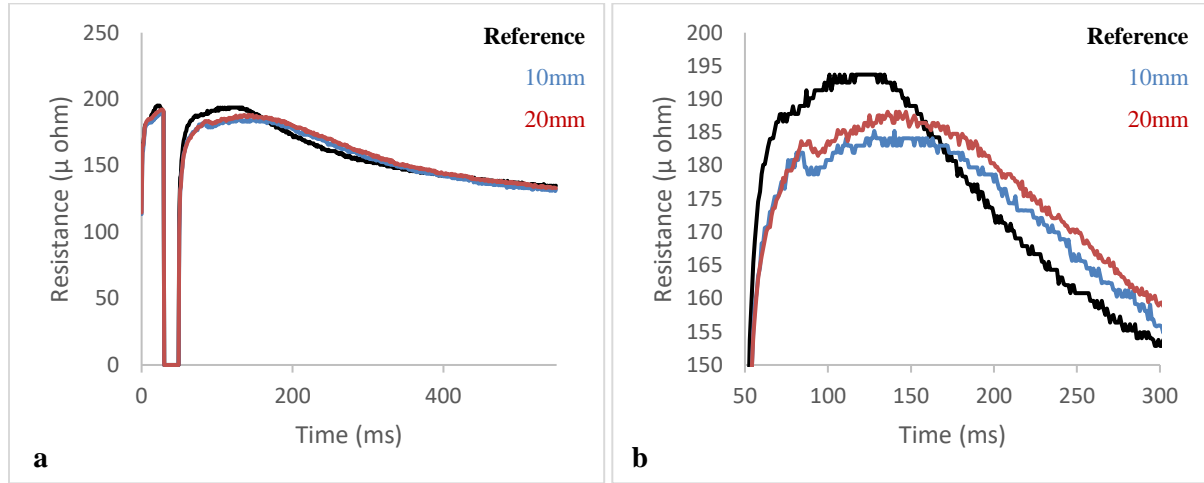
Figure 5.7. Full Schedule (a) and Main Weld (b) Dynamic Resistance Curve of Edge Welds with Pre-Pulse

The curves in Figure 5.7 follow the same pattern found in Chapter 4, where the beta peak resistance decreased and occurred later with a higher final resistance. A local peak and valley occur at 100ms in Figure 5.7b, which coincides with either a surface film breakdown or a coating melting. This is an interesting phenomenon as the pre-pulse was proven to be effective at removing the coating layer material from the interface surfaces and reduces roughness. This indicates that as the weld approaches the edge a residual roughness is more likely.
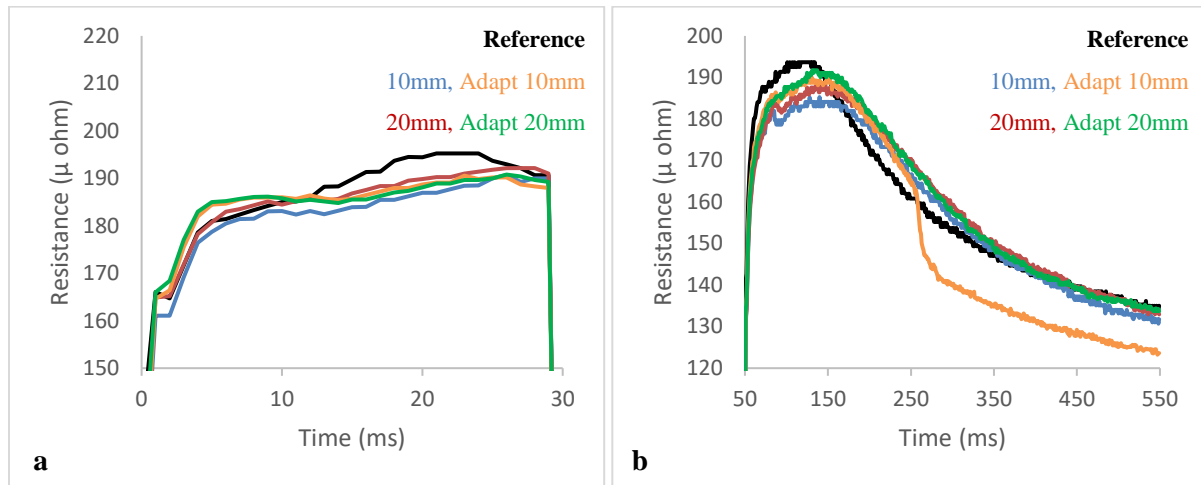
Figure 5.8. Pre-Pulse (a) and Main Weld (b) Dynamic Resistance Curves of Edge Welds with Adaptive and Constant Current Controls

With the implementation of the adaptive control, the localized peak and valley suspected to be residual roughness is removed with the adaptive functionality in Figure 5.8b. At an edge distance of 10mm, the risk of expulsion has increased, when it did not occur at constant current. This is likely due to the fluctuating current the controller is applying to the weld causing instability, and with a reduced distance of travel expulsion was more likely to occur. Comparing the UIP values found in Table 5.3, the application of adaptive welding seems to lower the values in contrast to shunting, where the values increased.

Table 5.3. Controller Values for Edge Welds with and Without Adaptive Control

Condition	Current (kA)	Resistance (μ ohm)	Energy (J)	UIP
Reference	7.63	160	5345	-
Edge 10mm	7.63	153	5048	107
Edge 15mm	7.63	155	5113	115
Adapt Edge 10mm	7.73	148	5014	100
Adapt Edge 15mm	7.71	156	5250	113
Over Edge 3mm	10.74	84	6028	30
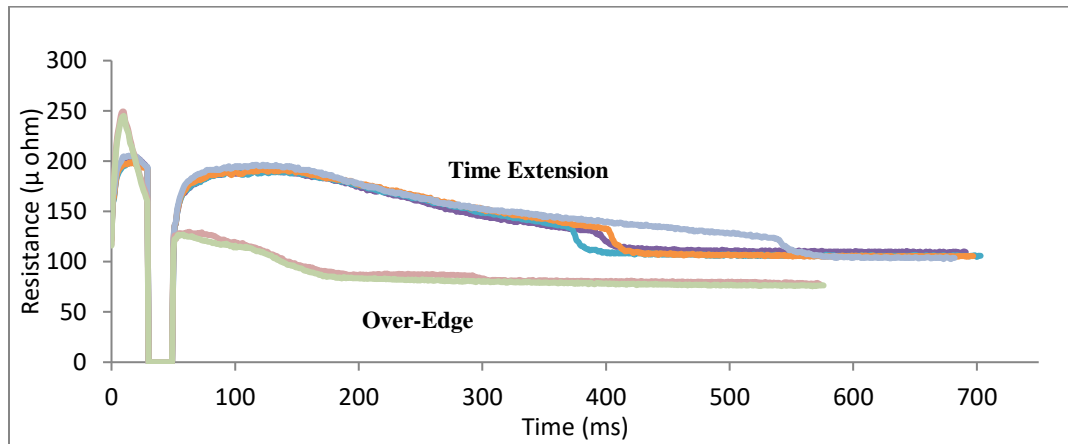
Figure 5.9. Dynamic Resistance Curves of Edge Welding with Adaptive Time Extension and Over-Edge Welding

When time extension setting was activated for 10mm edge welds, the expulsion time moved from 250 to 400ms shown in Figure 5.9 which may be accounted for by the controller reducing the severity of the current control as it now has the option to extend the time. Regardless, expulsion still occurred and the time for the weld was extended in efforts to increase the nugget growth stage. When observing the resistance curve of the over-edge welding condition in Figure 5.9, the curve is visually different from the others. When comparing the UIP values in Table 5.3, the controller output an average of 30, a substantial change in comparison to UIP values near 100, and extreme cases may be detected with UIP.
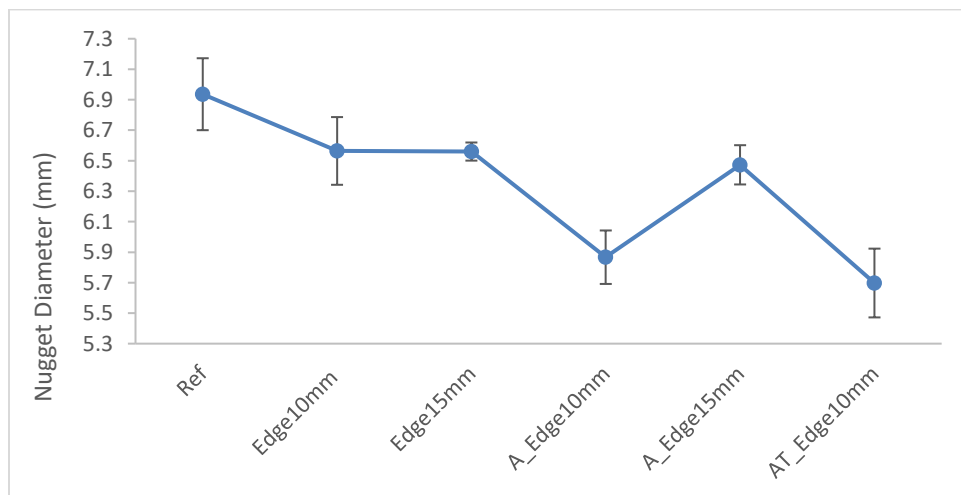
Figure 5.10. Measured Weld Nugget Diameter of Edge Welds

55

Figure 5.10 displays a general loss of nugget size with edge welding as found in the previous chapter. The introduction of adaptive welding worsened the nugget size as it caused expulsion, leading to a loss of material inside the weld. The application of time extension did not make a significant difference to the nugget size of a weld with expulsion as the 10mm edge weld with adaptive compared to the adaptive and time extension weld have weld nugget diameters of 5.87mm and 5.70mm respectively.

5.2.3 Influence of Sheet Separation using Shims

In this study, the same effective separation distance was used as the previous study in section 4.3 to compare the effect of adaptive welding. Welding with a gap on the robot produced the greatest difference in results in comparison to welds with pedestal welds. Welds performed with the pedestal welds produced dynamic resistance curves with lower and early beta peaks, while curves in Figure 5.11 have beta peaks that are higher and later. The main reason for this difference was accredited with the difference in the rigidity of the system which was the main cause of increased variance in spot welding [113]. During the application of the force, rigidity plays an influential role as deflections in the system may cause indirect reductions of force or change in electrode contact angles. The rigidity did not play a large role in prior studies with the robot as all of the workpieces were placed flat against each other but with a singular shim on one side of the workpiece, the impact would have been significant.
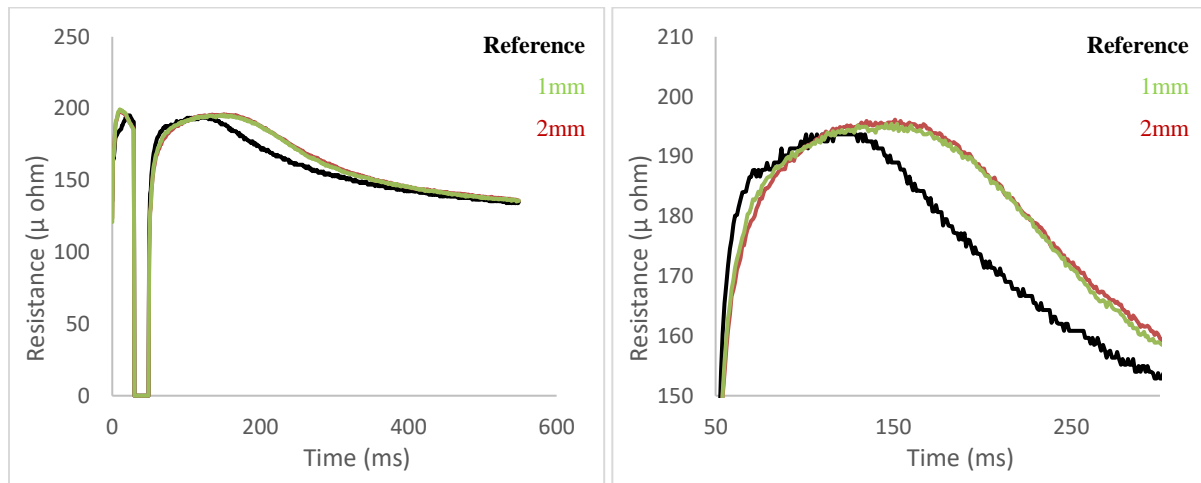
Figure 5.11. Dynamic Resistance Curve of Shim Welds with Pre-Pulse

56

The increase and delay of the beta peak in Figure 5.11 was due to the lack of contact caused by the deflection in the welding gun. This led to a reduction of force leading to higher surface roughness and an increased current path which consequentially delayed heat generation at the nugget.
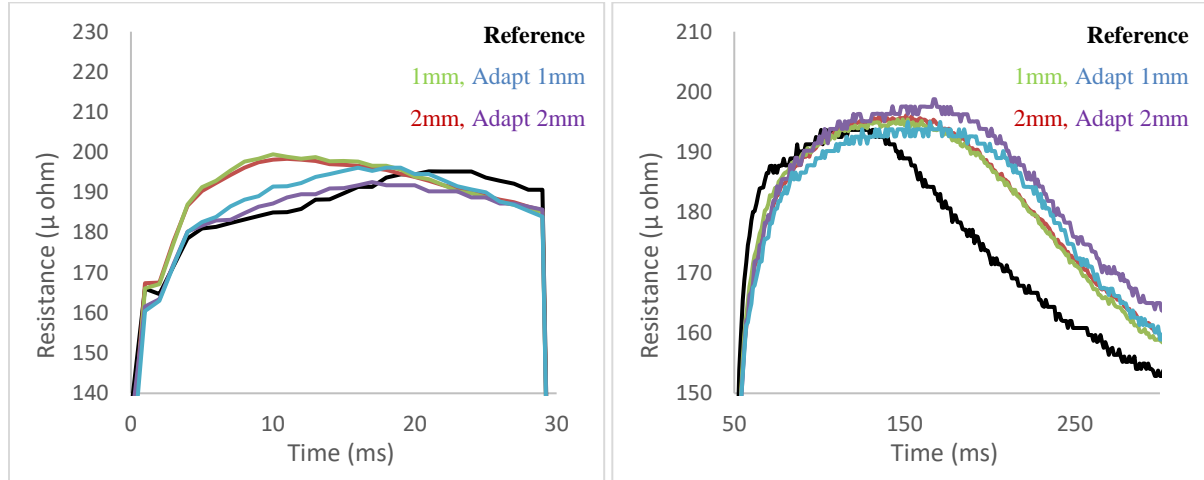
Figure 5.12. Pre-Pulse (Left) and Main Weld (Right) Dynamic Resistance Curves of Shim Welds with Adaptive and Constant Current Controls

In the pre-pulse section of the curves in Figure 5.12, the resistance changes from a high to low with constant current while with the adaptive welding the resistance follows the same behavior of low to high as the reference. In the main weld, there was no notable overall differences in the curves even with the time extension. The UIP values for the 1mm and 2mm were 111 and 119, while with the adaptive it was reported values of 107 and 120, respectively.
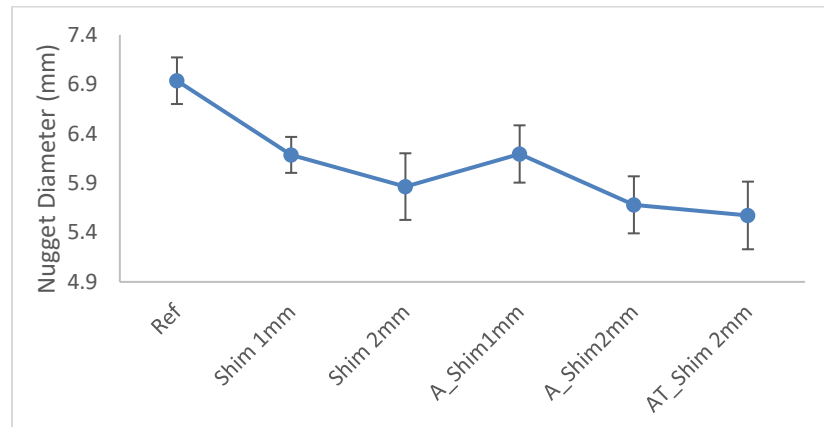
Figure 5.13. Measured Weld Nugget Diameter of Shim Welds

When comparing the nugget diameters as a function of the shimmed gap distance in Figure 5.13, there is a reduction of nugget diameter due to the introduced gap but no significant trend apart

57

from the initial observation. The increase in the distance between the constant current welds increased the variance in the nugget size but with adaptive the deviations were similar.

5.3 UIP

With the discovery that UIP does not directly reflect any minor changes in the process and could not differentiate any of the process changes aside from extreme cases such as over-edge welding, the origin of the UIP value comes into question. The origin of the quality indicator UIP and any correlation to the physical weld are explored. In the following section, the variables the controller most likely considers when outputting the UIP values are investigated.

5.3.1 Source of UIP

Figure 5.14 to Figure 5.16 compare the statistical analysis between the deviation of the variable from the reference curve against the average value. The summation of the deviation of the curve from the reference curve was calculated using a MATLAB code found in Appendix B. The data was set to best fit a singular variable model. All variables were found to be statistically significant at a P-value of less than 0.01. It is evident that the variation in the UIP values are explained better by the deviation from the reference current than the static average values. Thus, it was concluded that the basis of this adaptive controller is based on Kamat and Lagoo's theory of comparing dynamic resistances [91].
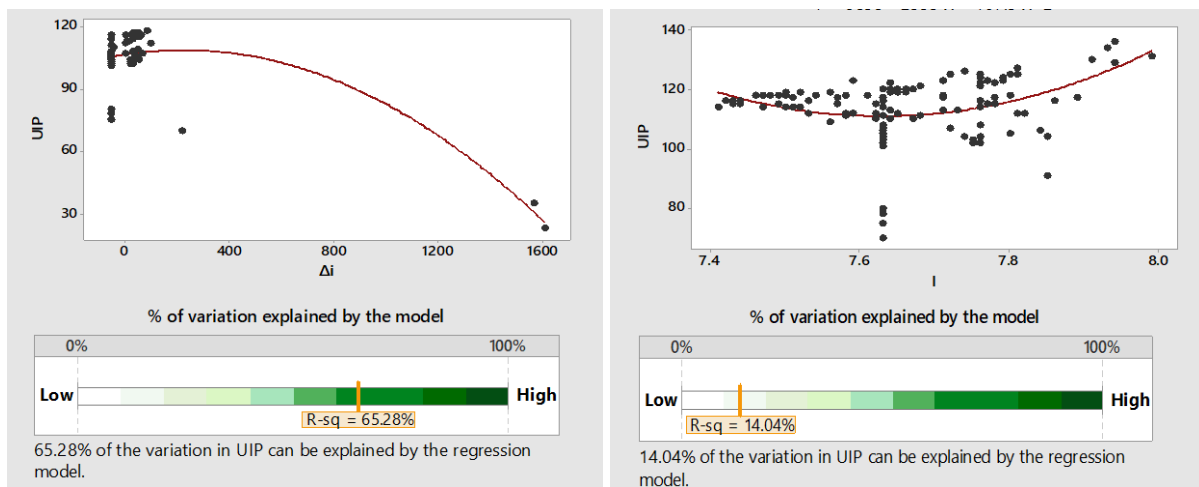
Figure 5.14. Statistical Analysis of UIP as a Function of Deviation of Current from Reference Curve (Left) and Average Current (Right)

58

In all of the deviation from reference plots exists data points that are not close to the majority groupings. These points were the result of over the edge welding where a portion of the electrode face was not in contact with the material to provide the worst-case scenario. While these data points may influence/skew the data, it is more important to determine if the quality variable does not change its calculations based on a "good" or "bad" weld situation. It was noted for later analysis that the poor welding condition of over-edge welding lay far outside of the main grouping the controller could weld.
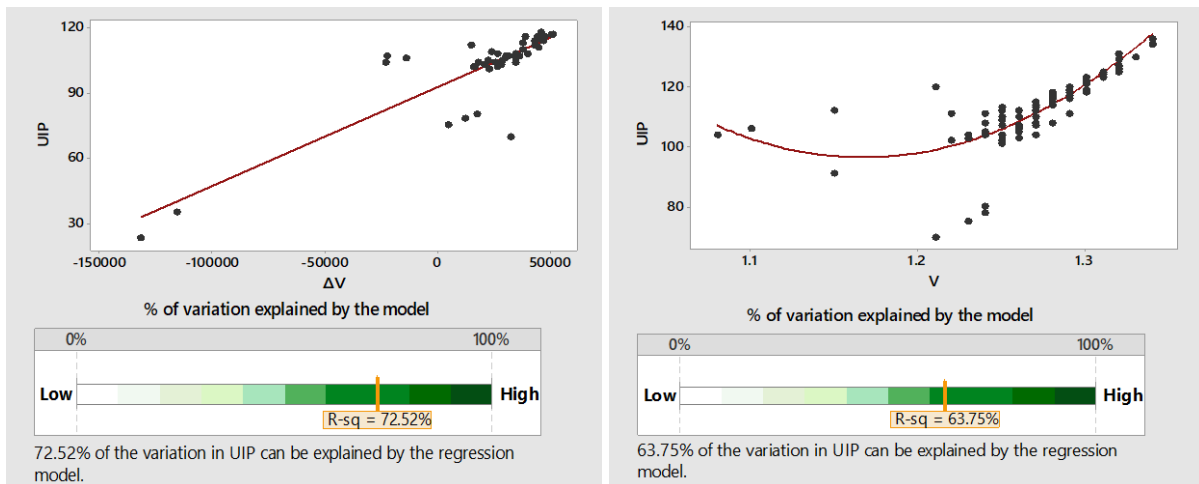
Figure 5.15. Statistical Analysis of Deviation of UIP as a Function of Voltage from Reference Curve (Left) and Average Voltage (Right)
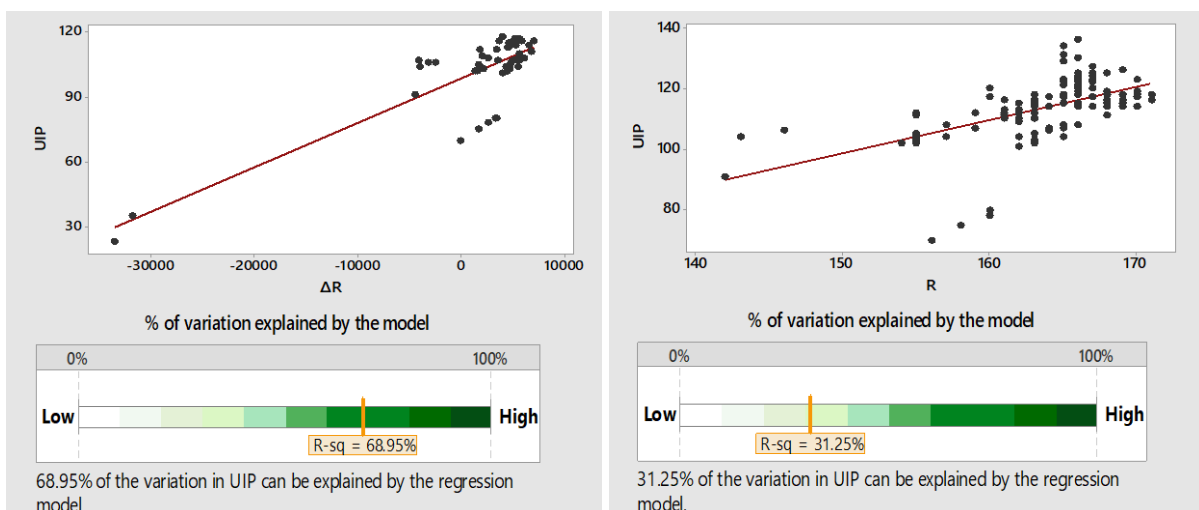
Figure 5.16. Statistical Analysis of UIP as a Function of Deviation of Resistance from Reference Curve (Left) and Average Voltage (Right)

A regression analysis was performed using the delta variables available from the output of the controller and resulted in the following model:

$$UIP = -4117 + 5.62\ \Delta I + 0.000407\ \Delta V + 0.00364\ \Delta R - 0.0513\ \Delta F + 4044\ UA$$
$$+ 0.000002\ \Delta I{*}\Delta R - 5.62\ \Delta I{*}UA - 0.005260\ \Delta R{*}UA + 0.0525\ \Delta F{*}UA$$

(Eq. 8)

where the constant *UA* is a Boolean variable to indicate if the weld was performed with adaptive control (1) or with constant current (0). The model calculated a 95.79% R-sq (adj) fit to the experimental data. Similar to the output of a neural network method, the constants could not be compared to any familiar constant values related to RSW. From the regression model, it is evident that there are the two-level interactions which change the UIP value significantly depending on if adaptive welding was active or not which reflects the results in section 5.2. The full regression analysis is included in Appendix B.

5.3.2 UIP vs Quality
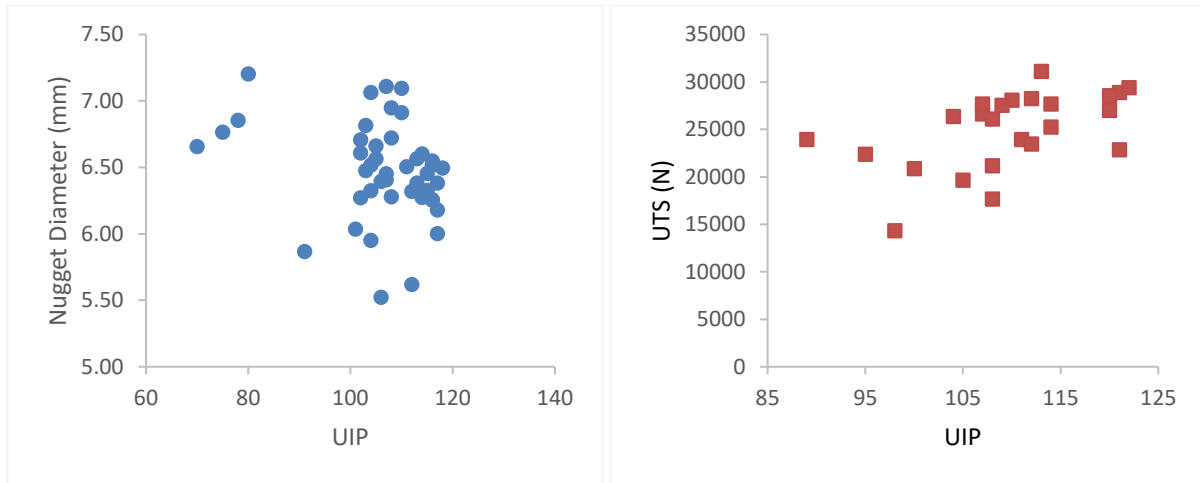
Figure 5.17. Nugget Diameter (Left) and Ultimate Tensile Strength (Right) as a Function of UIP

It is collective understanding that the strength of the weld and the nugget diameter possess a direct relationship. But with USIBOR® being an AHSS, the nugget diameter and the UTS do not have a clear relationship and thus cannot assume if the nugget reaches a specific size, it will perform well. Thus, both quality indicators were compared separately. Visually comparing the UIP value to the nugget diameter or the ultimate tensile strength (UTS) in Figure 5.17 show no clear trend. Upon running the variables in Minitab, the UIP variable was found to have a significant ($P<0.05$) relationship to both the nugget diameter and UTS but have a R-sq of 13.49% and 27.70% (respectively). This indicates that

60

the UIP variable alone cannot provide information on the quality of the weld. While UIP demonstrates a significant relationship to the destructive-tested weld nuggets, other variables may need to be incorporated to provide a more robust model. The full analysis performed with Minitab can be found in Appendix B.

5.4 Stability Factor

While not explicitly mentioned as a quality indicator, the function of the stabilization factor is a variable the controller calculates to provide feedback for the process. As the name suggests, this number fluctuates but did not appear to have a no direct correlation to the UIP (refer to Figure B.12 in Appendix B). Thus, the origin of the quality indicator stabilisationFactorActual was investigated.

5.4.1 Source of Stability Factor

In contrast to the UIP quality indicator, the Stabilization Factor in the controller outputs are not uniquely dependent on either the deviation from the reference curve or the average value the controller outputs. Comparing the R-sq values in Figure 5.18 to Figure 5.20, the average values provide a slightly higher R-sq value with the greatest difference in fit in Figure 5.18 comparing 98.18% to 98.84%. As seen in UIP as well as for stability, the introduction of the over-edge welding introduced points that lie far outside of the main grouping. For the same reason as UIP, they were kept to determine the source of the stabilization factor.
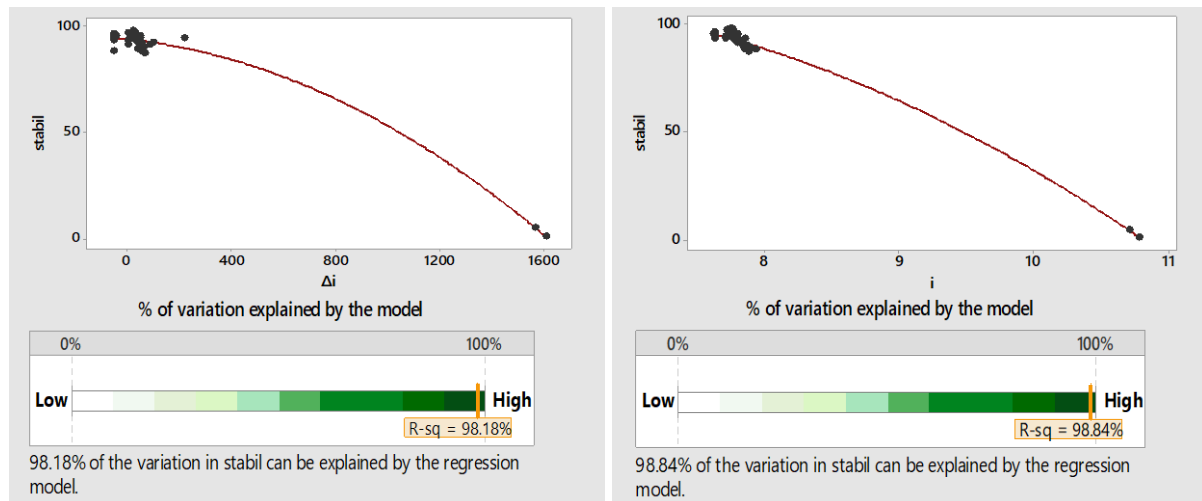
Figure 5.18. Statistical Analysis of Stabilization Factor as a Function of Deviation of Current from Reference Curve (Left) and Average Current (Right)

61
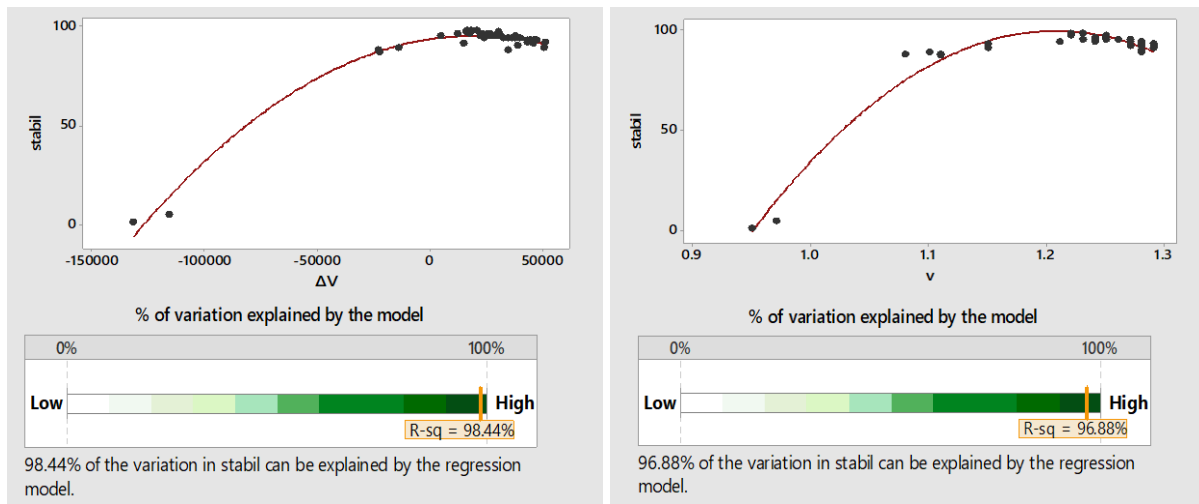
Figure 5.19. Statistical Analysis of Stabilization Factor as a Function of Deviation of Voltage from Reference Curve (Left) and Average Voltage (Right)
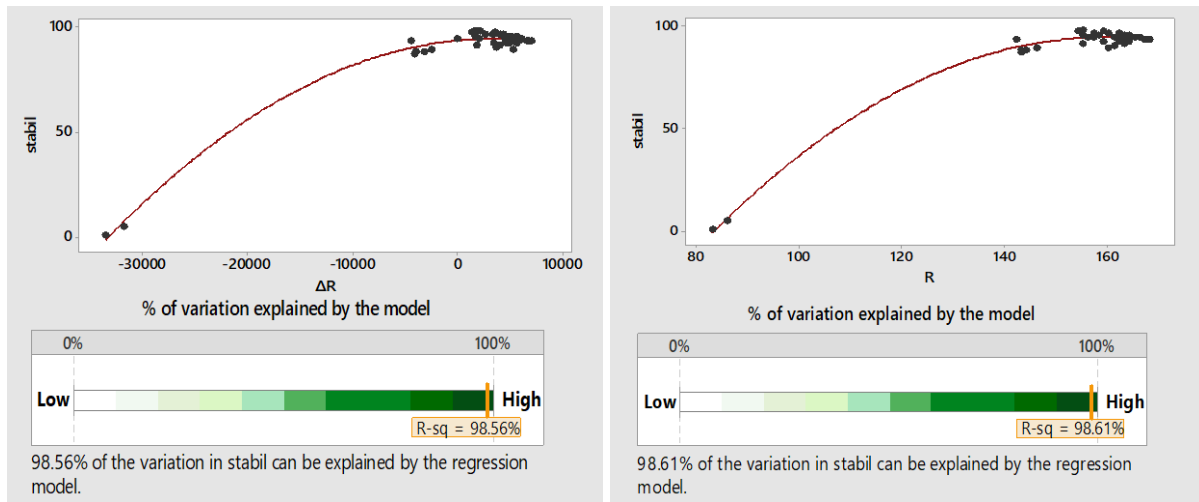
Figure 5.20. Statistical Analysis of Stabilization Factor as a Function of Deviation of Resistance from Reference Curve (Left) and Average Resistance (Right)

Based on the slightly higher fit using the average values, the calculated Energy and Power from the average values of the weld were incorporated into the analysis in Figure 5.21. Stabilization factor as a function of either energy or power is relatively low in comparison to the R-sq values found for current, voltage, or resistance, but cannot be ignored as they possess R-sq values of greater than 75%.
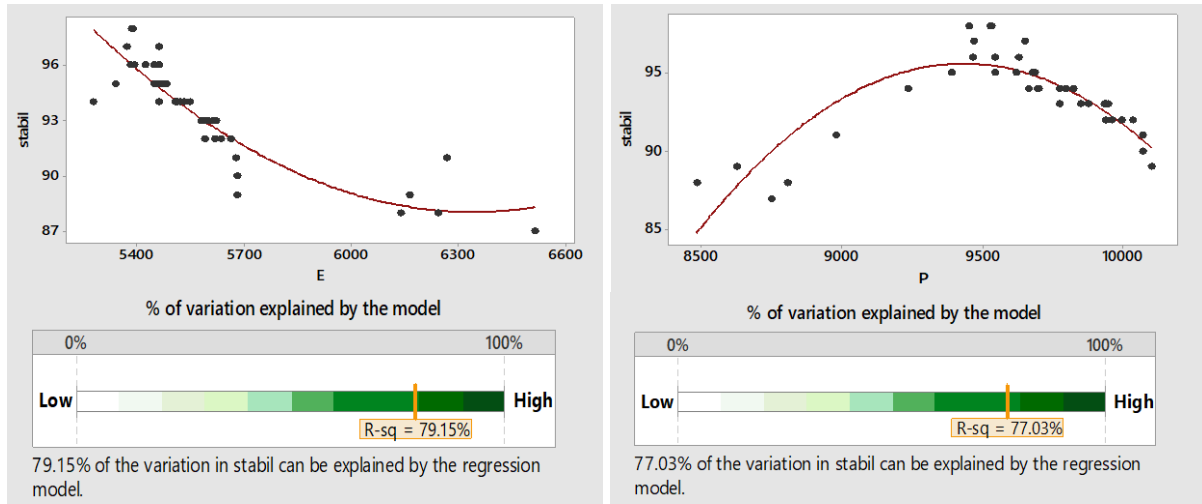
Figure 5.21. Statistical Analysis of Stabilization Factor as a Function of Energy (Left) and Power (Right)

Energy and power are functions of the voltage, resistance, current, and time which act as well-known interaction terms and contribute to explaining the variance in the stabilization factor. When performing the regression model, a variety of variables were used to model the data and the best combination was found to incorporate energy (E), power (P), current (I), voltage (V), and resistance (R) as follows:

$$\text{Stabilization Factor} = -3448 - 0.00549\ E - 0.0792\ P + 569.8\ I + 1188\ V + 4.220\ R$$
$$- 25.24\ I^2 - 0.000465\ P*R$$

(Eq. 9)

The model for stabilization factor, shown as (Eq. 9), resulted in a R-sq (adj) value of 99.78%, which is a suitable fit of experimental data to the modelled data. This fit helps explain that the stabilization factor is not based on any instantaneous values but dependent on the calculated values the controller outputs.

5.4.2 Stabilization Factor vs Quality

Based on the fact stabilization factor utilizes the average values, there is no expected direct correlation to quality indicators of nugget diameter or UTS. Visual inspection of Figure 5.22 shows a potential positive relationship of stabilization to nugget diameter and negative relation to the UTS. Using Minitab, it was found the stabilization factor has a significant relation ($P < 0.05$) to both nugget diameter and UTS with R-sq values of 46.55% and 35.01% (respectively). The R-sq values are much

higher than those calculated for the UIP values which may indicate that the use of the average values to determine the quality of the weld may not be easily dismissed.
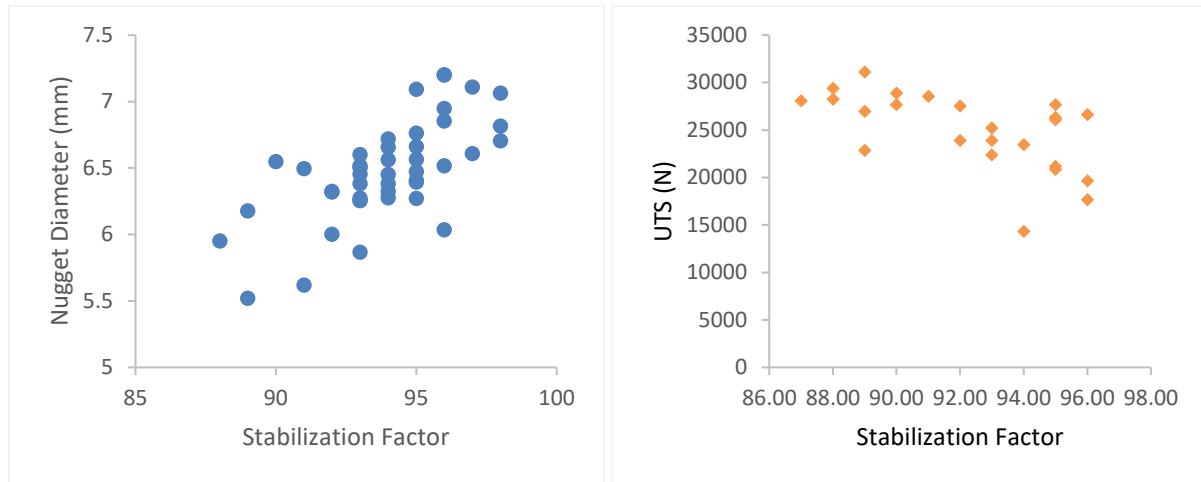
Figure 5.22. Nugget Diameter (Left) and Ultimate Tensile Strength (Right) as a Function of Stabilization Factor

5.5 Summary

With the introduction of adaptive current welding to the process conditions investigated in Chapter 4, there was a clear observation that the adaptive welding current did not operate by matching the weld to the reference dynamic resistance curve. The controller was free to vary the current by 50% and in all cases except the over-edge welding, and it did not exceed 10% of the control. Thus, only at extreme changes in the profile of the welding curve did the welder apply the full control of the welding procedure, and the associated UIP values were far below the others. When not welding extreme welding conditions, the application of adaptive welding was beneficial in some conditions and produced adverse effects to the nugget size. The related UIP values which were supposed to indicate quality abnormalities did not vary with the process condition, nor with incremental severity of the condition.

When investigating the UIP value, it was found that the deviation of the current, voltage, resistance, and force curves from the preset reference curve played the largest role in determining the UIP factor. Each variable possessed R-sq values of above 95%, and with the addition of the Boolean variable indicating the adaptive welding was active or not, could create a model that fit with a R-sq (adj) of a 95.79%. UIP was found to have no direct correlation to the nugget diameter or the tensile strength of a weld but was found to be significant ($P<0.05$) when comparing the data. The same procedure was performed for the stabilization factor and it was found that the average values the controller output would best explain this variable. With the average current, voltage, resistance, and the resulting energy and power, a model with a R-sq (adj) of 99.78% could be made. This variable was also not found to have any direct correlation to the nugget diameter or tensile strength but was also found to be significant ($P<0.05$).

Chapter 6

Identification of Potential Variables to Correlate the Nugget Size of USIBOR®

In the previous study, the most significant variables for UIP and Stabilization Factor were identified. It was concluded that there was a lack of evidence the variable UIP or Stabilization Factor could accurately be correlated to the quality of the weld, or even a change in the process. A further investigation into identifying significant variables in the models was conducted and reported in this chapter.

6.1 Nugget Diameter

The nugget diameter is a widely accepted criterion in the industry in determining if the weld is acceptable or not. While USIBOR® does not follow the common relation between larger nuggets providing higher strength, a loss of nugget size will negatively influence the strength of the weld. Thus, a model to identify if a nugget is undersized using the available information from the controller would be beneficial in reducing physical and destructive quality testing. Upon imputing all of the values into a regression analysis with the average values that the controller can output, the following ANOVA variables were determined (see Table 6.1).

Table 6.1. Summary of ANOVA values for Regression of Controller Variables

Source	DF	Adj SS	Adj MS	F-Value	P-Value
Regression	9	2.84580	0.31620	3.86	0.000
wear	1	0.01338	0.01338	0.16	0.687
voltageActualValue	1	0.79862	0.79862	9.74	0.002
currentActualValue	1	0.62087	0.62087	7.57	0.007
energyActualValue	1	0.11833	0.11833	1.44	0.233
powerActualValue	1	0.69972	0.69972	8.53	0.004
resistanceActualValue	1	0.36746	0.36746	4.48	0.037
stabilisationFactorActValue	1	0.63215	0.63215	7.71	0.007
uipActualValue	1	0.16682	0.16682	2.03	0.157
uipExpulsion	1	0.02490	0.02490	0.30	0.583
Error	85	6.97176	0.08202		
Total	94	9.81756			

The high *P-Value* variables indicate a low to insignificant variable in creating a robust model. Variables with values higher than an error level of 0.1 in Table 6.1 were the wear, energy, UIP and expulsion. The wear and energy term can be removed as the wear value provides information about the electrode condition and not about the individual weld, while the power value provides the same information as energy if time is held relatively constant. The UIP term remains included, as it provides indication of any large intermediate changes to the dynamic resistance curve which was proven to change significantly in Chapter 4. Expulsion possesses a relatively high *P-Value* as it is a Boolean which directly correlates poorly but may provide more information with interactions with other non-Boolean variables. When this model was derived based only on the average variables and no interactions, it possessed a R-sq (adj) value of 21.47%, further analysis can be seen in Appendix C. Once interactions were considered, various methods of removing the unnecessary terms were used to determine the best fitting model. The best result possible with the gathered data was a model with a R-sq (adj) of 40.29%. Table 6.2 contains all of the terms used in the model with corresponding *P-Values*. The full ANOVA analysis can be found in Appendix C.

Table 6.2. Segment of ANOVA Table for Full Model Displaying P-Values Used Variables

Term	P-Value
Constant	0.843
V	0.014
I	0.042
P	0.004
R	0.014
Stabil	0.095
UIP	0.374
Expl	0.044
$Stabil^2$	0.068
UIP^2	0.183
V*UIP	0.021
V*Expl	0.037
I*UIP	0.024
I*Expl	0.072
P*Expl	0.056
R*Stabil	0.019
Stabil*UIP	0.050
$V*UIP^2$	0.017
$I*UIP^2$	0.019
$Stabil^2*UIP$	0.057

Using the variables found to be important in Table 6.2, the model for nugget diameter labelled (Eq. 10) was made.

Nugget Diameter (mm) = -179 - 1654 V + 415 I + 0.02306 P + 1.443 R

- 26.2 Stabil + 15.6 UIP - 1320 Expl + 0.1532 Stabil^2 - 0.1198 UIP^2 + 26.V*UIP

+ 1195 V*Expl - 7.97 I*UIP + 139.0 I*Expl - 0.1288 P*Expl - 0.01531 R*Stabil   (Eq. 10)

+ 0.244 Stabil*UIP- 0.1188 V*UIP^2 + 0.0356 I*UIP^2 - 0.001300 UIP*Stabil^2

where *Expl* is the Boolean variable indicating if expulsion occurred, and *Stabil* is the stabilization factor previously modelled in Section 5.4. The coefficients did not match any known constants related to the resistance spot welding process and thus were qualitatively analyzed. Among the single order variables, the detection of expulsion (*Expl*) has the greatest negative impact on the nugget diameter. The second most influential parameter was the current, as it provided the most positive influence on the nugget diameter. Both of these variables aligned with known relations to the nugget diameter and thus was found reasonable. Of the second order variables, the controller quality indicators: stabilization factor (*Stabil*) and *UIP* were found to be the most frequently reoccurring and influential. The large role the two quality variables showed that there may be some quality detection capability with the variables, just not a direct relation.
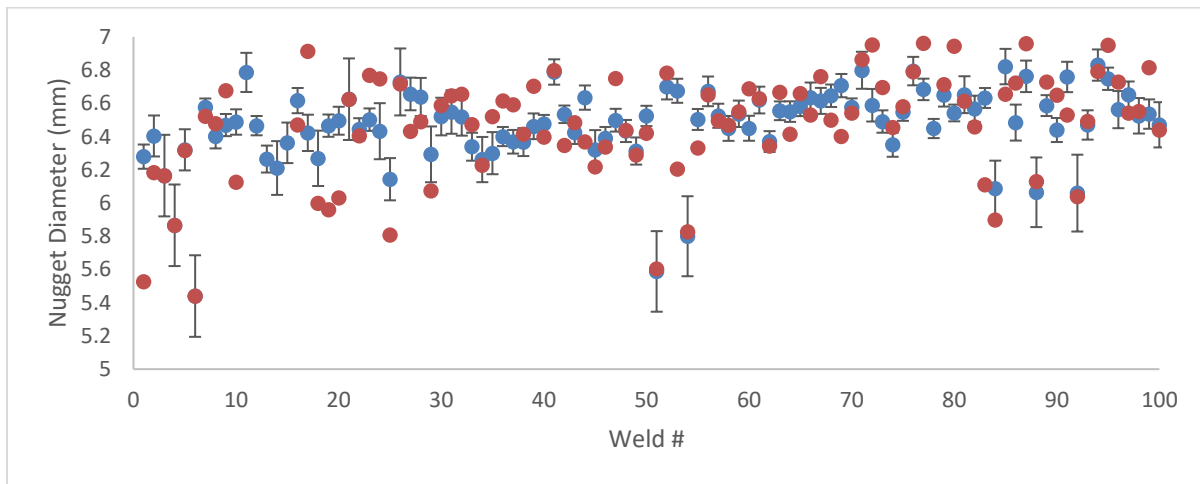
Figure 6.1. Predicted Nugget Diameter with Prediction Limits (Blue) Layered with Experimental (Red) of All Data Points

The data used to predict the model was used to determine the fit in Figure 6.1. Of the 100 data points used, 63 of the nugget diameters lie outside of the predicted limits, which links back to the R-sq

(adj) value of 40.29% output by the ANOVA analysis. The predicted data was plotted against the experimental data in Figure 6.2 to determine if the model was over- or underestimating the nugget size. It was concluded that the model could capture the general trend of the nugget diameter based on the weld controller outputs, when it did incorrectly predict, it tends to be overestimating the nugget size.
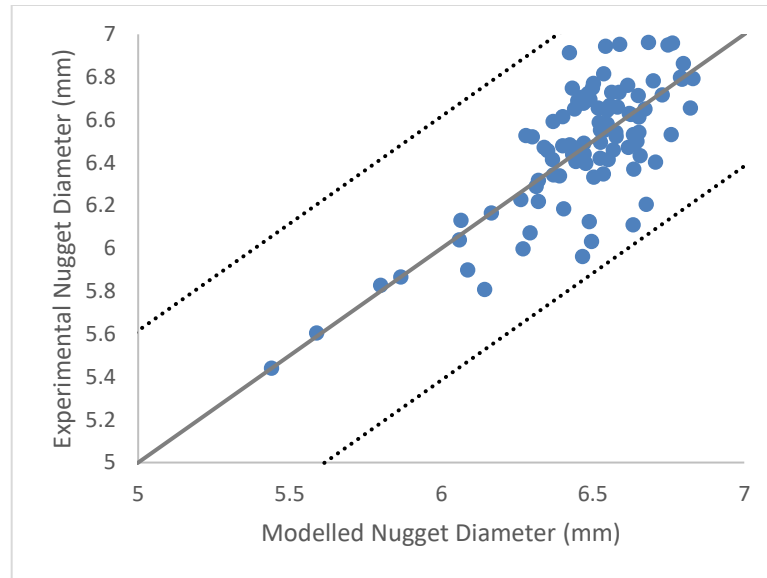
Figure 6.2. Plot of Experimental vs Modelled Nugget Diameter

6.1.1 Model Validation

A validation set of welds were made with a new reference curve for the adaptive feature to test the robustness of the model. The results based on the validation welds input into the model are shown in Figure 6.3 and Figure 6.4.
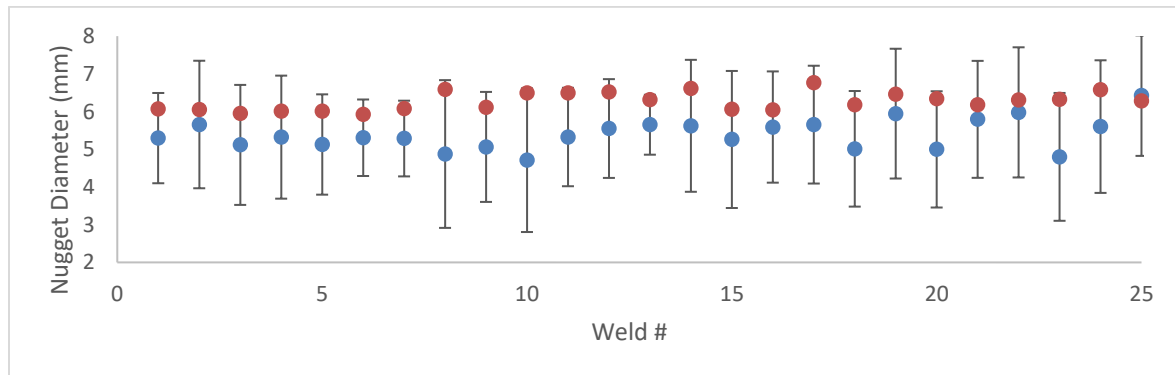
Figure 6.3. Predicted Nugget Diameter with Prediction Limits (Blue) Layered with Experimental (Red) of Validation Points
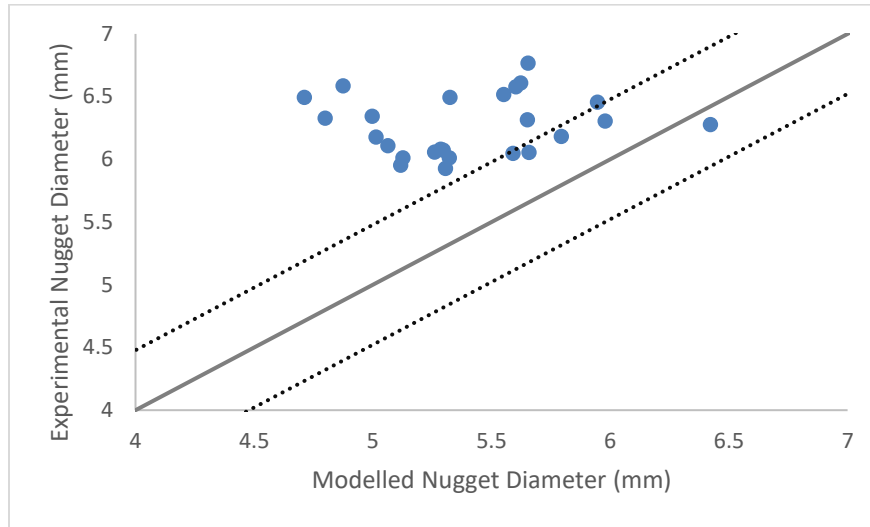
Figure 6.4. Plot of Experimental vs modelled Nugget Diameter Using New Reference Curve

Based on Figure 6.3, it would appear that the model is able to capture the experimental data within the prediction limits (to an error level of 0.1), but based on the variability of the new set of data, the error limits of each point ranges from 0.79 to 1.96 mm. To put the scale of the error bars into perspective, the data from Figure 6.1 displayed error bars ranging from 0.05 to 0.25 mm where nearly 37% of the data fit into the model. If the same error bars were used for this data set, 1 of the 25 data points would not fit, resulting in a 4% fit. When plotting the modelled nugget diameter to the experimental nugget in Figure 6.4, the lack of fit of the data is more evident. The model under-predicts the size of the nuggets as nuggets measured close to 6.5mm are predicted as close to 4.5 mm. This result demonstrates that the model using one reference curve is not robust enough to fit data of another reference curve and a more robust model is needed.

6.1.2 Creating a Robust Model

Combining the validation data points with the previous data set, a new model can be derived as (Eq. 11) to provide a stronger expression to capture and detect the fluctuation of the nugget diameter. The resulting model fit increased from a R-sq (adj) value of 40.29% to 45.71% indicating that this method should be chosen over creating separate models per each unique dynamic resistance curve. The model is shown in the following equation on the next page:

Nugget Diameter (mm) = -2232 + 388 I - 1402 Expl - 0.000071 P^2

   - 0.0863 R^2 + 0.384 V*P + 15.19 V*R - 3.623 V*Stabil + 1252 V*Expl

      - 2.469 I*UIP + 144.0 I*Expl + 0.000480 P*Stabil + 0.002784 P*UIP   (Eq. 11)

   - 0.1317 R*Expl + 0.0544 R*UIP - 889 V^3 + 0.000000 P^3 + 0.000113 R^3

      - 0.000267 UIP^3- 1.891 V*I*UIP + 0.01193 I*UIP^2 - 0.000006 P*R*UIP

It is evident there was a change in the variables used in attempting to correlate the controller's variables to the nugget diameter with the addition of the validation data set. All the variables and *P-Values* can be found in Table 6.3, where they were all found to be significant below an error level of 0.05. The first issue to note is the first order variables were not found to be significant to the data but still used in higher order terms, which indicates that with a new reference curve, the use of the variables themselves do not provide any useful information. The only single order terms were current and the Boolean term for expulsion, which are considered the two principal factors when investigating nugget sizes. The influence on the nugget diameter remained the same as higher current or no expulsion would produce a larger nugget. While it is customary to keep first order terms in the model, the missing first order variables were captured as either 2nd or 3rd order terms, and thus a decision was made to leave them out of the model.

Table 6.3. Segment of ANOVA Table for Robust Model Displaying P-Values Used Variables

Term	P-Value	Term	P-Value
Constant	0.001	P*Stabil	0.000
I	0.000	P*UIP	0.000
Expl	0.020	P*Expl	0.034
P^2	0.000	R*UIP	0.000
R^2	0.000	V^3	0.000
V*P	0.000	P^3	0.000
V*R	0.000	R^3	0.000
V*Stabil	0.000	UIP^3	0.000
V*Expl	0.016	V*I*UIP	0.000
I*UIP	0.000	$I*UIP^2$	0.000
I*Expl	0.047	P*R*UIP	0.000

The resulting model shown in Figure 6.5a, provides a much better fit to the data possessing standard deviation prediction limits of 0.13 and 0.44 while encapsulating 18 of the 25 validation data

points, a substantial improvement in comparison to the previous model. With the inclusion of all the previous data, shown in Figure 6.5b, the new model captured 50 of the 125 data points (~40%) within the prediction limits. It was concluded that including data from welds using a separate unique reference curve is able to improve the robustness of a model.

a

b
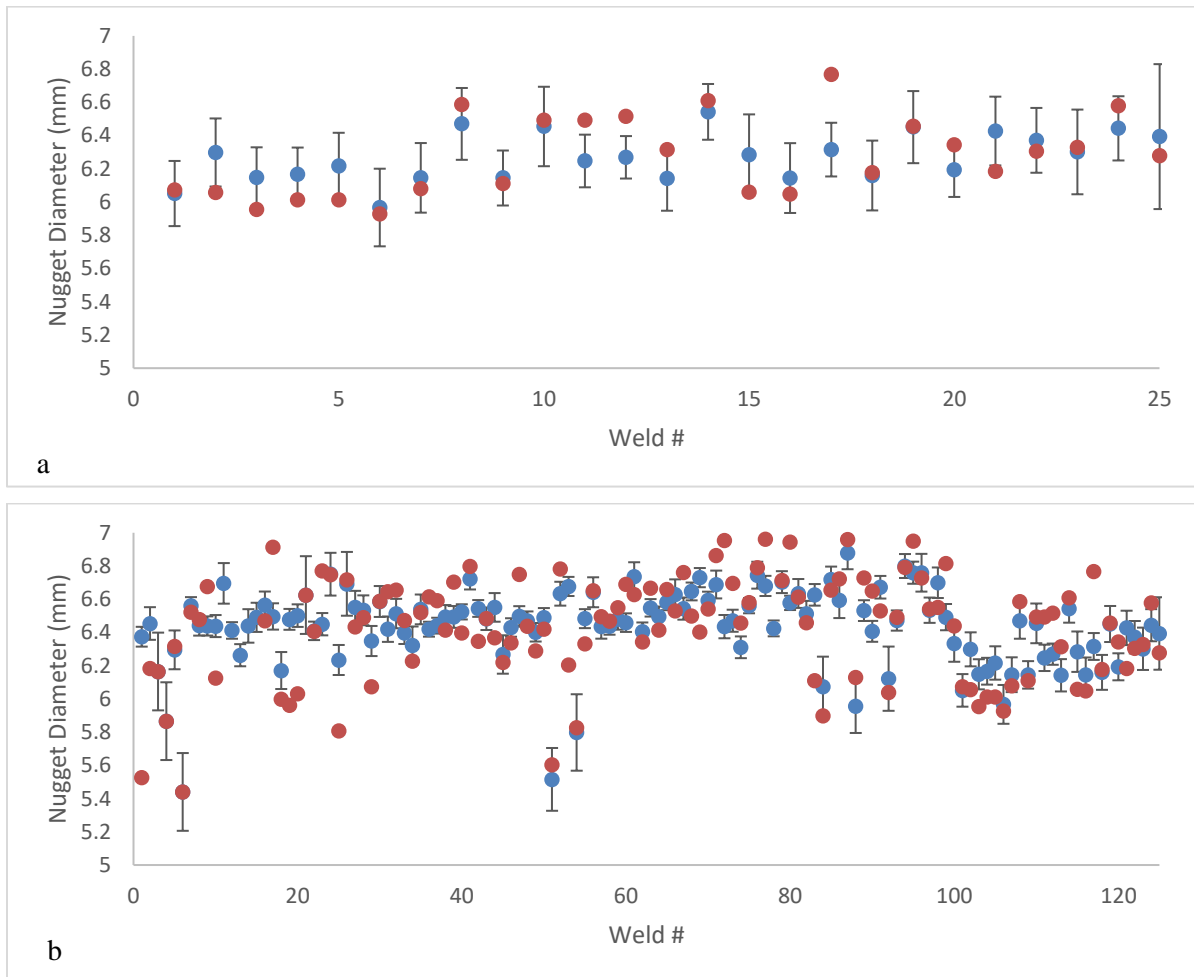
Figure 6.5. Predicted Nugget Diameter with Prediction Limits (Blue) Layered with Experimental (Red) with New Robust Model
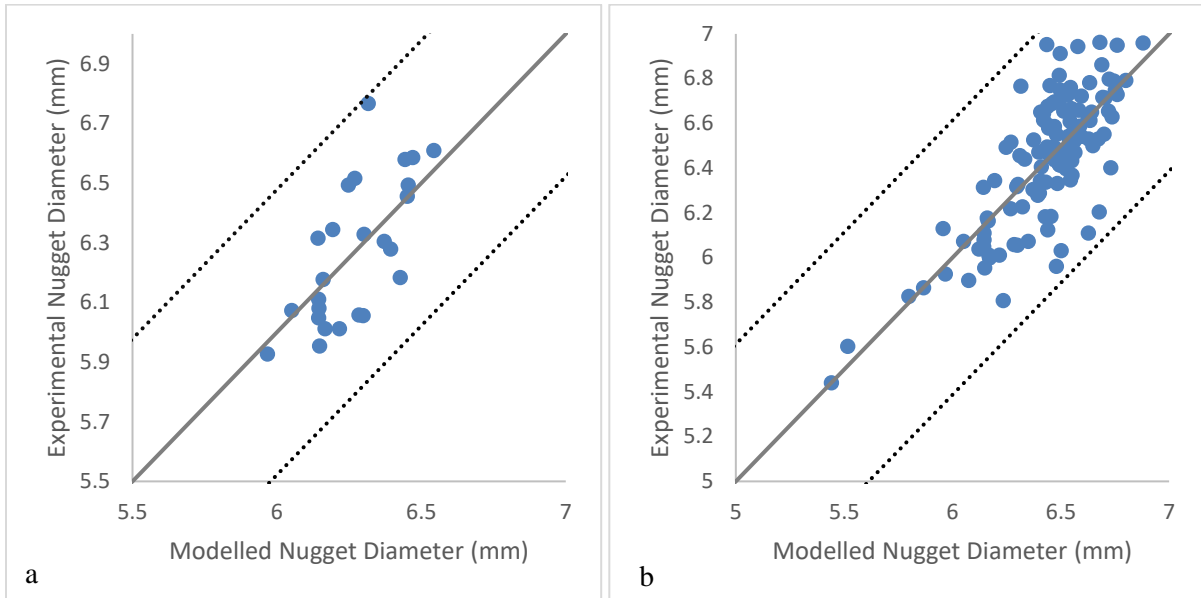
Figure 6.6. Plot of Experimental vs Modelled Nugget Diameter of Robust Model

When comparing the modelled nugget diameter to the experimental nugget diameter, Figure 6.6a displays the ability of the new model to capture the validation data while still capturing all of the original data in Figure 6.6b. It can be said that the addition of another reference curve will not skew the model and improve the ability to capture various reference curves.

6.2 Production Validation

To determine if the applicability of the findings in the laboratory setting could be directly applied to an automotive production setting, parts from the production line from Honda were supplied to be analyzed. The specific parts were the side stiff component, which consists of the a-pillar, and door frames, for the current production vehicle, as shown in Figure 6.7.
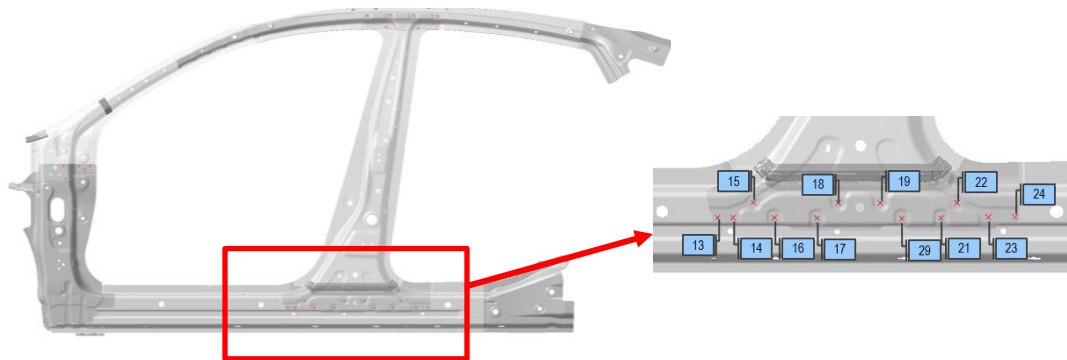
Figure 6.7. Outer Stiff Component (Left) and Analyzed Relevant Welds (Right)

The study performed in this thesis was intentionally based on the parameters and material stackup of the welds highlighted by Figure 6.7 to correlate to welds found on this component. For the specific two-stack, USIBOR® sheets were welded with a 12kA pre pulse and 7.8kA main pulse weld, with 12 welds along the bottom of the side component to be analyzed. Only one part for each side of the vehicle (driver and passenger) was provdied to be torn down and analyzed, totalling 24 welds to use as validation. In production, each of the 24 welds were welded with a unique reference curve that was set based on the specific weld location. Thus, the UIP values for all of the welds were not consistent as it changes as a function of the deviation from the set reference curve. The spread of the reference curves are shown in Figure 6.8, where the black line is the average of all of the curves. The widest spread is located during the pre-pulse with a standard deviation of 8.615. The second highest deviation was during the first 50ms of the second pulse ranging between 3 to 3.5. The level of deviation in Figure 6.8 from the reference curve was deemed acceptable to have minor effect on the UIP.
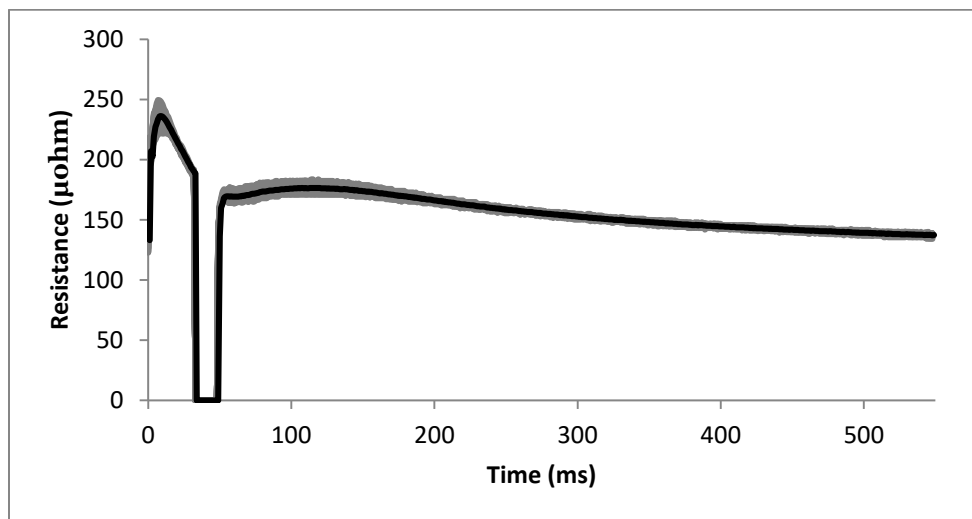
Figure 6.8. Compiled Reference Curves of All 24 Welds Used to Perform the Validation Welds

6.2.1 Nugget Diameter Validation

The statistical model formed in 6.1.2 was used to predict the nugget sizes based on the controller output signals from the production floor. The results shown in Figure 6.9, indicate that in comparison of the eperimental to the modelled data, it can be used to produce an acceptable linear correlation of the data, with 7 of the 24 data points found as outliers. The two predicted negative nugget diamters was found to be due to the expulsion. While expulsion was included in the model, it was found that the calculated power of the process was much higher. This was due to the adaptive welding

applying a higher current to mitigate high resistance situations caused by oils or dirt on the production parts in comparison to the cleaned workpieces in the lab. The prediction of the 9mm nugget was also due to the presence of expulsion. This indicates that the presence of expulsion in general was causing the model to produce poor fits. This is because it acts as a boolean variable and does not provide any addition information, but acts as a correction factor which activates other variables to correct any expulsion nugget diameters. This issue could be fixed by utilizing the production floor data to create the regression model and account for the higher power. The robustness of the model is limited to the boolean state of the expulsion variable.
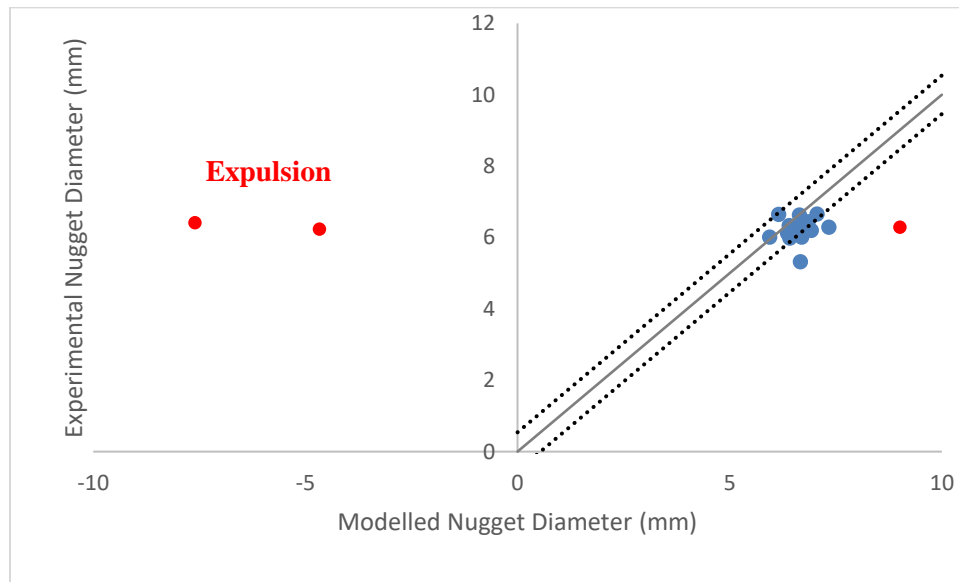
Figure 6.9. Plot of Experimental vs Modelled Nugget Diameter of Production Data using Robust Model

With results found comparing the laboratory setting and the production parts, the fit of the model was acceptable and possibly feasible with an in-depth investigation in determining what would make the model more robust.

6.2.2 Validation of Dissimilar Steel Stack Up

The side stiff components are fully composed of AHSS as it is a major component to the structural integrity of the vehicle. Al-Si coated USIBOR® and dual-phase (DP980) steels with a yield strength of 980 MPa made up the majority of the piece, each playing a different role. USIBOR® possesses a yield strength of 1500 MPa with low ductility, providing stiffness to prevent any deformation in the cabin. The DP980 possesses a lower yield strength because it is composed of a ferrite

matrix with martensite, or martensite-austenite islands to prevent dislocation, in comparison to USIBOR®'s full martensite composition [2], [114]. The presence of the ferrite matrix allows for improved ductility, and energy absorption to assist in protecting the cabin in the event of a collision.

With the introduction of a new material (DP980), the difference in bulk resistance of the different sheets would alter the dynamic resistance as well as the heat balance, as it is no longer symmetrical. These were deemed negligible to the performance of the adaptive welding capabilities of the controller as a unique reference curve for each weld in production is created. The reference curves of the production dissimilar welds can be seen in Figure 6.10 below. When comparing the production curves to the reference curve made in the laboratory setting at the university, the difference was notable. The beta peaks of the production curves range from 25 to 65% higher than the beta peaks observed in the laboratory setting. It was also noted the presence of two distinct groupings of the dynamic resistance curves (I and II in Figure 6.10). Upon investigation, the two groupings corresponded to the two separate robots used to weld the parts. In automotive production, multiple robots may simultaneously weld a larger component to meet the high demand. Thus, it should be noted that a specific robot may affect the dynamic resistance by contributing to the resistance path (through wires, wear on electrode guns, etc.).
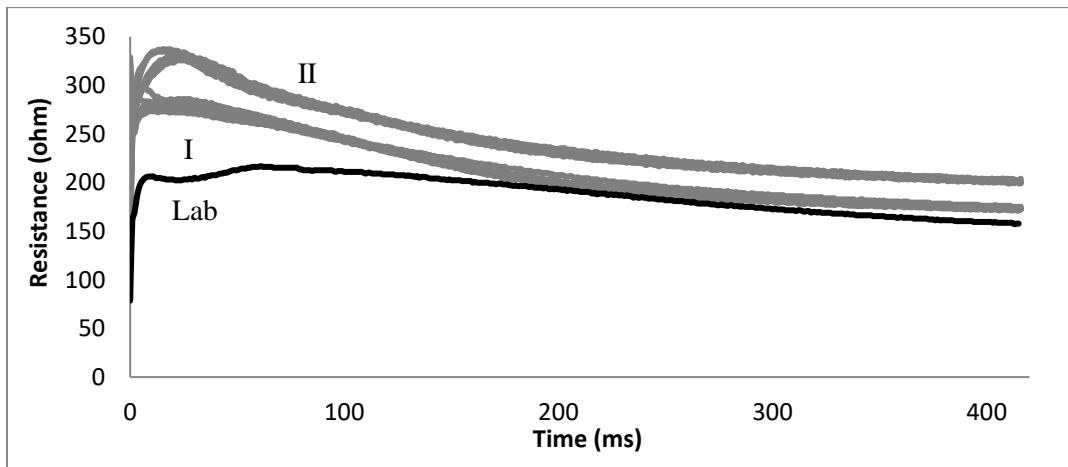
Figure 6.10. Reference Curves for All Dissimilar Welds, Production Curves in Grey and Lab Made Curves in Black

Various attempts to replicate the production setting dynamic resistance curves were made but could not be replicated without changing the test coupons. Acknowledging the discrepancy between the production data and the data collected in the lab setting, the same procedure for the same stack up

found earlier in this section was performed using 50 USIBOR®-DP980 welds. The resulting model is displayed below as (Eq. 12). The ANOVA analysis produced a R-sq (adj) value of 45.20% which was comparable to the previous models. All the first order terms were visible in this regression, but when comparing the previous models, the variable with the greatest positive influence was voltage (*V*) and *Expl* is not a negative influence. The *Expl* variable only appears once more as an interaction term with voltage (*V*) with a negative influence. This indicates that the nature of the welding behavior was not properly captured in this model and an extensive study similar to the one performed for the USIBOR® similar stack up is required for a robust model.

$$
\begin{aligned}
\textbf{Nugget Diameter (mm)} &= \text{-4526} + 22330\ V + 4375\ I - 1.52\ P - 223.8\ R \\
&\quad - 772\ \text{Stabil} + 432\ \text{UIP} + 1269\ \text{Expl} + 10.46\ \text{Stabil*Stabil} - 2.425\ \text{UIP*UIP} \\
&\quad + 158.2\ V\text{*}R - 337.1\ V\text{*Stabil} - 188.1\ V\text{*UIP} - 900\ V\text{*Expl} + 31.6\ I\text{*}R - 67.3\ I\text{*Stabil} \\
&\quad - 36.8\ I\text{*UIP} - 0.02230\ P\text{*}R + 0.0462\ P\text{*Stabil} - 0.0005\ P\text{*UIP} + 5.12\ \text{Stabil*UIP} \\
&\quad - 0.02666\ \text{Stabil*Stabil*Stabil} + 0.00336\ \text{UIP*UIP*UIP} + 0.000122\ P\text{*UIP*UIP} \\
&\quad - 0.02705\ \text{Stabil*Stabil*UIP}
\end{aligned}
$$

(Eq. 12)

The prediction capabilities of the model can be observed in Table 6.4. All error % found to be greater than 100% was highlighted red, leaving 1 of the 12 data points. The rest of the data produced unreasonable nugget diameters ranging from -7.9 to 118 mm nugget diameters (error % of -235.47% and 2083.85%). This indicates that the difference in the reference resistance curves and the lack of robustness of the model renders the model ineffective.

Table 6.4. Results of Implementation of Laboratory Created Model of Dissimilar Steel Stack Up

Weld #	Nugget Diameter (mm)	Predicted Nugget Diameter (mm)	Error %
11A_1	5.87	13.004	121.53%
11A_2	5.8	46.71553	705.44%
11A_3	5.61	40.18154	616.25%
11A_4	5.47	111.0839	1930.78%
11A_5	5.7	69.09023	1112.11%
11A_6	5.44	118.8015	2083.85%
11C_1	6.29	5.308053	-15.61%
11C_2	6.15	-0.60165	-109.78%
11C_3	6.05	-2.24254	-137.07%
11C_4	5.91	16.47872	178.83%
11C_5	5.84	-7.91152	-235.47%
11C_6	5.7	94.51068	1558.08%

6.3 Summary

From the findings of section 6.1, a regression model of the same stack up weld using the variables output by the controller is possible to make with a fit of 40.29%. To achieve such a fit, the sample was composed of welds made under various process conditions such as edge welding, shunting, poor fitment, etc. The models were able to reflect the known relations between the nugget diameter and process variables such as the direct relation with current or the negative influence of expulsion. When implementing the model to the data collected from the production floor and comparing the nugget diameters, there was reasonable fit hinting that this process has potential to be a feasible solution if more research is conducted.

With the implementation of the dissimilar steel stack up, there were findings that were not captured by the similar stack up. The first being that different welding robots create notably different reference curves which will reduce the effectivity of the model (as the adaptive controller will behave differently under the different resistance curves). This ultimately will change the UIP values and in turn no longer be viable to use one model for the specific stack up. The second is that the model created in the lab must be made with varying process conditions or else the model will not accurately reflect the relations the nugget diameter has with the process variables as demonstrated by the results with the dissimilar welding. There is a possibility that the dissimilar welding itself had caused error in the regression methods and requires further investigation. Lastly, the statistical model should reflect the known physical relations between the quality indicator and the model variables regardless of the fit (R-sq adj) for it to be viable.

Chapter 7
Conclusion and Final Remarks

The intention of the thesis was to provide a compiled report of all the findings with the use of the dynamic resistance curve and the adaptive welding controller which utilizes it. The findings were broken down by the investigation process performed. Firstly, the effect of process parameters on a constant parameter welding condition were investigated to see if there were any detection capability. Secondly, the capability of the weld controller was investigated to determine how it achieved the results it claimed it did. Lastly the quality of the weld represented by the weld nugget diameter and a statistical analysis of important variables along with a potential model was proposed, along with the problems of the method.

7.1 Process Conditions on the Dynamic Resistance Curve

The dynamic resistance curve had been used synonymously with the real-time condition of the welding process. With the first introduction of the breakdown of the dynamic resistance curve by Dickinson, research focused on this curve had been extensive [48]. The dynamic resistance is sensitive to an introduction of change in the material or type of coating [57]. With such sensitivity, the response of the dynamic resistance curve under various process conditions was tested. The results showed for extreme cases of shunting, edge welding, and shim gap, the dynamic resistance curve was significantly different from the standard reference weld. In the case of shunted welds, at a distance of 10mm between the center of a pre-existing weld to the new weld lead to a lower resistance and later beta peak resulting in a smaller nugget. During edge welding, a critical distance of approximately half of the electrode face exists where expulsion occurs and at smaller distances the shape of the curve drops quicker due to the nugget growing outside of the workpieces. For shimmed welds, the beta peak was reached earlier due to the change in current density and contact area as the required pressure of the electrodes increased. Through these findings, it is possible to justify the use of a reference resistance curve to detect a change in the process condition.

7.2 Adaptive Control

The adaptive controller promoted claims to detect the quality of the weld in real time. The claim was based on the ability of the controller to utilize a predetermined reference curve. Since the dynamic resistance curve varied significantly due to extreme changes in the process, the quality output

variables of the controller were thoroughly investigated. The ability of the adaptive controller to follow the reference curve was tested by applying the same extreme process conditions that were found to significantly change the curves. Comparing the adaptive welds with the welds performed with a constant current, it was found that in a laboratory setting the controller did not change the current by more than 10% even with the option to change up to 50%. The adaptive curves did not fit the reference any better than without, but the measured welds provided mixed results. All adaptive welds did not result in any larger nuggets except with the use of time extension for shunted welds. For edge welds it was found to be greatly detrimental, inducing expulsion.

Statistical regression analysis was performed to determine what the variable UIP was actually measuring or indicating. UIP was found to be a function of the deviation of the current, voltage, resistance, and force curves collected by the controller against the set reference curve. In addition, the stability variable was found to be a function of the average values of the energy, power, current, voltage, and resistance. Both quality indicators were found to have no correlation to the nugget diameter or the tensile strength.

7.3 Nugget Diameter Modelling

With the capability of the UIP and Stabilization determined to have no relation the quality of the weld, a model incorporating other variables in conjunction with the quality indicators. A regression of the same stack up weld was conducted to reach a maximum fit of (R-sq adj) 40.29%. This meant that the best achievable prediction of the weld was close to half of the welds performed, which is not ideal for any production setting. The model was verified against a part off of the production like and found to have an acceptable fit. While the modelling was to be as robust as possible, there were certain steps taken that could help further studies but were not done in this thesis. The data collected was from an assortment of process conditions but was limited to the time required for each stage of analysis and more process conditions could not be incorporated. This could have filled in any of the gaps between the points which appear to skew the data and may help build a better model and explanation. Further modelling could be done using normalized data which was not considered in this thesis as the effect of the raw data on the model/nugget was used to decipher the model and helped determine the validity. Given a normalized data set, the spread of the data would not be as wide considering the parameters were fixed with adaptive welding and only the variance caused by the controller would have been normalized. The analysis and interpretations of the controller is best used as the first step in moving forward in using a statistical approach of modelling nugget diameter. While it may not be the ideal

method as it neglects a lot of the physical phenomena and importance of the coefficients as a black box (neural network) would do, it is an alternative method to utilize the large amounts of data collected from the controllers.

The same investigation was performed with dissimilar materials to determine if the modelling process is robust to accommodate the effect of change in bulk resistance of other materials. It was found that the specific robot played an influential role in the resistance dynamic resistance curve, changing the adaptive control of the process. It was also discovered that the coefficients of the model should reflect the natural relations inherent to the welding process. Even with a better fit of 45.20%, the use of the model on the production part predicted error rate of over 2000%. Thus, the capabilities of this process ranges from acceptable to unusable, and further investigation is required into making this process more robust.

7.4 Future Recommendations

The following recommendations are based on the findings enclosed in this thesis:

1. The phenomena of the critical edge distance (approximately half of the electrode face) is worth investigating as all literature states the weld will experience expulsion, however no expulsion was observed below the critical edge distance.

2. An investigation into producing a more robust model is necessary if this method is to be successfully implemented as a quality monitoring tool. This may include other process conditions not covered in this study such as electrode wear (change in electrode face diameter).

3. The UIP value utilizes the force readings from the robot servo motors but the accuracy as force measurements are not precise as the robot controller does not gather data to the millisecond scale. This may improve the UIP readings in detecting and accounting for the fluctuations of the change in force.

4. The significance of the robot on the dynamic resistance is another area of interest as the dynamic resistance curves for the same weld schedule and same materials produced two unique curves based on two separate robots with the same tooling.

Bibliography

[1] Z. Hou, I. S. Kim, Y. Wang, C. Li, and C. Chen, "Finite element analysis for the mechanical features of resistance spot welding process," *J. Mater. Process. Technol.*, vol. 185, no. 1–3, pp. 160–165, 2007.

[2] World Auto Steel, *Advanced High-Strength Steels Application Guidelines*, no. 6.0. 2007.

[3] M. Ouisse and S. Cogan, "Robust design of spot welds in automotive structures: A decision-making methodology," *Mech. Syst. Signal Process.*, vol. 24, no. 4, pp. 1172–1190, 2010.

[4] A. H. Ertas and F. O. Sonmez, "Design optimization of spot-welded plates for maximum fatigue life," *Finite Elem. Anal. Des.*, vol. 47, no. 4, pp. 413–423, 2011.

[5] American Welding Society, *Recommended Practices for Test Methods for Evaluating the Resistance Spot Welding Behavior of Automotive Sheet Steel Materials*, AWS D8.9M. Miami, FL, 2012.

[6] American Welding Society, *Specification for Automotive Weld Quality-Resistance Spot Welding of Steel*, AWS D8.1M. Miami, FL, 2013.

[7] G.E. Schmidt, "Welding Issue and Cause Matrix," 2013. [Online]. Available: http://geschmidt.com/wp-content/uploads/2017/08/weldhelp_matrix_geschmidt.pdf. [Accessed: 23-Apr-2019].

[8] X. Wan, Y. Wang, and C. Fang, "Welding Defects Occurrence and Their Effects on Weld Quality in Resistance Spot Welding of AHSS Steel," *ISIJ Int.*, vol. 54, no. 8, pp. 1883–1889, 2014.

[9] J. E. Gould, S. P. Khurana, and T. Li, "Predictions of Microstructures when Welding Automotive Advanced High-Strength Steels," *Weld. J.*, vol. 85, pp. 111s-116s, 2006.

[10] Y. J. Chao, "Failure mode of spot welds: interfacial versus pullout," *Sci. Technol. Weld. Join.*, vol. 8, no. 2, pp. 133–137, 2003.

[11] D. J. Radakovic and M. Tumuluru, "Predicting resistance spot weld failure modes in shear tension tests of advanced high-strength automotive steels," *Weld. J. (Miami, Fla)*, vol. 87, no. 4, pp. 96–105, 2008.

[12] D. Zhao, Y. Wang, S. Sheng, and Z. Lin, "Real time monitoring weld quality of small scale resistance spot welding for titanium alloy," *Meas. J. Int. Meas. Confed.*, vol. 46, no. 6, pp. 1957–1963, 2013.

[13] M. Jou, "Real time monitoring weld quality of resistance spot welding for the fabrication of sheet metal assemblies," *J. Mater. Process. Technol.*, vol. 132, no. 1–3, pp. 102–113, 2003.

[14] J. Wen, C. S. Wang, G. C. Xu, and X. Q. Zhang, "Real Time Monitoring Weld Quality of Resistance Spot Welding for Stainless Steel," *ISIJ Int.*, vol. 49, no. 4, pp. 553–556, 2009.

[15] C. Summerville, P. Compston, and M. Doolan, "A comparison of resistance spot weld quality assessment techniques," *Procedia Manuf.*, vol. 29, pp. 305–312, 2019.

[16] R. Koganti, A. Elliott, and D. F. Maatz, "Resistance Spot Welding (RSW) Evaluation of 1.0 mm Usibor® 1500 P to 2.0 mm Usibor® 1500 P Steel for Automotive Body Structure Applications," 2012, pp. 639–645.

[17]   N. T. Williams and J. D. Parker, "Review of resistance spot welding of steel sheets Part 1 Modelling and control of weld nugget formation," *Int. Mater. Rev.*, vol. 49, no. 2, pp. 45–75, 2004.

[18]   N. T. Williams and J. D. Parker, "Review of resistance spot welding of steel sheets Part 2 Factors influencing electrode life," *Int. Mater. Rev.*, vol. 49, no. 2, pp. 77–108, 2004.

[19]   H. Zhang and J. Senkara, *Resistance Spot Welding Fundamentals and Applications*. Boca Raton, FL: Taylor & Francis Group, LLC, 2006.

[20]   E. Thomson, "Method of Electric Welding," United States of America Patent 451345, 1891.

[21]   W. Li, D. Cerjanex, and G. A. Grzadzinski, "A Comparative Study of Single-Phase AC and Multi-Phase DC Resistance Spot Welding," *J. Manuf. Sci. Eng.*, vol. 127, no. 3, pp. 583–589, 2004.

[22]   B. M. Brown, "A Comparison of AC and DC current in the Resistance Spot Welding of Automotive Steels," *Weld. J.*, vol. 66, no. 1, pp. 18–23, 1987.

[23]   R. Söderberg, K. Wärmefjord, L. Lindkvist, and R. Berlin, "The influence of spot weld position variation on geometrical quality," *CIRP Ann. - Manuf. Technol.*, vol. 61, no. 1, pp. 13–16, 2012.

[24]   J. S. Carlson, D. Spensieri, K. Wärmefjord, J. Segeborn, and R. Söderberg, "Minimizing dimensional variation and robot traveling time in welding stations," *Procedia CIRP*, vol. 23, no. C, pp. 77–82, 2014.

[25]   P. Bozek, "Robot Path Optimization for Spot Welding Applications in Automotive Industry," *Teh. Vjesn. Gaz.*, vol. 20, no. 5, pp. 913–917, 2013.

[26]   R. G. Selfridge, "Analysis of robot manipulators," *ACM SIGAPL APL Quote Quad*, vol. 19, no. 4, pp. 312–319, 2007.

[27]   C. Ma, D. L. Chen, S. D. Bhole, G. Boudreau, A. Lee, and E. Biro, "Microstructure and fracture characteristics of spot-welded DP600 steel," *Mater. Sci. Eng. A*, vol. 485, no. 1–2, pp. 334–346, 2008.

[28]   Z. Han, J. Orozco, J. E. Indacochea, and C. H. Chen, "Resistance Spot Welding: A Heat Transfer Study," *Weld. J.*, vol. 73, pp. 362s-371s, 1989.

[29]   C. L. Tsai, J. C. Papritan, D. W. Dickinson, and O. Jammal, "Modeling of resistance spot weld nugget growth," *Weld. J.*, vol. 71, no. 2, p. 47, 1992.

[30]   B. H. Chang, M. V. Li, and Y. Zhou, "Comparative study of small scale and 'large scale' resistance spot welding," *Sci. Technol. Weld. Join.*, vol. 6, no. 5, pp. 273–280, 2004.

[31]   M. Pouranvari and S. P. H. Marashi, "Factors affecting mechanical properties of resistance spot welds," *Mater. Sci. Technol.*, vol. 26, no. 9, pp. 1137–1144, 2009.

[32]   Y. J. Chao, "Ultimate Strength and Failure Mechanism of Resistance Spot Weld Subjected to Tensile, Shear, or Combined Tensile/Shear Loads," *J. Eng. Mater. Technol.*, vol. 125, no. 2, p. 125, 2003.

[33]   M. Pouranvari, A. Abedi, P. Marashi, and M. Goodarzi, "Effect of expulsion on peak load and energy absorption of low carbon steel resistance spot welds," *Sci. Technol. Weld. Join.*, vol. 13, no. 1, pp. 39–43, 2008.

[34]   T. Sadasue, S. Igi, K. Taniguchi, R. Ikeda, and K. Oi, "Fracture behaviour and numerical study

of resistance spot welded joints in high-strength steel sheet*," *Weld. Int.*, vol. 30, no. 8, pp. 602–613, 2016.

[35] D. R. B. and Y. Z. S.Fukumoto, I.Lum, E.Biro, "Effects of Electrode Degradation on Electrode Life in Resistance Spot Welding of Aluminum Alloy 5182," *Weld. J.*, no. November, pp. 307–312, 2003.

[36] Amada Miyachi, "The Effects of Polarity on the Resistance Welding Process," vol. 3, no. 2, pp. 1–2, 2015.

[37] Y. B. Li, Q. X. Zhang, L. Qi, and S. A. David, "Improving austenitic stainless steel resistance spot weld quality using external magnetic field," *Sci. Technol. Weld. Join.*, vol. 23, no. 7, pp. 619–627, 2018.

[38] E. E. Ferrenz, A. Amare, and C. R. Arumainayagam, "An improved method to spot-weld difficult junctions," *Rev. Sci. Instrum.*, vol. 72, no. 12, pp. 4474–4476, 2001.

[39] L. Han, M. Thornton, D. Boomer, and M. Shergold, "Effect of aluminium sheet surface conditions on feasibility and quality of resistance spot welding," *J. Mater. Process. Technol.*, vol. 210, no. 8, pp. 1076–1082, 2010.

[40] C. T. Lane, C. D. Sorensen, G. B. Hunter, S. A. Gedeon, and T. W. Eagar, "Cinematography of Resistance Spot Welding of Galvanized Steel Sheet," *Weld. Res.*, no. September, pp. 260–265, 1987.

[41] C. Sawanishi *et al.*, "Mechanical properties and microstructures of resistance spot welded DP980 steel joints using pulsed current pattern," *Sci. Technol. Weld. Join.*, vol. 19, no. 1, pp. 52–59, 2013.

[42] M. Mimer, L. E. Svensson, and R. Johansson, "Process adjustments to improve fracture behaviour in resistance spot welds of ehss and uhss," *Weld. World*, vol. 48, no. 3–4, pp. 14–18, 2004.

[43] X. Liao, X. Wang, Z. Guo, M. Wang, Y. Wu, and Y. Rong, "Microstructures in a resistance spot welded high strength dual phase steel," *Mater. Charact.*, vol. 61, no. 3, pp. 341–346, 2010.

[44] S. To and T. H. E. Welding, "Development of Appropriate Resistance Spot Welding Practice for Transformation-Hardened Steels," *Weld. J.*, no. January, pp. 1–7, 2002.

[45] J. Senkara, H. Zhang, and S. J. Hu, "Expulsion Prediction in Resistance Spot Welding," *Weld. J.*, vol. 83, no. 4, pp. 123s-132s, 2004.

[46] N. Charde, "Effects of Electrode Deformation of Resistance Spot Welding on 304 Austenitic Stainless Steel Weld Geometry," *J. Mech. Eng. Sci.*, vol. 3, no. December, pp. 261–270, Dec. 2012.

[47] Shinkokiki Co. Ltd, "Basis and Point of Resistance Welding (1)," *Shinkokiki Co., Ltd*, 2014. [Online]. Available: https://shinkokiki.co.jp/en/knowledge/miracle. [Accessed: 06-May-2019].

[48] D. W. Dickinson, J. E. Franklin, and A. Stanya, "Characterization of Spot Welding Behavior by Dynamic Electrical Parameter Monitoring The use of two parameters-dynamic resistance and critical expulsion energy-is proposed for controlling resistance spot welding," no. June, 1980.

[49] Y. Cho and S. Rhee, "Experimental study of nugget formation in resistance spot welding," *Weld. J.*, vol. 82, no. 8, pp. 195S-201S, 2003.

[50] M. Kimchi and D. H. Phillips, "Resistance Spot Welding: Fundamentals and Applications for the Automotive Industry," *Synth. Lect. Mech. Eng.*, vol. 1, no. 2, pp. i–115, Sep. 2017.

[51] M. R. Finlay, "Resistance Spot Welding of Metallic Coated Steels and PVD Coated Electrodes," *Aust. Weld. Res.*, vol. 18, p. 18, 1996.

[52] S. A. Gedeon, C. D. Sorensen, K. T. Ulrich, and T. W. Eagar, "Measurement of Dynamic Electrical and Mechanical Properties of Resistance Spot Welds," *Weld. J.*, vol. 66, no. 2, pp. 378s-385s, 1987.

[53] P. H. Thornton, A. R. Krause, and R. G. Davies, "Contact Resistances in Spot Welding," *Weld. Reseach Suppl.*, vol. 75, no. December, pp. 402–412, 1996.

[54] S. C. Wang and P. S. Wei, "Modeling Dynamic Electrical Resistance During Resistance Spot Welding," *J. Heat Transfer*, vol. 123, no. 3, p. 576, 2002.

[55] S. A. Gedeon and T. W. Eagar, "Resistance spot welding of galvanized steel: Part II. Mechanisms of spot weld nugget formation," *Metall. Trans. B*, vol. 17, no. 4, pp. 887–901, 1986.

[56] F. Savage, E. F. Nippes, and F. a Wassell, "Static Contact Resistance of Series Spot Welds," *Weld. Reseach Suppl.*, pp. 365–370, 1977.

[57] O. L. R. Ighodaro, E. Biro, and Y. N. Zhou, "Study and Applications of Dynamic Resistance Profiles During Resistance Spot Welding of Coated Hot-Stamping Steels," *Metall. Mater. Trans. A Phys. Metall. Mater. Sci.*, vol. 48, no. 2, pp. 745–758, 2017.

[58] D. Q. Sun, B. Lang, D. X. Sun, and J. B. Li, "Microstructures and mechanical properties of resistance spot welded magnesium alloy joints," *Mater. Sci. Eng. A*, vol. 460–461, pp. 494–498, 2007.

[59] J. Sankara and H. Zhang, "Cracking in Spot Welding Aluminum Alloy AA5754," *Weld. Res. Suppl.*, no. July, pp. 194–201, 2000.

[60] S. To, T. H. E. Welding, C. V Robino, T. J. Headley, and J. R. Michael, "Weld Solidification and Cracking Behavior of Free-Machining Stainless Steel," *Society*, no. March, pp. 51–64, 2003.

[61] S. Fukumoto, K. Fujiwara, S. Toji, and A. Yamamoto, "Small-scale resistance spot welding of austenitic stainless steels," *Mater. Sci. Eng. A*, vol. 492, no. 1–2, pp. 243–249, 2008.

[62] J. A. Brooks, M. I. Baskes, and F. A. Greulich, "Solidification Modeling and Solid-State Transformations in High-Energy Density Stainless Steel Welds," *Metall. Trans. A*, vol. 22A, pp. 915–926, 1991.

[63] M. G. Nicholas and C. F. Old, "Liquid metal embrittlement," *J. Mater. Sci.*, vol. 14, no. 1, pp. 1–18, Jan. 1979.

[64] C. Beal, X. Kleber, D. Fabregue, and M. Bouzekri, "Liquid zinc embrittlement of twinning-induced plasticity steel," *Scr. Mater.*, vol. 66, no. 12, pp. 1030–1033, 2012.

[65] Y. G. Kim, I. J. Kim, J. S. Kim, Y. Il Chung, and D. Y. Choi, "Evaluation of Surface Crack in Resistance Spot Welds of Zn-Coated Steel," *Mater. Trans.*, vol. 55, no. 1, pp. 171–175, 2014.

[66] Z. Ling, M. Wang, and L. Kong, "Liquid Metal Embrittlement of Galvanized Steels During Industrial Processing: A Review," pp. 25–42, 2018.

[67] "ISO 14329:2003: Resistance welding – Destructive tests of welds – Failure types and geometric measurements for resistance spot, seam and projection welds." .

[68] Y. Ma, P. Wu, C. Xuan, Y. Zhang, and H. Su, "Review on techniques for on-line monitoring of resistance spot welding process," *Adv. Mater. Sci. Eng.*, vol. 2013, 2013.

[69] M. Thornton, L. Han, and M. Shergold, "Progress in NDT of resistance spot welding of aluminium using ultrasonic C-scan," *NDT E Int.*, vol. 48, pp. 30–38, 2012.

[70] R. J. Ditchburn, S. K. Burke, and C. M. Scala, "NDT of welds: state of the art," *NDT E Int.*, vol. 29, no. 2, pp. 111–117, Apr. 1996.

[71] D. Zhao, Y. Wang, Z. Lin, and S. Sheng, "An effective quality assessment method for small scale resistance spot welding based on process parameters," *NDT E Int.*, vol. 55, pp. 36–41, 2013.

[72] C. Hellier, *Handbook of Nondestructive Evaluation*, vol. 1. US: McGraw-Hill Professional, 2001.

[73] Ó. Martín, M. Pereda, J. I. Santos, and J. M. Galán, "Assessment of resistance spot welding quality based on ultrasonic testing and tree-based techniques," *J. Mater. Process. Technol.*, vol. 214, no. 11, pp. 2478–2487, 2014.

[74] A. M. Chertov, R. G. Maev, and F. M. Severin, "Acoustic microscopy of internal structure of resistance spot welds," *IEEE Trans. Ultrason. Ferroelectr. Freq. Control*, vol. 54, no. 8, pp. 1521–1529, 2007.

[75] H. T. Lee, M. Wang, R. Maev, and E. Maeva, "A study on using scanning acoustic microscopy and neural network techniques to evaluate the quality of resistance spot welding," *Int. J. Adv. Manuf. Technol.*, vol. 22, no. 9–10, pp. 727–732, 2003.

[76] M. Takuma, N. Shinke, and H. Motono, "Evaluation of Function of Spot-Welded Joint Using Ultrasonic Inspection," *JSME Int. J. Ser. A*, vol. 39, no. 4, pp. 626–632, 1996.

[77] D. Türler, D. Hopkins, and F. Reverdy, "Nondestructive Evaluation of Spot Welds Using Acoustic and Thermographic Imaging Techniques," 2003.

[78] R. G. Maev, A. Ptchelintsev, and A. A. Denissov, "Ultrasonic Imaging with 2D Matrix Transducers," in *Acoustical Imaging*, Boston: Kluwer Academic Publishers, 2002, pp. 157–162.

[79] A. A. Denisov, C. M. Shakarji, B. B. Lawford, R. G. Maev, and J. M. Paille, "Spot weld analysis with 2D ultrasonic Arrays," *J. Res. Natl. Inst. Stand. Technol.*, vol. 109, no. 2, p. 233, 2012.

[80] A. A. Denisov, R. G. Maev, J. Erlewein, and H. Römmer, "Advanced Ultrasonic Imaging for Automotive Spot Weld Quality Testing," *Pam Am. Conf. NDT*, no. October, 2011.

[81] F. Schubert, R. Hipp, and A. Gommlich, "Determination of Diameter and Thickness of Weld Nuggets in Resistance Spot Weldings by High Frequency Ultrasound Inspection," *11th Eur. Conf. Non-Destructive Test. (ECNDT 2014)*, no. Ecndt, pp. 1–10, 2014.

[82] J. Ruisz, J. Biber, and M. Loipetsberger, "Quality evaluation in resistance spot welding by analysing the weld fingerprint on metal bands by computer vision," *Int. J. Adv. Manuf. Technol.*, vol. 33, no. 9–10, pp. 952–960, 2007.

[83] S. M. Shepard, B. B. Chaudhry, R. L. Predmesky, and M. J. Zaluzec, "Pulsed thermographic inspection of spot welds," *Proc. SPIE, Thermosense XX*, vol. 3361, pp. 320–324, 1998.

[84] W. Woo *et al.*, "Application of infrared imaging for quality inspection in resistance spot welds," *Proc. SPIE, Thermosense XXXI*, vol. 7299, p. 729912, 2009.

[85] J. Schlichting, S. Brauser, L. A. Pepke, C. Maierhofer, M. Rethmeier, and M. Kreutzbruck, "Thermographic testing of spot welds," *NDT E Int.*, vol. 48, pp. 23–29, 2012.

[86] C. S. Chien and E. Kannatey-Asibu Jr., "Investigation of Monitoring Systems for Resistance Spot WElding," *Weld. Journal-New York*, vol. 81, no. 9, pp. 195–199, 2002.

[87] Y. J. Park and H. Cho, "Quality evaluation by classification of electrode force patterns in the resistance spot welding process using neural networks," *Proc. Inst. Mech. Eng. Part B J. Eng. Manuf.*, vol. 218, no. 11, pp. 1513–1524, Nov. 2004.

[88] H. Wang, Y. Zhang, and G. Chen, "Resistance spot welding processing monitoring based on electrode displacement curve using moving range chart," *Meas. J. Int. Meas. Confed.*, vol. 42, no. 7, pp. 1032–1038, 2009.

[89] X. Lai, X. Zhang, Y. Zhang, and G. Chen, "Weld quality inspection based on on-line measured indentation from servo encoder in resistance spot welding," *Conf. Rec. - IEEE Instrum. Meas. Technol. Conf.*, vol. 56, no. 4, pp. 1501–1505, 2006.

[90] S. M. Van Bohemen, M. J. Hermans, and G. Den Ouden, "Monitoring of martensite formation during welding by means of acoustic emission," *J. Phys. D. Appl. Phys.*, vol. 34, no. 22, p. 3312, 2001.

[91] Y. V. Kamat and K. D. Lagoo, "In-process monitoring of resistance spot welding," in *Measurement Technology and Intelligent Instruments*, 1993, vol. 2101, no. September 1993, p. 650.

[92] M. Hao, K. A. Osman, D. R. Boomer, and C. J. Newton, "Developments in Characterization of Resistance Spot Welding of Aluminum," *Weld. J.*, vol. 75, no. 1, pp. 1-s-8-s, 1996.

[93] R. K. Cohen, "Resistance spot welder adaptive control," US 4447700A, 1982.

[94] A. G. Livshits, "Universal Quality Assurance Method for Resistance Spot Welding Based on Dynamic Resistance," *Weld. Res. Suppl.*, pp. 383–390, 1997.

[95] Y. Cho and S. Rhee, "Primary Circuit Dynamic Resistance Monitoring and its Application to Quality Estimation during Resistance Spot Welding," *Weld. J.*, no. June, pp. 104–111, 2002.

[96] Y. Cho and S. Rhee, "New technology for measuring dynamic resistance and estimating strength in resistance spot welding," *Meas. Sci. Technol.*, vol. 11, no. 8, pp. 1173–1178, 2000.

[97] M. F. A. Zaharuddin, D. Kim, and S. Rhee, "An ANFIS based approach for predicting the weld strength of resistance spot welding in artificial intelligence development," *J. Mech. Sci. Technol.*, vol. 31, no. 11, pp. 5467–5476, 2017.

[98] T. Kim, Y. S. Lee, J. Lee, and S. H. Rhee, "A Study of Nondestructive Weld Quality Inspection and Estimation during Resistance Spot Welding," *Key Eng. Mater.*, vol. 270–273, pp. 2338–2344, 2009.

[99] C. Summerville, D. Adams, P. Compston, and M. Doolan, "Process Monitoring of Resistance Spot Welding Using Dynamic Resistance.pdf," *Suppl. to Weld. J.*, vol. 96, pp. 403–412, 2017.

[100] F. Garza and M. Das, "On real time monitoring and control of resistance spot welds using dynamic resistance signatures," *Midwest Symp. Circuits Syst.*, vol. 1, pp. 41–44, 2001.

[101] Arcelor Mittal, "Steels for hot stamping - Usibor and Ductibor." [Online]. Available: https://automotive.arcelormittal.com/products/global_offering/PHS/usibor_ductibor. [Accessed: 07-May-2019].

[102] H. Karbasian and A. E. Tekkaya, "A review on hot stamping," *J. Mater. Process. Technol.*, vol. 210, no. 15, pp. 2103–2118, 2010.

[103] M. C. J. Marker, B. Skolyszewska-Kühberger, H. S. Effenberger, C. Schmetterer, and K. W. Richter, "Phase equilibria and structural investigations in the system Al-Fe-Si," *Intermetallics*, vol. 19, no. 12, pp. 1919–1929, 2011.

[104] E. Biro, J. R. McDermid, J. D. Embury, and Y. Zhou, "Softening kinetics in the subcritical heat-affected zone of dual-phase steel welds," *Metall. Mater. Trans. A Phys. Metall. Mater. Sci.*, vol. 41, no. 9, pp. 2348–2356, 2010.

[105] Y. Lu, A. Peer, T. Abke, M. Kimchi, and W. Zhang, "Subcritical heat affected zone softening in hot-stamped boron steel during resistance spot welding," *Mater. Des.*, vol. 155, pp. 170–184, 2018.

[106] J. K. Larson, "Optimizing the Resistance Spot Welding Process for High Quality Welding of Press-Hardened Steel," in *EUROJOIN 8*, 2012.

[107] T. Huin, S. Dancette, D. Fabrègue, and T. Dupuy, "Investigation of the Failure of Advanced High Strength Steels Heterogeneous Spot Welds," *Metals (Basel).*, vol. 6, no. 5, p. 111, 2016.

[108] B. Xing, Y. Xiao, and Q. H. Qin, "Characteristics of shunting effect in resistance spot welding in mild steel based on electrode displacement," *Meas. J. Int. Meas. Confed.*, vol. 115, no. June 2017, pp. 233–242, 2018.

[109] H. S. Chang and H. S. Cho, "A Study on the Shunt Effect in Resistance Spot Welding," *Weld. J.*, vol. 69, no. 8, pp. 308–317, 1990.

[110] B. B. Wang, M. Lou, Q. Shen, y. . Li, and H. Zhang, "Shunting Effect in Resistance Spot Welding Steels - Part1: Experimental Study," *Weld. J.*, vol. 92, no. June, pp. 1–8, 2013.

[111] J. Shen, Y. S. Zhang, and X. M. Lai, "Influence of initial gap on weld expulsion in resistance spot welding of dual phase steel," *Sci. Technol. Weld. Join.*, vol. 15, no. 5, pp. 386–392, 2010.

[112] J. S. Hou, "Resistance Spot Welding and In-Process Heat Treatment of Hot Stamped Boron Steel," 2016.

[113] O. Andersson, "Process planning of resistance spot welding," 2013.

[114] J. Galán, L. Samek, P. Verleysen, K. Verbeken, and Y. Houbaert, "Advanced high strength steels for automotive industry," *Rev. Metal.*, vol. 48, no. 2, pp. 118–131, Apr. 2012.

Appendix A

Chapter 4 Supplementary Data

Table A.1. Data for 6 Variables for Shunt Welds

Shunt	max_resist	max_time	final_resist	form_slope	grow_slope	avg
10.00	237.72	42.42	135.29	5.60	0.22	158.13
10.00	215.93	64.06	136.55	3.37	0.18	152.90
10.00	228.73	32.43	131.83	7.05	0.21	155.09
10.00	228.72	36.99	130.70	6.18	0.21	152.90
10.00	217.75	38.58	130.43	5.64	0.19	150.62
10.00	216.23	43.18	130.80	5.01	0.19	148.48
10.00	220.52	40.68	132.32	5.42	0.19	150.08
10.00	219.20	47.44	129.22	4.62	0.20	149.75
20.00	244.43	31.54	130.13	7.75	0.24	156.64
20.00	235.41	29.77	127.48	7.91	0.23	152.52
20.00	231.26	40.24	126.01	5.75	0.23	149.37
20.00	229.24	37.04	126.64	6.19	0.22	150.77
20.00	224.27	49.94	126.37	4.49	0.22	148.86
20.00	226.97	43.82	127.02	5.18	0.22	149.12
20.00	229.00	44.84	125.93	5.11	0.23	148.63
20.00	224.54	52.60	126.87	4.27	0.22	148.16
30.00	243.89	33.14	129.60	7.36	0.24	151.91
30.00	248.51	32.92	130.36	7.55	0.25	152.69
30.00	235.38	42.32	126.04	5.56	0.24	150.25
30.00	240.20	41.24	129.33	5.82	0.24	153.38
30.00	239.04	35.91	129.74	6.66	0.24	153.70
30.00	226.92	48.57	124.32	4.67	0.23	147.54
30.00	239.15	43.04	129.50	5.56	0.24	153.73
30.00	232.13	44.92	127.54	5.17	0.23	150.69
40.00	248.79	27.26	130.38	9.13	0.25	155.24
40.00	243.91	31.84	128.86	7.66	0.25	152.69
40.00	235.38	44.84	124.84	5.25	0.24	150.03
40.00	235.15	33.84	127.45	6.95	0.23	149.95
40.00	233.78	38.82	125.80	6.02	0.23	151.27
40.00	233.78	42.60	125.84	5.49	0.24	148.04
40.00	234.25	43.18	128.36	5.42	0.23	152.04
40.00	240.73	34.67	129.73	6.94	0.24	154.13

Table A.2. Data for 6 Variables for Edge Welds

Edge	max_resist	max_time	final_resist	form_slope	grow_slope	avg
1	224.1	25.25	110.7	8.876	0.2388	132.7
1	222.6	27.73	107.4	8.028	0.2438	129.0
2	230.2	35.47	114.7	6.490	0.2485	136.7
2	227.5	36.30	115.1	6.267	0.2424	135.5
2	233.1	25.12	116.5	9.278	0.2454	138.6
3	225.1	49.89	122.3	4.512	0.2284	136.7
3	218.4	45.50	117.6	4.800	0.2218	135.7
3	218.9	48.02	122.0	4.558	0.2142	139.7
5	237.1	47.83	128.3	4.957	0.2406	145.9
5	221.1	43.03	129.9	5.137	0.1995	148.4
5	221.8	48.75	127.7	4.550	0.2085	149.1
10	224.2	49.52	128.6	4.527	0.2121	149.6
10	231.4	45.17	130.4	5.122	0.2220	152.6
10	230.	40.84	130.7	5.648	0.2177	152.0
15	241.6	41.49	126.9	5.824	0.2502	149.4
15	235.1	33.84	127.4	6.948	0.2310	149.9
15	233.7	42.60	125.8	5.487	0.2359	148.0
15	240.7	34.66	129.7	6.943	0.2385	154.1
1	231.7	19.78	105.1	11.70	0.2635	130.1
1	245.9	17.52	105.7	14.02	0.2904	133.2
1	257.2	17.83	104.0	14.42	0.3175	136.8
2	213.1	29.57	114.7	7.207	0.2091	133.1
2	218.0	29.65	112.2	7.352	0.2249	130.9
2	216.8	26.15	110.7	8.289	0.2239	129.7

Table A.3. Data for 6 Variables for Shim Welds

| Fit Up	max_resist	max_time	final_resist	form_slope	grow_slope	avg
1mm	217.1	17	131.7	12.77	0.1767	175.8
1mm	230.8	19	137.2	12.14	0.1946	178.8
1mm	230.5	19	137.4	12.13	0.1935	179.2
1mm	217.4	16	136.7	13.59	0.1668	178.1
1mm	229.3	15	137.3	15.28	0.1895	180.6
2mm	250.9	15	139.7	16.73	0.2294	190.5
2mm	236.0	13	137.1	18.15	0.2031	180.8
2mm	250.3	15	133.9	16.69	0.2401	186.8
2mm	236.4	18	134.9	13.13	0.2105	183.2
2mm	259.8	14	132.2	18.55	0.2625	190.7
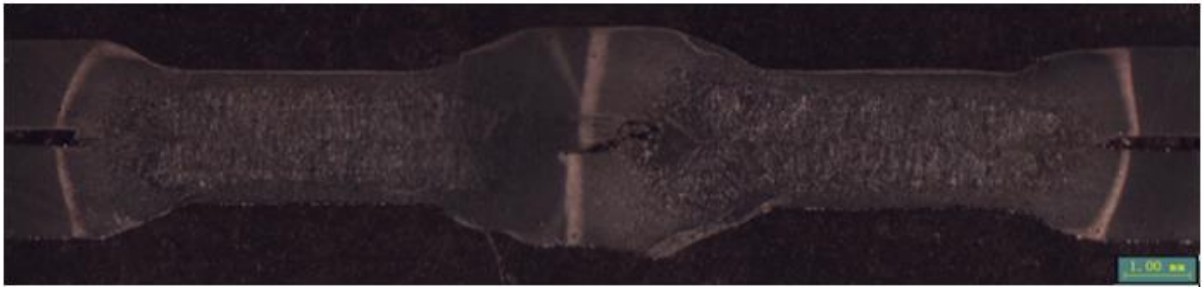
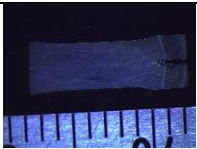**Figure A.1. Macroscopic Cross Section of Shunted 10mm Weld**
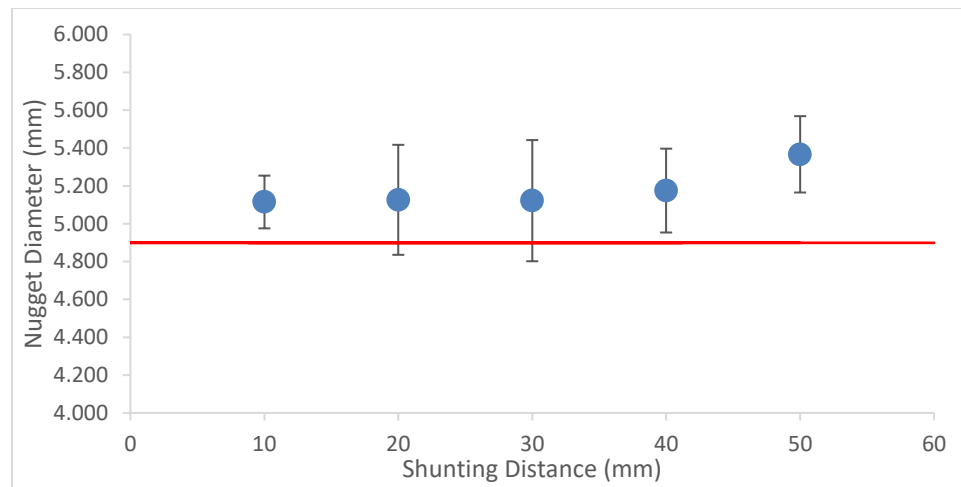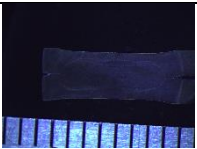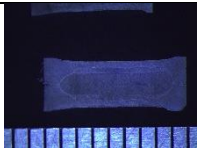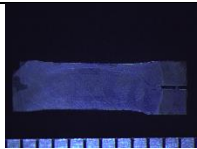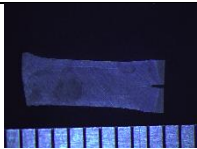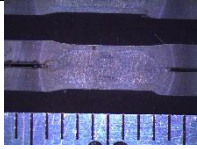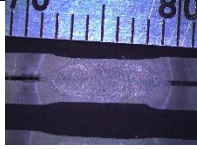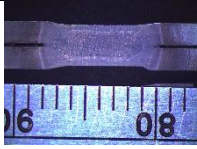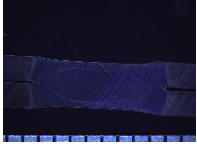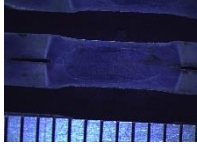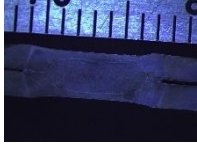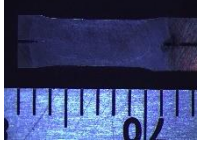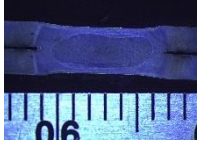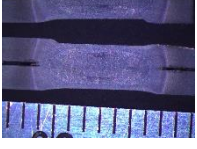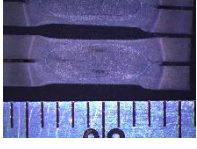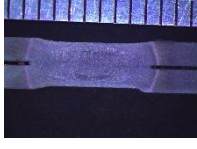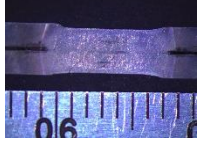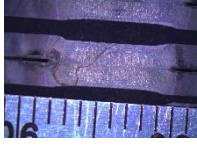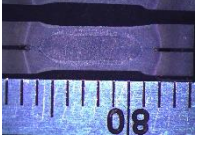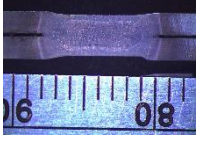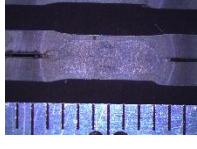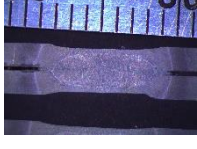
Figure A.2. Nugget Diameter of Shunted Welds with 2 Standard Deviation Bars

Table A.4. Macroscopic Images of Cross-Sectioned and Etched Shunted Welds

10mm					
20mm					
30mm					
40mm					
Ref					

Figure A.3. Macroscopic Cross Section of Edge Weld at 2mm
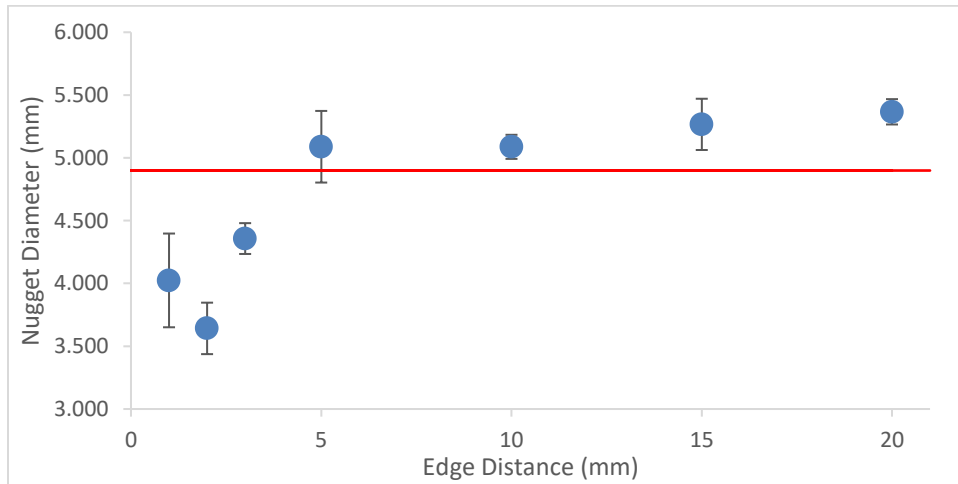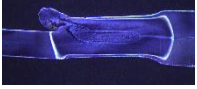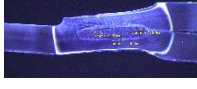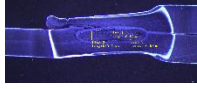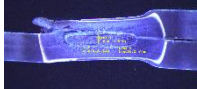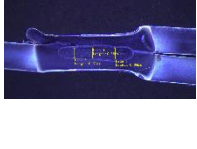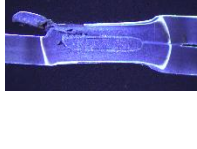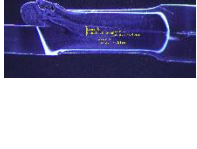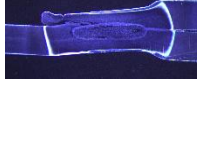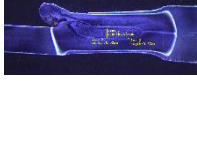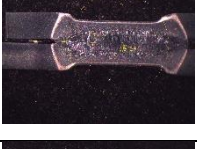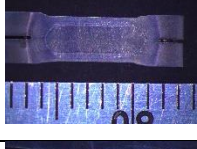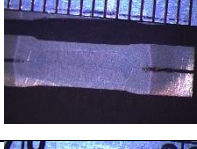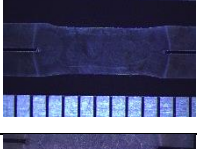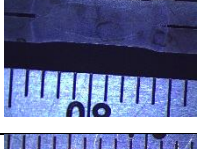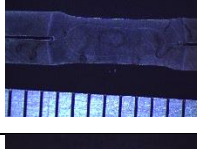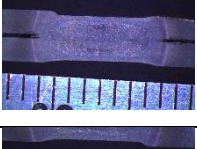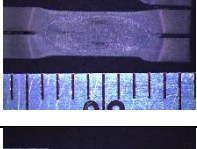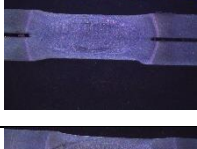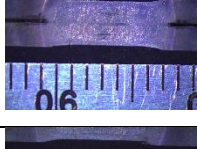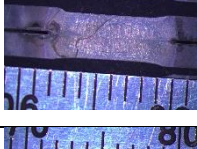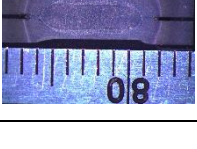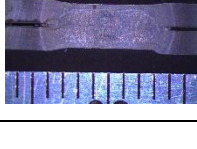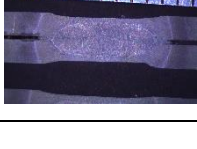
Figure A.4. Nugget Diameter of Edge Welds with 2 Standard Deviation Bars

Table A.5. Macroscopic Images of Cross-Sectioned and Etched Edge Welds

1mm					
2mm					
3mm					
5mm					
10mm					
15mm					
Ref					
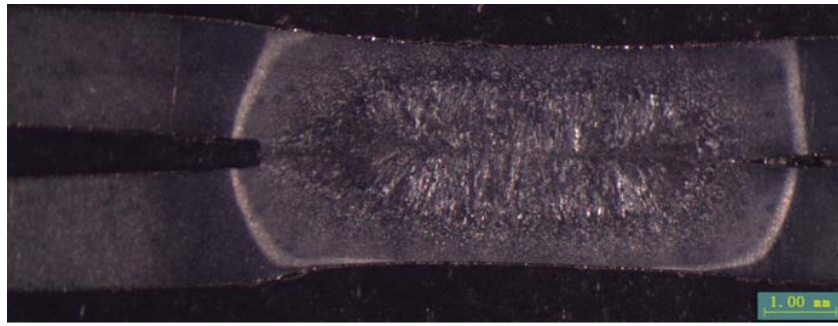
Figure A.5. Macroscopic Cross Section of Shim Weld

Table A.6. Macroscopic Images of Cross-Sectioned and Etched Shim Welds
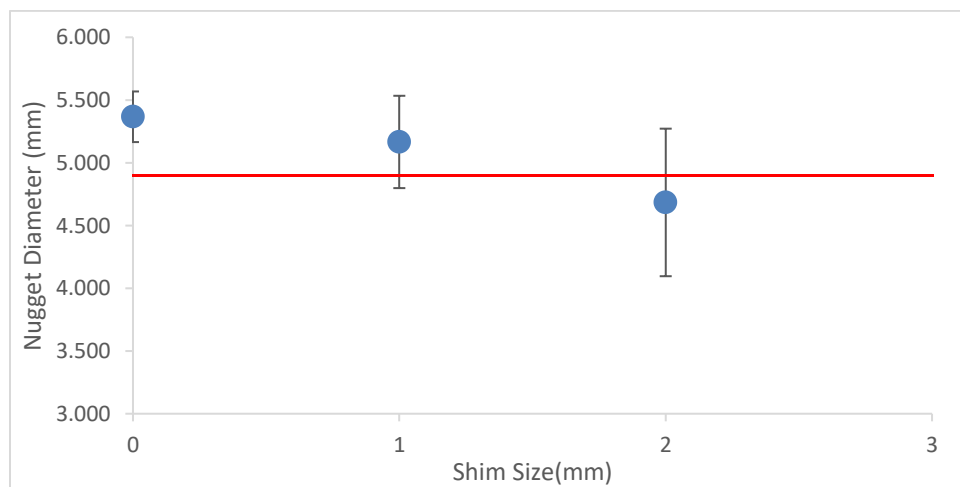
Figure A.6. Nugget Diameter of Shim Welds with 2 Standard Deviation Bars

Appendix B

Chapter 5 Supplementary Data

MATLAB Code

```matlab
clear all
close all

% reading the data in
data_dir = 'C:\Users\Kyu Won Choi\Documents\MASc\2018 Data\Experiments\Robot\1.5mm usibor\Matlab';

dat1 = importdata('TimeExt.txt');
dat2 = importdata('Compile.txt');
dat3 = zeros(550,186);
dat3 = importdata('Validate.txt');

%Offset: 1time2current3voltage4resist5zwxks6force
offset = 2;

%Compare Resistance
for k=1:1:16
    for i=1:1:length(dat1)
        compare1(i,k)=dat1(i,(offset+6*(k-1)))-dat1(i,90+offset);
    end
end

%Compare Resistance
for k=1:1:38
    for i=1:1:length(dat2)
        compare2(i,k)=dat2(i,(offset+6*(k-1)))-dat1(i,90+offset);
    end
end

%Compare Resistance
for k=1:1:31
    for i=1:1:length(dat3)
        compare3(i,k)=dat3(i,(offset+6*(k-1)))-dat3(i,180+offset);
    end
end

compare1(isnan(compare1))=0;
compare2(isnan(compare2))=0;
compare3(isnan(compare3))=0;

totaldiff1=sum(compare1);
totaldiff2=sum(compare2);
totaldiff3=sum(compare3);

abstotaldiff1=sum(abs(compare1));
abstotaldiff2=sum(abs(compare2));
abstotaldiff3=sum(abs(compare3));
```

Statistical Analysis of UIP
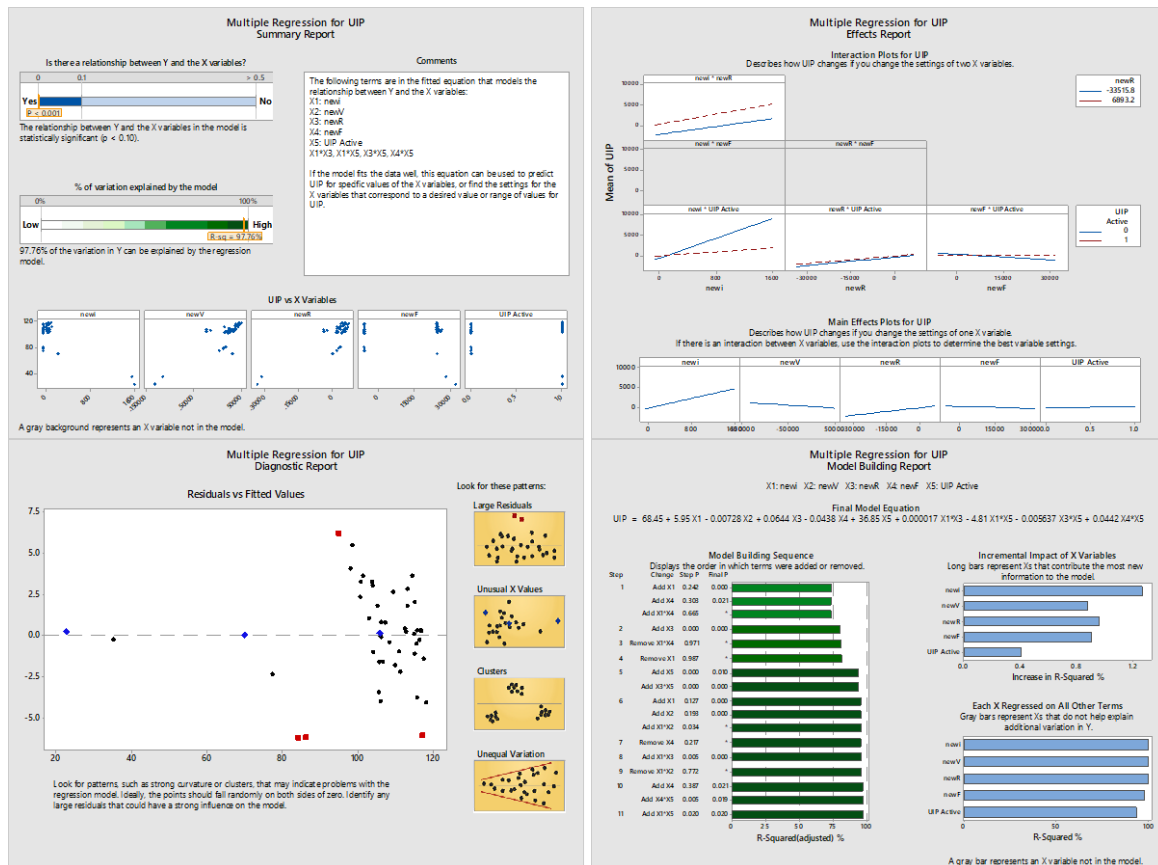
Figure B.7. MiniTab Initial Regression Data for Delta

Regression Analysis: UIP versus X1, X2, X3, X4, X5, X1*X3, ... *X5, X4*X5

Analysis of Variance

Source	DF	Adj SS	Adj MS	F-Value	P-Value
Regression	9	16358.2	1817.58	125.02	0.000
X1	1	76.0	75.98	5.23	0.028
X2	1	32.2	32.20	2.21	0.145
X3	1	36.9	36.87	2.54	0.119
X4	1	77.0	76.99	5.30	0.027
X5	1	80.8	80.77	5.56	0.023

X1*X3	1	81.4	81.39	5.60	0.023
X1*X5	1	75.9	75.89	5.22	0.028
X3*X5	1	524.1	524.07	36.05	0.000
X4*X5	1	80.2	80.24	5.52	0.024
Error	40	581.5	14.54		
Lack-of-Fit	38	581.5	15.30	*	*
Pure Error	2	0.0	0.00		
Total	49	16939.8			

Model Summary

S	R-sq	R-sq(adj)
3.81293	96.57%	95.79%

Coefficients

Term	Coef	SE Coef	T-Value	P-Value	VIF
Constant	-4117	1723	-2.39	0.022	
X1	5.62	2.46	2.29	0.028	2057366.94
X2	0.000407	0.000274	1.49	0.145	310.14
X3	0.00364	0.00229	1.59	0.119	1016.13
X4	-0.0513	0.0223	-2.30	0.027	373758.13
X5	4044	1716	2.36	0.023	2385001.37
X1*X3	0.000002	0.000001	2.37	0.023	182.87
X1*X5	-5.62	2.46	-2.28	0.028	1970758.22
X3*X5	-0.005260	0.000876	-6.00	0.000	135.29
X4*X5	0.0525	0.0223	2.35	0.024	1102463.05

Regression Equation

UIP = -4117 + 5.62 X1 + 0.000407 X2 + 0.00364 X3 - 0.0513 X4 + 4044 X5 + 0.000002 X1*X3
- 5.62 X1*X5 - 0.005260 X3*X5 + 0.0525 X4*X5

Fits and Diagnostics for Unusual Observations

Obs	UIP	Fit	Resid	Std Resid		
9	106.00	104.49	1.51	3.75	R	X
13	35.00	31.71	3.29	3.50	R	X
14	23.00	26.07	-3.07	-3.49	R	X
44	78.00	85.72	-7.72	-2.34	R	

46   70.00   70.00   0.00   *   X

R Large residual
X Unusual X

Residual Plots for UIP
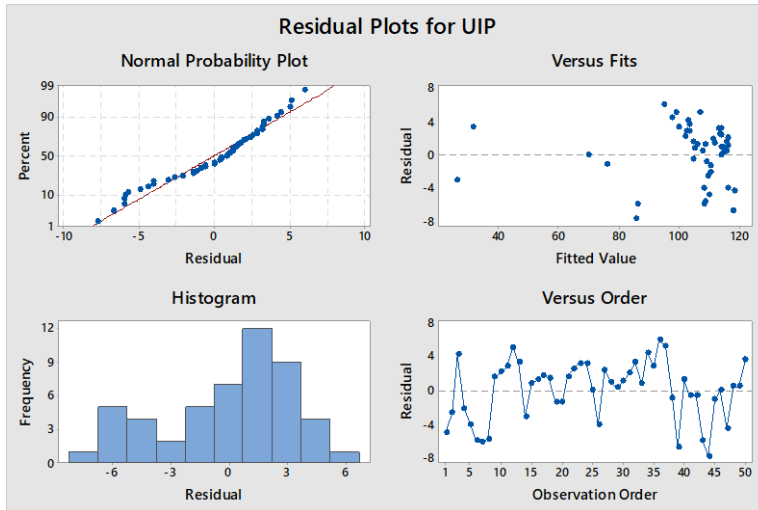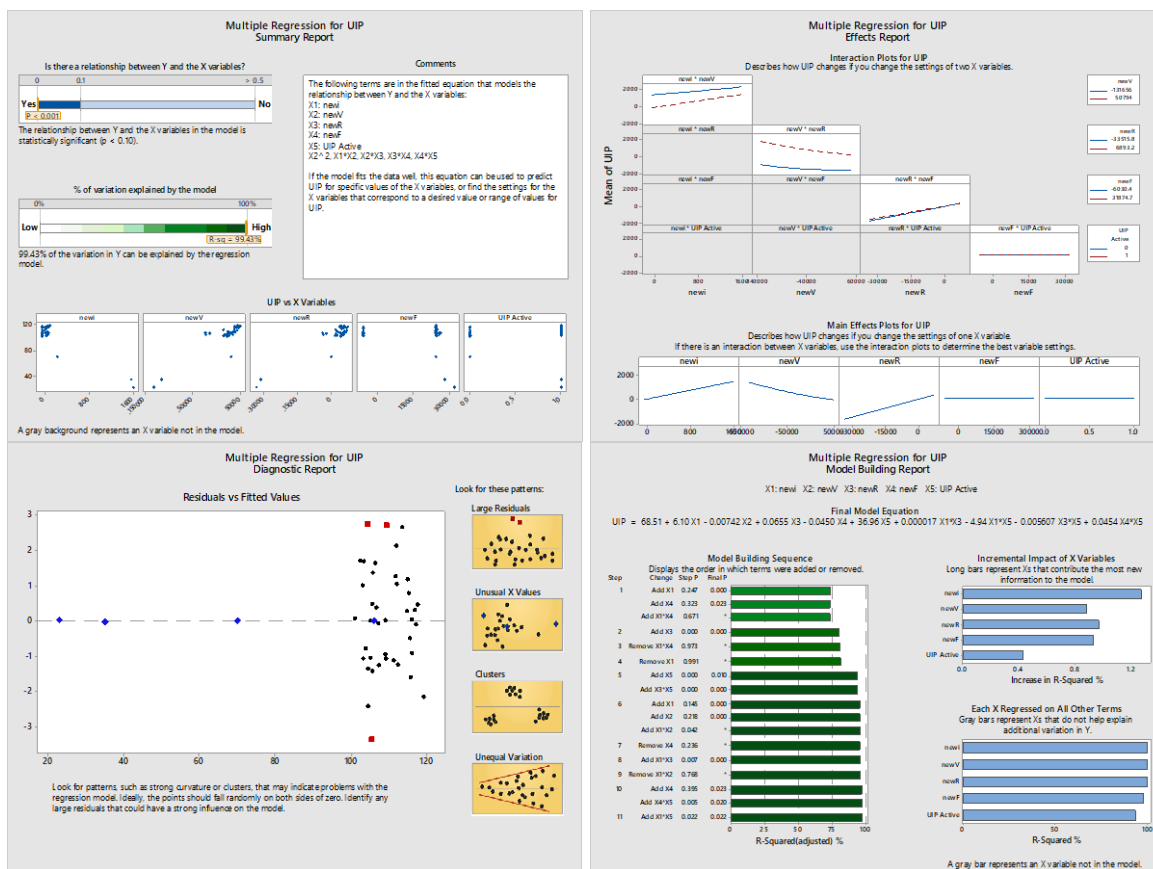
Figure B.8. MiniTab Removal of Outlier Regression Data for Delta
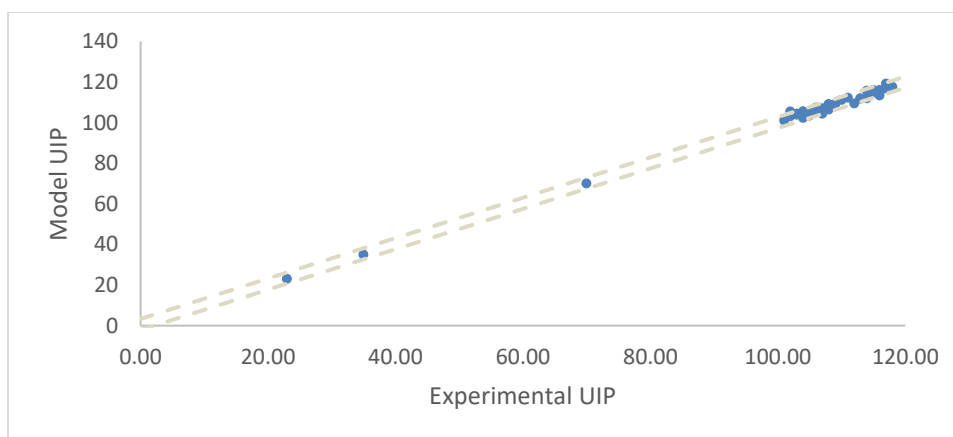
Figure B.9. Plot of Experimental vs Model UIP

Regression Analysis: UIP versus X1, X2, X3, X4, X5, X2^2, ... *X4, X4*X5

Analysis of Variance

Source	DF	Adj SS	Adj MS	F-Value	P-Value
Regression	10	14671.6	1467.16	537.07	0.000
X1	1	89.0	89.03	32.59	0.000
X2	1	83.2	83.16	30.44	0.000
X3	1	75.3	75.33	27.57	0.000
X4	1	44.7	44.70	16.36	0.000
X5	1	10.6	10.56	3.87	0.057
X2^2	1	50.5	50.47	18.48	0.000
X1*X2	1	36.0	35.98	13.17	0.001
X2*X3	1	38.0	38.02	13.92	0.001
X3*X4	1	98.9	98.87	36.19	0.000
X4*X5	1	19.6	19.59	7.17	0.011
Error	35	95.6	2.73		
Lack-of-Fit	33	95.6	2.90	*	*
Pure Error	2	0.0	0.00		
Total	45	14767.2			

Model Summary

S	R-sq	R-sq(adj)
1.65281	99.35%	99.17%

Coefficients

Term	Coef	SE Coef	T-Value	P-Value	VIF
Constant	25.2	12.7	1.99	0.055	
X1	0.909	0.159	5.71	0.000	45547.78
X2	-0.00721	0.00131	-5.52	0.000	36314.55
X3	0.04451	0.00848	5.25	0.000	73690.42
X4	-0.000715	0.000177	-4.05	0.000	109.96
X5	-161.5	82.1	-1.97	0.057	25768.22
X2^2	0.000000	0.000000	4.30	0.000	10325.99

X1*X2	0.000001	0.000000	3.63	0.001	2962.16
X2*X3	-0.000000	0.000000	-3.73	0.001	44639.59
X3*X4	-0.000000	0.000000	-6.02	0.000	2706.13
X4*X5	-0.00417	0.00156	-2.68	0.011	25262.32

Regression Equation

UIP = 25.2 + 0.909 X1 - 0.00721 X2 + 0.04451 X3 - 0.000715 X4 - 161.5 X5 + 0.000000 X2^2
+ 0.000001 X1*X2 - 0.000000 X2*X3 - 0.000000 X3*X4 - 0.00417 X4*X5

Fits and Diagnostics for Unusual Observations

Obs	UIP	Fit	Resid	Std Resid	
3	107.00	104.55	2.45	2.07	R
6	102.00	105.18	-3.18	-2.03	R
9	106.00	107.17	-1.17	-2.06	R X
12	112.00	109.04	2.96	2.26	R
13	35.00	35.16	-0.16	-1.28	X
14	23.00	22.87	0.13	1.21	X
42	70.00	70.00	-0.00	*	X

R Large residual
X Unusual X

Residual Plots for UIP

Residual Plots for UIP
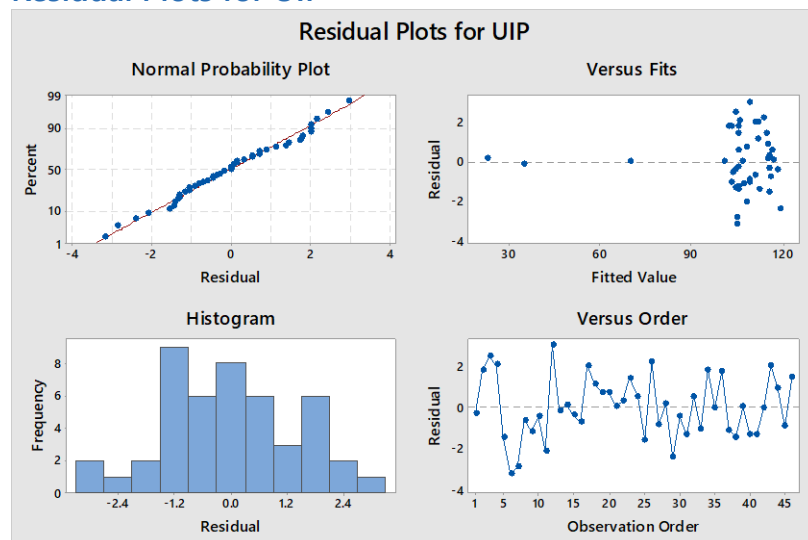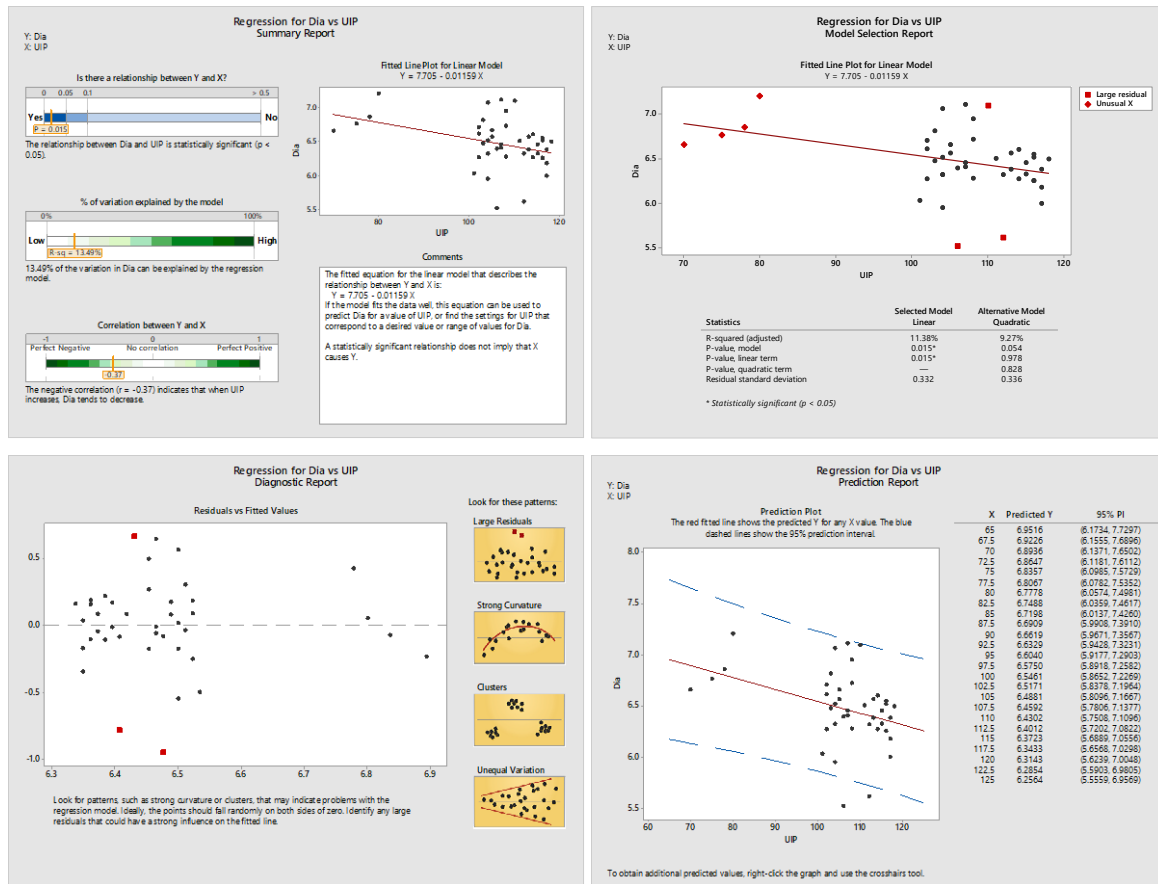
Figure B.10. MiniTab Analysis of Nugget Diameter as a Function of UIP
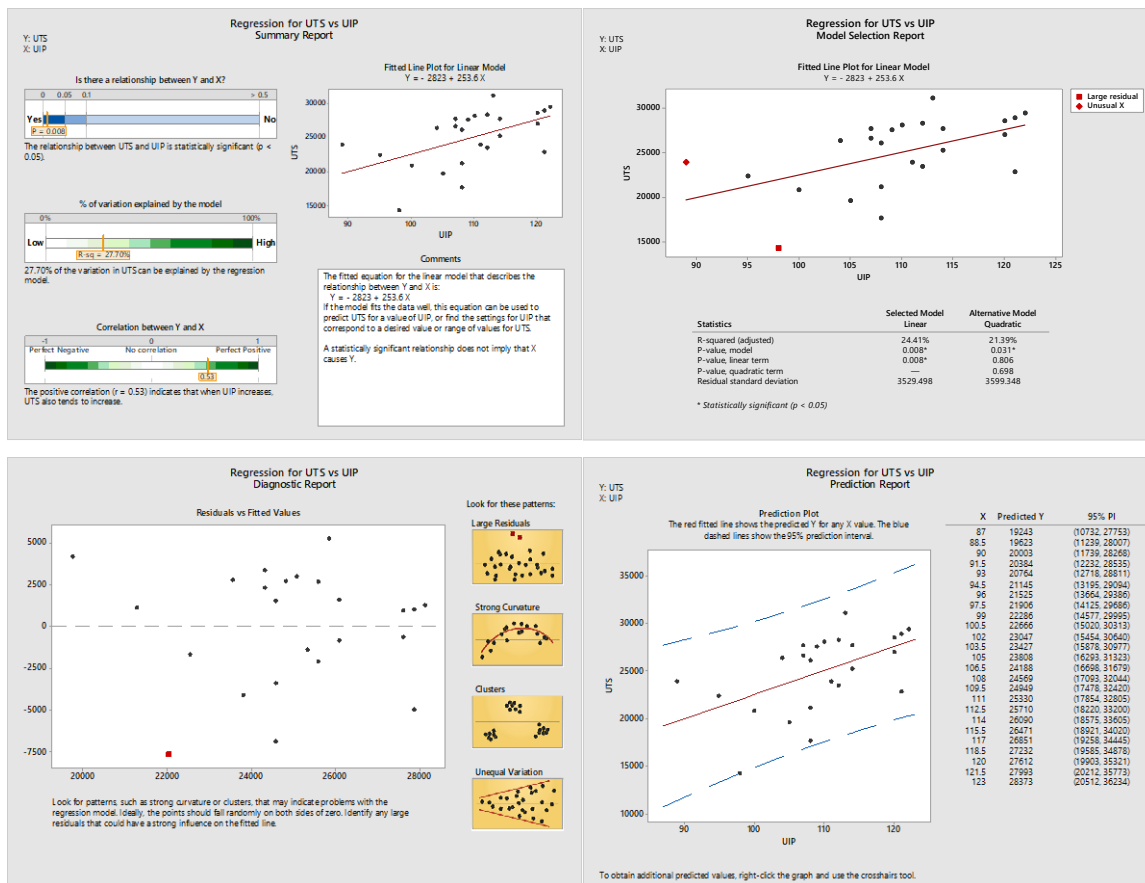
Figure B.11. MiniTab Analysis of UTS as a Function of UIP
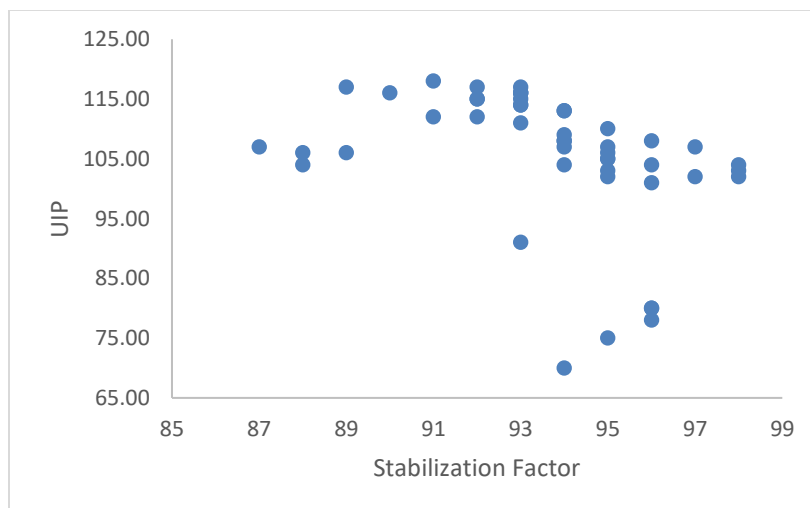
Figure B.12. Plot of UIP as a Function of Stabilization Factor

Statistical Analysis of Stabilization
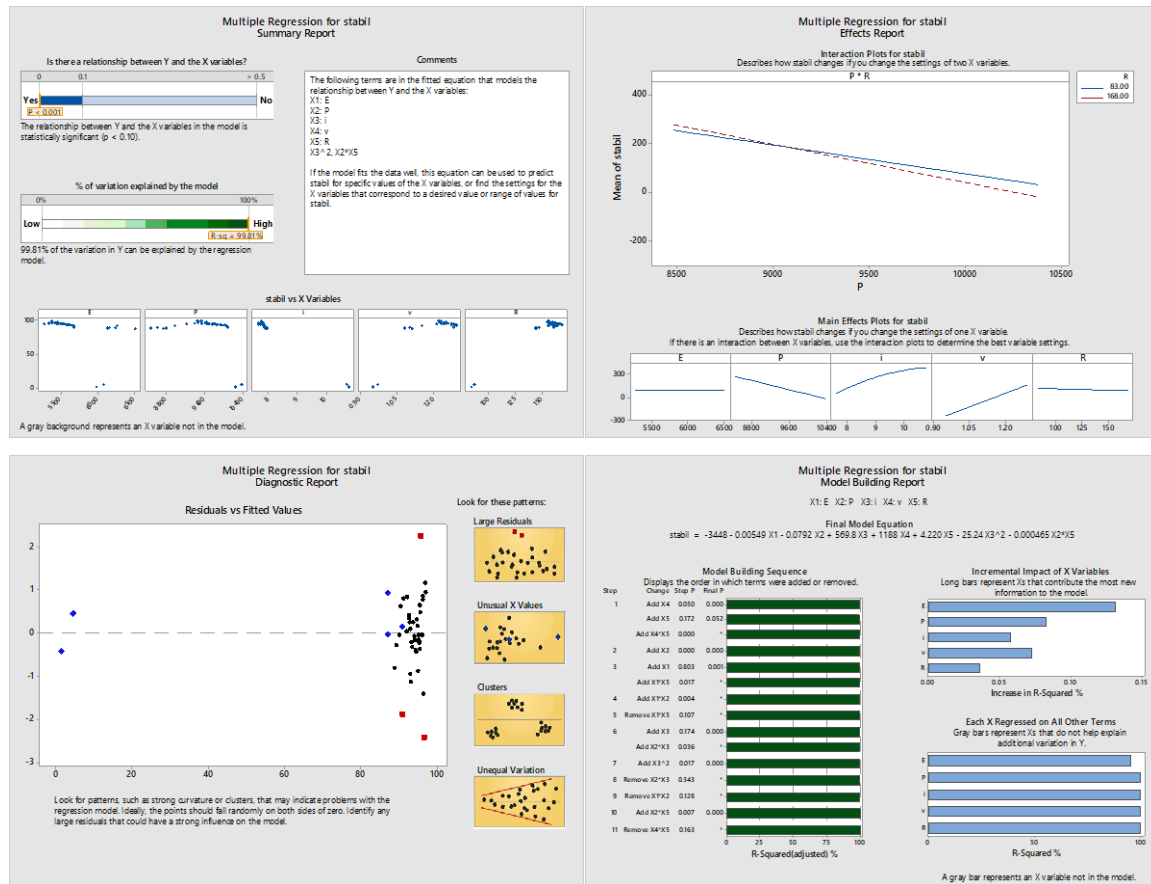
Figure B.13. MiniTab Regression Data for Stability
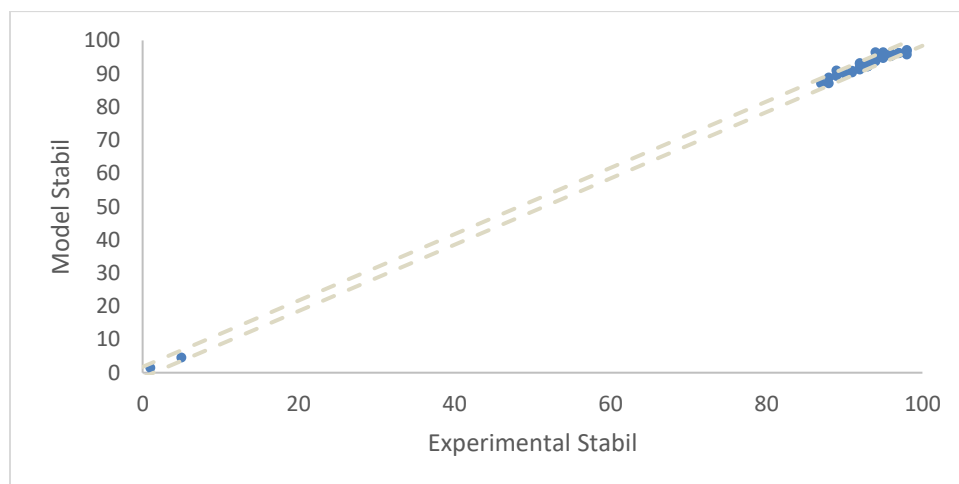
Figure B.14. Plot of Experimental vs Model Stabilization Factor

Regression Analysis: stabil versus X1, X2, X3, X4, X5, X3^2, X2*X5

Analysis of Variance

Source	DF	Adj SS	Adj MS	F-Value	P-Value
Regression	7	16054.1	2293.44	3119.11	0.000
X1	1	10.2	10.24	13.92	0.001
X2	1	7.0	6.99	9.51	0.004
X3	1	32.1	32.07	43.62	0.000
X4	1	19.0	19.04	25.90	0.000
X5	1	27.2	27.20	36.99	0.000
X3^2	1	45.8	45.79	62.28	0.000
X2*X5	1	29.5	29.46	40.06	0.000
Error	42	30.9	0.74		
Lack-of-Fit	40	30.9	0.77	*	*
Pure Error	2	0.0	0.00		
Total	49	16085.0			

Model Summary

S	R-sq	R-sq(adj)	R-sq(pred)
0.857489	99.81%	99.78%	99.65%

Coefficients

Term	Coef	SE Coef	T-Value	P-Value	VIF
Constant	-3448	546	-6.31	0.000	
X1	-0.00549	0.00147	-3.73	0.001	10.21
X2	-0.0792	0.0257	-3.08	0.004	6498.80
X3	569.8	86.3	6.60	0.000	180842.26
X4	1188	233	5.09	0.000	20816.97
X5	4.220	0.694	6.08	0.000	8260.35
X3^2	-25.24	3.20	-7.89	0.000	84184.09
X2*X5	-0.000465	0.000073	-6.33	0.000	10288.45

Regression Equation

stabil = -3448 - 0.00549 X1 - 0.0792 X2 + 569.8 X3 + 1188 X4 + 4.220 X5 - 25.24 X3^2
        - 0.000465 X2*X5

Fits and Diagnostics for Unusual Observations

Obs	stabil	Fit	Resid	Std Resid	
3	87.000	87.036	-0.036	-0.09	X
5	98.000	95.749	2.251	2.77	R
10	88.000	87.077	0.923	1.71	X
12	91.000	90.848	0.152	0.33	X
13	5.000	4.541	0.459	1.21	X
14	1.000	1.423	-0.423	-1.18	X
30	89.000	90.894	-1.894	-2.40	R
46	94.000	96.442	-2.442	-3.20	R

R Large residual
X Unusual X

Residual Plots for stabil

107
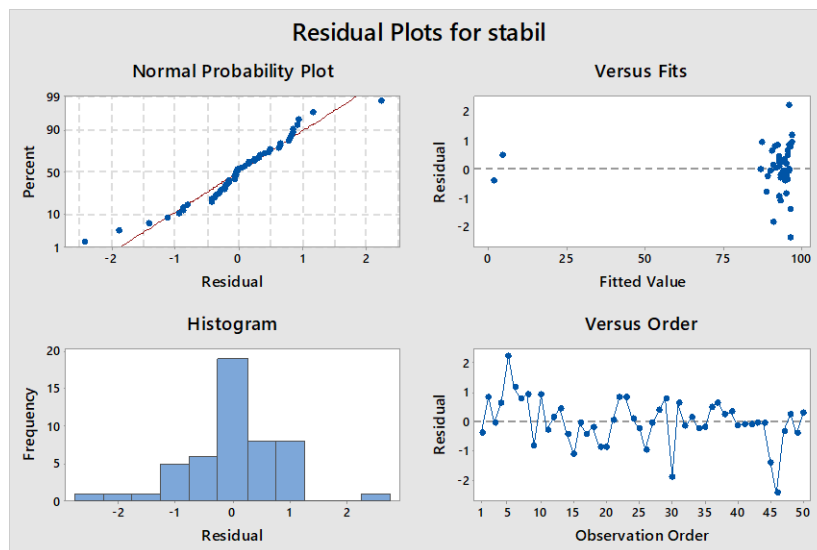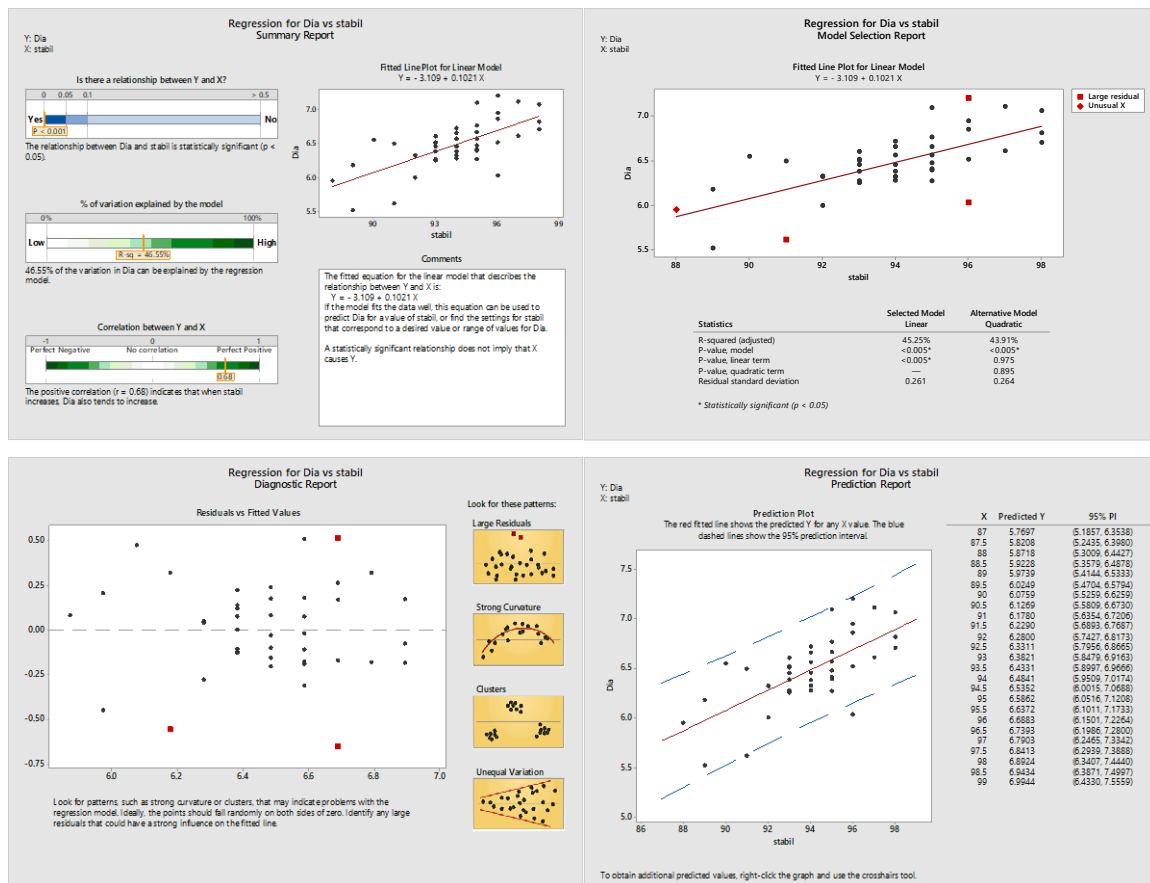
Figure B.15. MiniTab Analysis of Nugget Diameter as a Function of Stabilization
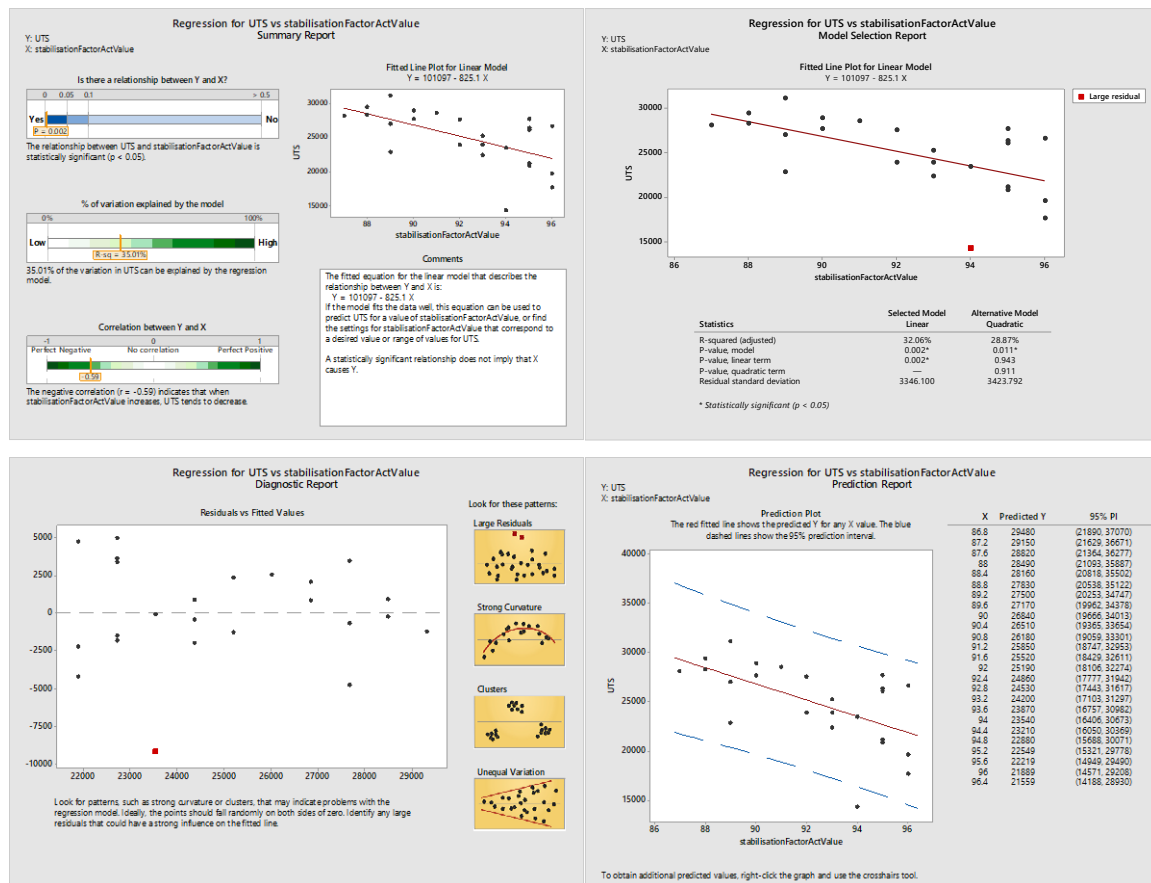
Figure B.16. MiniTab Analysis of UTS as a Function of Stabilization

Appendix C

Chapter 6 Supplementary Data

Regression of Nugget Diameter with No Interactions

Regression Analysis: Nug Dia versus wear, ... ActualValue, uipExpulsion

Method

Rows unused   5

Analysis of Variance

Source	DF	Adj SS	Adj MS	F-Value	P-Value
Regression	9	2.84580	0.31620	3.86	0.000
wear	1	0.01338	0.01338	0.16	0.687
voltageActualValue	1	0.79862	0.79862	9.74	0.002
currentActualValue	1	0.62087	0.62087	7.57	0.007
energyActualValue	1	0.11833	0.11833	1.44	0.233
powerActualValue	1	0.69972	0.69972	8.53	0.004
resistanceActualValue	1	0.36746	0.36746	4.48	0.037
stabilisationFactorActValue	1	0.63215	0.63215	7.71	0.007
uipActualValue	1	0.16682	0.16682	2.03	0.157
uipExpulsion	1	0.02490	0.02490	0.30	0.583
Error	85	6.97176	0.08202		
Total	94	9.81756			

Model Summary

S	R-sq	R-sq(adj)
0.286393	28.99%	21.47%

Coefficients

Term	Coef	SE Coef	T-Value	P-Value	VIF
Constant	171.2	60.4	2.83	0.006	
wear	0.00074	0.00184	0.40	0.687	2.36
voltageActualValue	-157.0	50.3	-3.12	0.002	1990.39
currentActualValue	-22.53	8.19	-2.75	0.007	1620.91

energyActualValue	-0.000491	0.000409	-1.20	0.233	9.23
powerActualValue	0.01877	0.00643	2.92	0.004	5025.00
resistanceActualValue	0.1110	0.0524	2.12	0.037	42.61
stabilisationFactorActValue	0.0586	0.0211	2.78	0.007	4.01
uipActualValue	0.0325	0.0228	1.43	0.157	24.99
uipExpulsion	0.161	0.293	0.55	0.583	4.01

Regression Equation

Nug Dia   =   171.2 + 0.00074 wear - 157.0 voltageActualValue - 22.53 currentActualValue
- 0.000491 energyActualValue + 0.01877 powerActualValue
+ 0.1110 resistanceActualValue + 0.0586 stabilisationFactorActValue
+ 0.0325 uipActualValue + 0.161 uipExpulsion

Fits and Diagnostics for Unusual Observations

Obs	Nug Dia	Fit	Resid	Std Resid		
1	5.526	6.387	-0.861	-3.11	R	
3	6.165	5.671	0.494	2.33	R	X
4	5.866	5.924	-0.058	-0.25		X
6	5.440	6.079	-0.639	-2.89	R	X
19	5.961	6.582	-0.621	-2.25	R	
21	6.625	6.422	0.203	0.95		X
25	5.808	6.425	-0.617	-2.26	R	
26	6.717	6.349	0.368	1.65		X
51	5.604	5.904	-0.300	-1.41		X
54	5.827	5.832	-0.005	-0.08		X
78	7.070	6.488	0.582	2.08	R	

R Large residual
X Unusual X

Durbin-Watson Statistic

Durbin-Watson Statistic =   1.59254

Residual Plots for Nug Dia
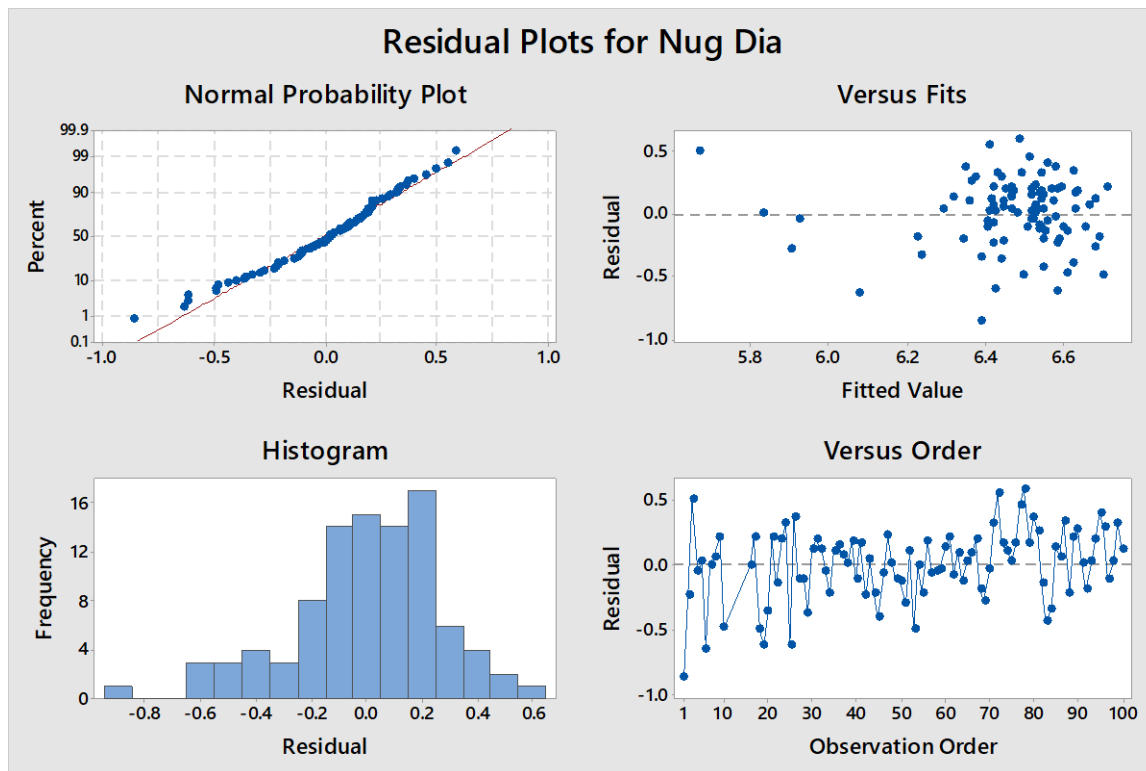
Regression of Nugget Diameter with Interactions

Regression Analysis: Nug Dia versus voltageActualValue, ... pExpulsion

The following terms cannot be estimated and were removed:
currentActualValue*powerActualValue, powerActualValue*resistanceActualValue,
resistanceActualValue*uipExpulsion, stabilisationFactorActValue*uipExpulsion,
uipActualValue*uipExpulsion, voltageActualValue*voltageActualValue*voltageActualValue,
currentActualValue*currentActualValue*currentActualValue,
voltageActualValue*voltageActualValue*currentActualValue,
voltageActualValue*voltageActualValue*powerActualValue,
voltageActualValue*voltageActualValue*resistanceActualValue,
voltageActualValue*voltageActualValue*stabilisationFactorActValue,
voltageActualValue*voltageActualValue*uipActualValue,
voltageActualValue*voltageActualValue*uipExpulsion,
voltageActualValue*currentActualValue*currentActualValue,
voltageActualValue*currentActualValue*powerActualValue,
voltageActualValue*currentActualValue*resistanceActualValue,
voltageActualValue*currentActualValue*stabilisationFactorActValue,

voltageActualValue*currentActualValue*uipActualValue,
voltageActualValue*currentActualValue*uipExpulsion,
voltageActualValue*powerActualValue*powerActualValue,
voltageActualValue*resistanceActualValue*resistanceActualValue,
currentActualValue*currentActualValue*powerActualValue,
currentActualValue*currentActualValue*resistanceActualValue,
currentActualValue*currentActualValue*stabilisationFactorActValue,
currentActualValue*currentActualValue*uipActualValue,
currentActualValue*currentActualValue*uipExpulsion,
currentActualValue*powerActualValue*powerActualValue,
currentActualValue*powerActualValue*resistanceActualValue,
currentActualValue*powerActualValue*stabilisationFactorActValue,
currentActualValue*powerActualValue*uipActualValue,
currentActualValue*powerActualValue*uipExpulsion,
currentActualValue*resistanceActualValue*resistanceActualValue,
powerActualValue*powerActualValue*resistanceActualValue,
powerActualValue*powerActualValue*stabilisationFactorActValue,
powerActualValue*powerActualValue*uipActualValue,
powerActualValue*powerActualValue*uipExpulsion,
powerActualValue*resistanceActualValue*resistanceActualValue,
powerActualValue*resistanceActualValue*stabilisationFactorActValue,
powerActualValue*resistanceActualValue*uipActualValue,
powerActualValue*resistanceActualValue*uipExpulsion,
powerActualValue*stabilisationFactorActValue*stabilisationFactorActValue,
powerActualValue*uipActualValue*uipActualValue,
resistanceActualValue*resistanceActualValue*stabilisationFactorActValue,
resistanceActualValue*resistanceActualValue*uipActualValue,
resistanceActualValue*resistanceActualValue*uipExpulsion,
resistanceActualValue*stabilisationFactorActValue*stabilisationFactorActValue,
resistanceActualValue*stabilisationFactorActValue*uipExpulsion,
stabilisationFactorActValue*stabilisationFactorActValue*uipExpulsion,
stabilisationFactorActValue*uipActualValue*uipExpulsion,
uipActualValue*uipActualValue*uipExpulsion

Method

Rows unused   5

Backward Elimination of Terms

α to remove = 0.1

Analysis of Variance

Source	DF	Adj SS
Regression	19	5.29687
voltageActualValue	1	0.38441
currentActualValue	1	0.25723

113

powerActualValue	1	0.52907
resistanceActualValue	1	0.37816
stabilisationFactorActValue	1	0.17244
uipActualValue	1	0.04814
uipExpulsion	1	0.25256
stabilisationFactorActValue*stabilisationFactorActValue	1	0.20729
uipActualValue*uipActualValue	1	0.10882
voltageActualValue*uipActualValue	1	0.33759
voltageActualValue*uipExpulsion	1	0.27231
currentActualValue*uipActualValue	1	0.31936
currentActualValue*uipExpulsion	1	0.20063
powerActualValue*uipExpulsion	1	0.22796
resistanceActualValue*stabilisationFactorActValue	1	0.34640
stabilisationFactorActValue*uipActualValue	1	0.23963
voltageActualValue*uipActualValue*uipActualValue	1	0.36237
currentActualValue*uipActualValue*uipActualValue	1	0.34465
stabilisationFactorActValue*stabilisationFactorActValue*uipActualValue	1	0.22468
Error	75	4.52069
Total	94	9.81756

Source	Adj MS	F-Value
Regression	0.27878	4.63
voltageActualValue	0.38441	6.38
currentActualValue	0.25723	4.27
powerActualValue	0.52907	8.78
resistanceActualValue	0.37816	6.27
stabilisationFactorActValue	0.17244	2.86
uipActualValue	0.04814	0.80
uipExpulsion	0.25256	4.19
stabilisationFactorActValue*stabilisationFactorActValue	0.20729	3.44
uipActualValue*uipActualValue	0.10882	1.81
voltageActualValue*uipActualValue	0.33759	5.60

voltageActualValue*uipExpulsion	0.27231	4.52
currentActualValue*uipActualValue	0.31936	5.30
currentActualValue*uipExpulsion	0.20063	3.33
powerActualValue*uipExpulsion	0.22796	3.78
resistanceActualValue*stabilisationFactorActValue	0.34640	5.75
stabilisationFactorActValue*uipActualValue	0.23963	3.98
voltageActualValue*uipActualValue*uipActualValue	0.36237	6.01
currentActualValue*uipActualValue*uipActualValue	0.34465	5.72
stabilisationFactorActValue*stabilisationFactorActValue*uipActualValue	0.22468	3.73
Error	0.06028	
Total		

Source	P-Value
Regression	0.000
voltageActualValue	0.014
currentActualValue	0.042
powerActualValue	0.004
resistanceActualValue	0.014
stabilisationFactorActValue	0.095
uipActualValue	0.374
uipExpulsion	0.044
stabilisationFactorActValue*stabilisationFactorActValue	0.068
uipActualValue*uipActualValue	0.183
voltageActualValue*uipActualValue	0.021
voltageActualValue*uipExpulsion	0.037
currentActualValue*uipActualValue	0.024
currentActualValue*uipExpulsion	0.072
powerActualValue*uipExpulsion	0.056
resistanceActualValue*stabilisationFactorActValue	0.019
stabilisationFactorActValue*uipActualValue	0.050
voltageActualValue*uipActualValue*uipActualValue	0.017
currentActualValue*uipActualValue*uipActualValue	0.019

stabilisationFactorActValue*stabilisationFactorActValue*uipActualValue	0.057
Error	
Total	

Model Summary

S	R-sq	R-sq(adj)
0.245512	53.95%	42.29%

Coefficients

Term	Coef	SE Coef
Constant	-179	901
voltageActualValue	-1654	655
currentActualValue	415	201
powerActualValue	0.02306	0.00778
resistanceActualValue	1.443	0.576
stabilisationFactorActValue	-26.2	15.5
uipActualValue	15.6	17.5
uipExpulsion	-1320	645
stabilisationFactorActValue*stabilisationFactorActValue	0.1532	0.0826
uipActualValue*uipActualValue	-0.1198	0.0892
voltageActualValue*uipActualValue	26.5	11.2
voltageActualValue*uipExpulsion	1195	562
currentActualValue*uipActualValue	-7.97	3.46
currentActualValue*uipExpulsion	139.0	76.2
powerActualValue*uipExpulsion	-0.1288	0.0662
resistanceActualValue*stabilisationFactorActValue	-0.01531	0.00639
stabilisationFactorActValue*uipActualValue	0.244	0.122
voltageActualValue*uipActualValue*uipActualValue	-0.1188	0.0485
currentActualValue*uipActualValue*uipActualValue	0.0356	0.0149
stabilisationFactorActValue*stabilisationFactorActValue*uipActualValue	-0.001300	0.000673

Term	T-Value	P-Value
Constant	-0.20	0.843
voltageActualValue	-2.53	0.014

Term		
currentActualValue	2.07	0.042
powerActualValue	2.96	0.004
resistanceActualValue	2.50	0.014
stabilisationFactorActValue	-1.69	0.095
uipActualValue	0.89	0.374
uipExpulsion	-2.05	0.044
stabilisationFactorActValue*stabilisationFactorActValue	1.85	0.068
uipActualValue*uipActualValue	-1.34	0.183
voltageActualValue*uipActualValue	2.37	0.021
voltageActualValue*uipExpulsion	2.13	0.037
currentActualValue*uipActualValue	-2.30	0.024
currentActualValue*uipExpulsion	1.82	0.072
powerActualValue*uipExpulsion	-1.94	0.056
resistanceActualValue*stabilisationFactorActValue	-2.40	0.019
stabilisationFactorActValue*uipActualValue	1.99	0.050
voltageActualValue*uipActualValue*uipActualValue	-2.45	0.017
currentActualValue*uipActualValue*uipActualValue	2.39	0.019
stabilisationFactorActValue*stabilisationFactorActValue*uipActualValue	-1.93	0.057

Term	VIF
Constant	
voltageActualValue	458786.81
currentActualValue	1329126.49
powerActualValue	10029.22
resistanceActualValue	6995.88
stabilisationFactorActValue	2927762.92
uipActualValue	20130732.29
uipExpulsion	26419464.24
stabilisationFactorActValue*stabilisationFactorActValue	2688541.18
uipActualValue*uipActualValue	28335291.65
voltageActualValue*uipActualValue	24020832.95
voltageActualValue*uipExpulsion	30276607.43

currentActualValue*uipActualValue	69759881.28
currentActualValue*uipExpulsion	21299831.03
powerActualValue*uipExpulsion	24340684.92
resistanceActualValue*stabilisationFactorActValue	14064.74
stabilisationFactorActValue*uipActualValue	6044798.50
voltageActualValue*uipActualValue*uipActualValue	18729907.52
currentActualValue*uipActualValue*uipActualValue	57595765.76
stabilisationFactorActValue*stabilisationFactorActValue*uipActualValue	2284034.31

Regression Equation

Nug   =   -179 - 1654 voltageActualValue + 415 currentActualValue
Dia   + 0.02306 powerActualValue
        + 1.443 resistanceActualValue - 26.2 stabilisationFactorActValue
        + 15.6 uipActualValue - 1320 uipExpulsion
        + 0.1532 stabilisationFactorActValue*stabilisationFactorActValue
        - 0.1198 uipActualValue*uipActualValue + 26.5 voltageActualValue*uipActualValue
        + 1195 voltageActualValue*uipExpulsion - 7.97 currentActualValue*uipActualValue
        + 139.0 currentActualValue*uipExpulsion - 0.1288 powerActualValue*uipExpulsion
        - 0.01531 resistanceActualValue*stabilisationFactorActValue
        + 0.244 stabilisationFactorActValue*uipActualValue
        - 0.1188 voltageActualValue*uipActualValue*uipActualValue
        + 0.0356 currentActualValue*uipActualValue*uipActualValue
        - 0.001300 stabilisationFactorActValue*stabilisationFactorActValue*uipActualValue

Fits and Diagnostics for Unusual Observations

Obs	Nug Dia	Fit	Resid	Std Resid	
1	5.526	6.279	-0.753	-3.21	R
3	6.165	6.165	-0.000	*	X
4	5.866	5.866	-0.000	-0.00	X
6	5.440	5.440	-0.000	-0.00	X
17	6.913	6.422	0.491	2.23	R
19	5.961	6.466	-0.505	-2.14	R
20	6.032	6.495	-0.463	-2.01	R
21	6.625	6.625	-0.000	*	X
26	6.717	6.729	-0.012	-0.08	X
51	5.604	5.588	0.016	0.42	X

53	6.205	6.676	-0.471	-2.01	R
54	5.827	5.800	0.027	0.57		X
78	7.070	6.449	0.621	2.60	R
83	6.110	6.632	-0.522	-2.19	R
88	6.130	6.065	0.065	0.51		X
92	6.039	6.060	-0.021	-0.25		X

R Large residual
X Unusual X

Durbin-Watson Statistic

Durbin-Watson Statistic =   1.45400

Residual Plots for Nug Dia
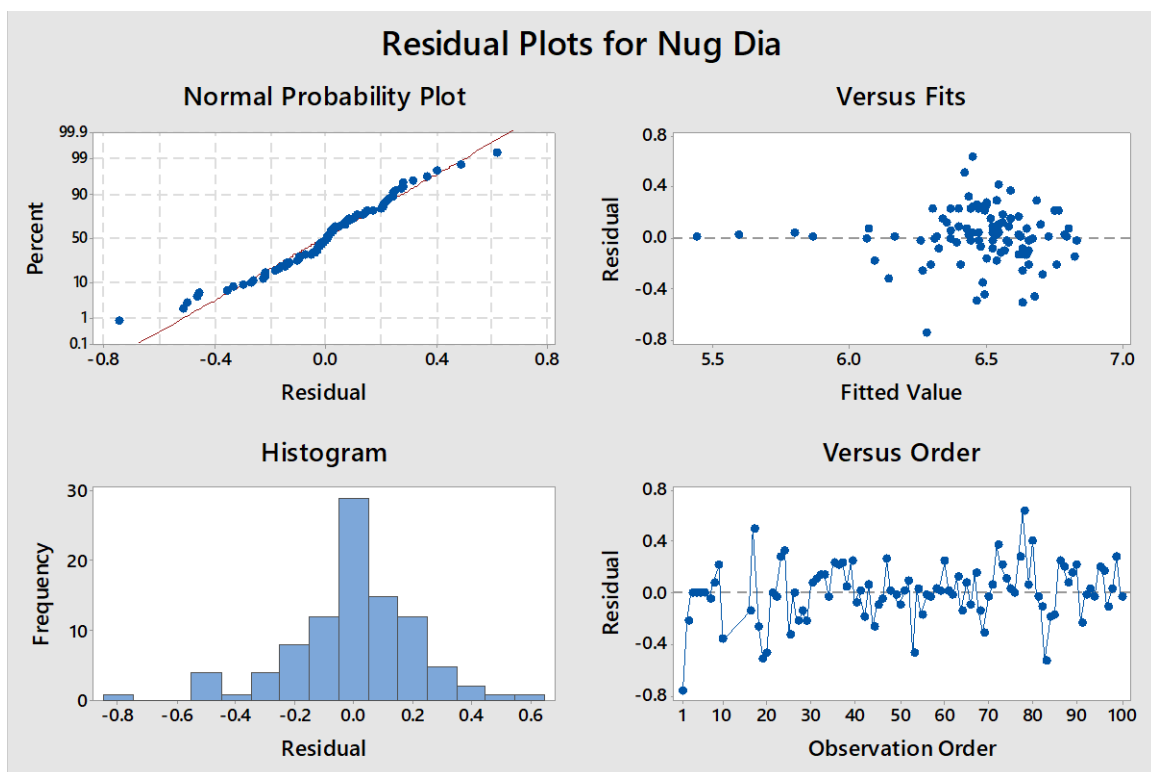
Regression of Nugget Diameter with Inclusion of Validation Data

Regression Analysis: Nug Dia versus voltageActualValue, ... pExpulsion

The following terms cannot be estimated and were removed:
currentActualValue*powerActualValue, powerActualValue*resistanceActualValue,
resistanceActualValue*uipExpulsion, stabilisationFactorActValue*uipExpulsion,
uipActualValue*uipExpulsion, currentActualValue*currentActualValue*currentActualValue,
voltageActualValue*voltageActualValue*currentActualValue,
voltageActualValue*voltageActualValue*powerActualValue,
voltageActualValue*voltageActualValue*resistanceActualValue,
voltageActualValue*voltageActualValue*uipExpulsion,
voltageActualValue*currentActualValue*currentActualValue,
voltageActualValue*currentActualValue*powerActualValue,
voltageActualValue*currentActualValue*resistanceActualValue,
voltageActualValue*currentActualValue*stabilisationFactorActValue,
voltageActualValue*currentActualValue*uipExpulsion,
voltageActualValue*powerActualValue*powerActualValue,
voltageActualValue*resistanceActualValue*resistanceActualValue,
currentActualValue*currentActualValue*powerActualValue,
currentActualValue*currentActualValue*resistanceActualValue,
currentActualValue*currentActualValue*stabilisationFactorActValue,
currentActualValue*currentActualValue*uipExpulsion,
currentActualValue*powerActualValue*powerActualValue,
currentActualValue*powerActualValue*resistanceActualValue,
currentActualValue*powerActualValue*stabilisationFactorActValue,
currentActualValue*powerActualValue*uipActualValue,
currentActualValue*powerActualValue*uipExpulsion,
currentActualValue*resistanceActualValue*resistanceActualValue,
powerActualValue*powerActualValue*uipActualValue,
powerActualValue*powerActualValue*uipExpulsion,
powerActualValue*resistanceActualValue*resistanceActualValue,
powerActualValue*resistanceActualValue*stabilisationFactorActValue,
powerActualValue*resistanceActualValue*uipExpulsion,
powerActualValue*stabilisationFactorActValue*stabilisationFactorActValue,
powerActualValue*uipActualValue*uipActualValue,
resistanceActualValue*resistanceActualValue*stabilisationFactorActValue,
resistanceActualValue*resistanceActualValue*uipExpulsion,
resistanceActualValue*stabilisationFactorActValue*stabilisationFactorActValue,
resistanceActualValue*stabilisationFactorActValue*uipExpulsion,
stabilisationFactorActValue*stabilisationFactorActValue*uipExpulsion,
stabilisationFactorActValue*uipActualValue*uipExpulsion,
uipActualValue*uipActualValue*uipExpulsion

Method

120

Rows unused   5

Backward Elimination of Terms

α to remove = 0.1

Beginning with step 1, the model may not be hierarchical because some required terms are impossible to estimate.

Analysis of Variance

Source	DF	Adj SS	Adj MS
Regression	21	6.6346	0.31593
currentActualValue	1	0.8101	0.81015
uipExpulsion	1	0.3039	0.30391
powerActualValue*powerActualValue	1	0.9522	0.95216
resistanceActualValue*resistanceActualValue	1	1.4929	1.49286
voltageActualValue*powerActualValue	1	0.7891	0.78910
voltageActualValue*resistanceActualValue	1	1.1577	1.15767
voltageActualValue*stabilisationFactorActValue	1	1.1312	1.13125
voltageActualValue*uipExpulsion	1	0.3322	0.33221
currentActualValue*uipActualValue	1	1.2702	1.27016
currentActualValue*uipExpulsion	1	0.2213	0.22129
powerActualValue*stabilisationFactorActValue	1	1.1771	1.17707
powerActualValue*uipActualValue	1	0.8363	0.83628
powerActualValue*uipExpulsion	1	0.2530	0.25302
resistanceActualValue*uipActualValue	1	1.2794	1.27935
voltageActualValue*voltageActualValue*voltageActualValue	1	1.0258	1.02576
powerActualValue*powerActualValue*powerActualValue	1	1.0428	1.04279
resistanceActualValue*resistanceActualValue*resistanceActualValue	1	1.1909	1.19093
uipActualValue*uipActualValue*uipActualValue	1	1.4608	1.46082
voltageActualValue*currentActualValue*uipActualValue	1	0.8500	0.84997
currentActualValue*uipActualValue*uipActualValue	1	1.4913	1.49126
powerActualValue*resistanceActualValue*uipActualValue	1	1.0715	1.07152
Error	98	5.3654	0.05475
Total	119	11.9999	

Source	F-Value	P-Value

Regression	5.77	0.000
currentActualValue	14.80	0.000
uipExpulsion	5.55	0.020
powerActualValue*powerActualValue	17.39	0.000
resistanceActualValue*resistanceActualValue	27.27	0.000
voltageActualValue*powerActualValue	14.41	0.000
voltageActualValue*resistanceActualValue	21.15	0.000
voltageActualValue*stabilisationFactorActValue	20.66	0.000
voltageActualValue*uipExpulsion	6.07	0.016
currentActualValue*uipActualValue	23.20	0.000
currentActualValue*uipExpulsion	4.04	0.047
powerActualValue*stabilisationFactorActValue	21.50	0.000
powerActualValue*uipActualValue	15.27	0.000
powerActualValue*uipExpulsion	4.62	0.034
resistanceActualValue*uipActualValue	23.37	0.000
voltageActualValue*voltageActualValue*voltageActualValue	18.74	0.000
powerActualValue*powerActualValue*powerActualValue	19.05	0.000
resistanceActualValue*resistanceActualValue*resistanceActualValue	21.75	0.000
uipActualValue*uipActualValue*uipActualValue	26.68	0.000
voltageActualValue*currentActualValue*uipActualValue	15.52	0.000
currentActualValue*uipActualValue*uipActualValue	27.24	0.000
powerActualValue*resistanceActualValue*uipActualValue	19.57	0.000
Error		
Total		

Model Summary

S	R-sq	R-sq(adj)
0.233985	55.29%	45.71%

Coefficients

Term	Coef	SE Coef
Constant	-2232	631
currentActualValue	388	101

Term		
uipExpulsion	-1402	595
powerActualValue*powerActualValue	-0.000071	0.000017
resistanceActualValue*resistanceActualValue	-0.0863	0.0165
voltageActualValue*powerActualValue	0.384	0.101
voltageActualValue*resistanceActualValue	15.19	3.30
voltageActualValue*stabilisationFactorActValue	-3.623	0.797
voltageActualValue*uipExpulsion	1252	508
currentActualValue*uipActualValue	-2.469	0.513
currentActualValue*uipExpulsion	144.0	71.7
powerActualValue*stabilisationFactorActValue	0.000480	0.000104
powerActualValue*uipActualValue	0.002784	0.000712
powerActualValue*uipExpulsion	-0.1317	0.0613
resistanceActualValue*uipActualValue	0.0544	0.0113
voltageActualValue*voltageActualValue*voltageActualValue	-889	205
powerActualValue*powerActualValue*powerActualValue	0.000000	0.000000
resistanceActualValue*resistanceActualValue*resistanceActualValue	0.000113	0.000024
uipActualValue*uipActualValue*uipActualValue	-0.000267	0.000052
voltageActualValue*currentActualValue*uipActualValue	-1.891	0.480
currentActualValue*uipActualValue*uipActualValue	0.01193	0.00229
powerActualValue*resistanceActualValue*uipActualValue	-0.000006	0.000001

Term	T-Value	P-Value
Constant	-3.54	0.001
currentActualValue	3.85	0.000
uipExpulsion	-2.36	0.020
powerActualValue*powerActualValue	-4.17	0.000
resistanceActualValue*resistanceActualValue	-5.22	0.000
voltageActualValue*powerActualValue	3.80	0.000
voltageActualValue*resistanceActualValue	4.60	0.000
voltageActualValue*stabilisationFactorActValue	-4.55	0.000
voltageActualValue*uipExpulsion	2.46	0.016
currentActualValue*uipActualValue	-4.82	0.000

Term		
currentActualValue*uipExpulsion	2.01	0.047
powerActualValue*stabilisationFactorActValue	4.64	0.000
powerActualValue*uipActualValue	3.91	0.000
powerActualValue*uipExpulsion	-2.15	0.034
resistanceActualValue*uipActualValue	4.83	0.000
voltageActualValue*voltageActualValue*voltageActualValue	-4.33	0.000
powerActualValue*powerActualValue*powerActualValue	4.36	0.000
resistanceActualValue*resistanceActualValue*resistanceActualValue	4.66	0.000
uipActualValue*uipActualValue*uipActualValue	-5.17	0.000
voltageActualValue*currentActualValue*uipActualValue	-3.94	0.000
currentActualValue*uipActualValue*uipActualValue	5.22	0.000
powerActualValue*resistanceActualValue*uipActualValue	-4.42	0.000

Term	VIF
Constant	
currentActualValue	453888.26
uipExpulsion	25016437.70
powerActualValue*powerActualValue	25662108.24
resistanceActualValue*resistanceActualValue	812461.63
voltageActualValue*powerActualValue	9388268.48
voltageActualValue*resistanceActualValue	1474029.86
voltageActualValue*stabilisationFactorActValue	33180.77
voltageActualValue*uipExpulsion	27505831.65
currentActualValue*uipActualValue	2880249.29
currentActualValue*uipExpulsion	20935486.96
powerActualValue*stabilisationFactorActValue	48187.14
powerActualValue*uipActualValue	11468049.65
powerActualValue*uipExpulsion	23132883.94
resistanceActualValue*uipActualValue	690227.83
voltageActualValue*voltageActualValue*voltageActualValue	1474791.31
powerActualValue*powerActualValue*powerActualValue	5195303.99
resistanceActualValue*resistanceActualValue*resistanceActualValue	106024.47

124

uipActualValue*uipActualValue*uipActualValue	675608.11
voltageActualValue*currentActualValue*uipActualValue	5214853.40
currentActualValue*uipActualValue*uipActualValue	2811521.34
powerActualValue*resistanceActualValue*uipActualValue	1164445.77

Regression Equation

Nug Dia = -2232 + 388 currentActualValue - 1402 uipExpulsion
- 0.000071 powerActualValue*powerActualValue
- 0.0863 resistanceActualValue*resistanceActualValue
+ 0.384 voltageActualValue*powerActualValue
+ 15.19 voltageActualValue*resistanceActualValue
- 3.623 voltageActualValue*stabilisationFactorActValue
+ 1252 voltageActualValue*uipExpulsion - 2.469 currentActualValue*uipActualValue
+ 144.0 currentActualValue*uipExpulsion
+ 0.000480 powerActualValue*stabilisationFactorActValue
+ 0.002784 powerActualValue*uipActualValue
- 0.1317 powerActualValue*uipExpulsion
+ 0.0544 resistanceActualValue*uipActualValue
- 889 voltageActualValue*voltageActualValue*voltageActualValue
+ 0.000000 powerActualValue*powerActualValue*powerActualValue
+ 0.000113 resistanceActualValue*resistanceActualValue*resistanceActualValue
- 0.000267 uipActualValue*uipActualValue*uipActualValue
- 1.891 voltageActualValue*currentActualValue*uipActualValue
+ 0.01193 currentActualValue*uipActualValue*uipActualValue
- 0.000006 powerActualValue*resistanceActualValue*uipActualValue

Fits and Diagnostics for Unusual Observations

Obs	Nug Dia	Fit	Resid	Std Resid	
1	5.526	6.374	-0.848	-3.75	R
3	6.165	6.165	-0.000	*	X
4	5.866	5.866	-0.000	-0.00	X
6	5.440	5.440	-0.000	-0.00	X
19	5.961	6.479	-0.518	-2.30	R
20	6.032	6.501	-0.469	-2.10	R
21	6.625	6.625	-0.000	*	X
26	6.717	6.693	0.024	0.18	X
51	5.604	5.515	0.089	0.64	X
53	6.205	6.677	-0.472	-2.08	R
54	5.827	5.798	0.029	0.68	X

72	6.953	6.435	0.518	2.32	R	
78	7.070	6.424	0.646	2.82	R	
83	6.110	6.626	-0.516	-2.30	R	
84	5.899	6.074	-0.175	-1.18		X
92	6.039	6.122	-0.083	-0.63		X
117	6.767	6.316	0.451	2.06	R	
125	6.279	6.394	-0.115	-1.36		X

R Large residual
X Unusual X

Durbin-Watson Statistic

Durbin-Watson Statistic =   1.46314
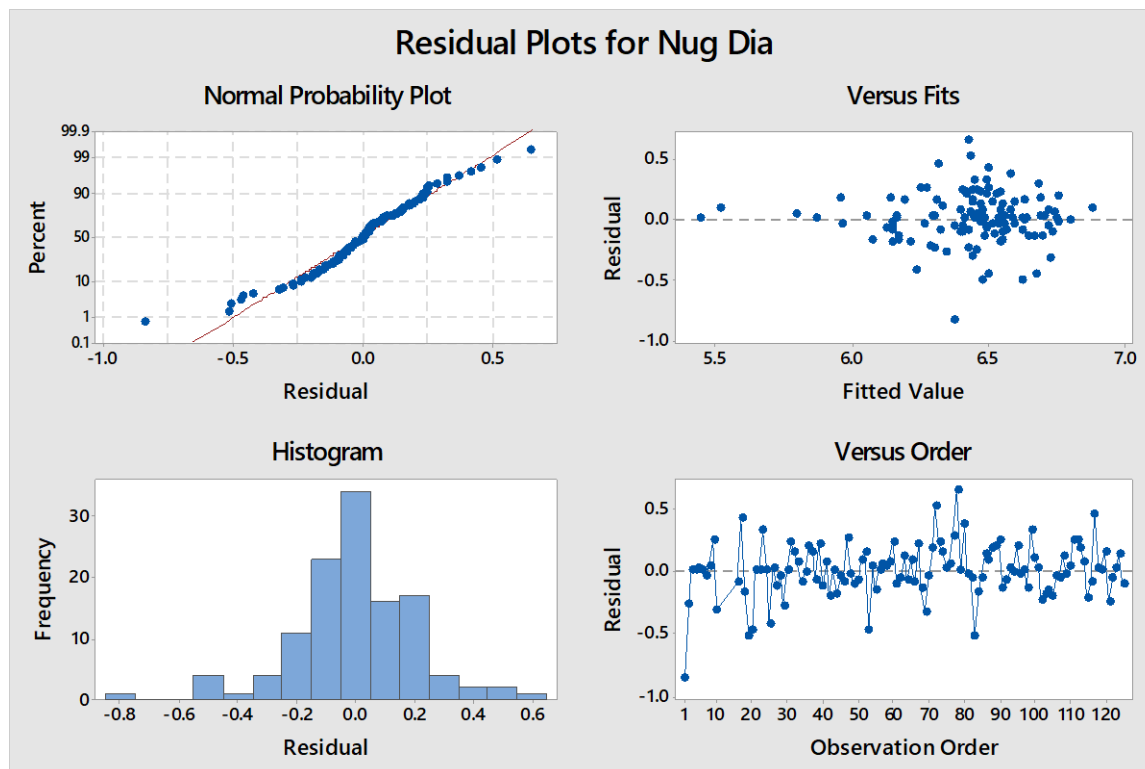
Residual Plots for Nug Dia

Regression Analysis: Nugget Dia versus V, I, P, R, Stabil, UIP, Expl

Analysis of Variance

Source	DF	Adj SS	Adj MS	F-Value	P-Value
Regression	7	1.68188	0.24027	5.22	0.000
V	1	0.03959	0.03959	0.86	0.359
I	1	0.05792	0.05792	1.26	0.268
P	1	0.04202	0.04202	0.91	0.345
R	1	0.03902	0.03902	0.85	0.362
Stabil	1	0.02250	0.02250	0.49	0.488
UIP	1	0.09411	0.09411	2.05	0.160
Expl	1	0.30125	0.30125	6.55	0.014
Error	42	1.93184	0.04600		
Total	49	3.61372			

Model Summary

S	R-sq	R-sq(adj)	R-sq(pred)
0.214467	46.54%	37.63%	31.53%

Coefficients

Term	Coef	SE Coef	T-Value	P-Value	VIF
Constant	98.9	73.5	1.35	0.186	
V	-46.6	50.2	-0.93	0.359	1533.27
I	-10.97	9.78	-1.12	0.268	846.83
P	0.00635	0.00665	0.96	0.345	1397.28
R	-0.0684	0.0743	-0.92	0.362	138.17
Stabil	-0.0203	0.0291	-0.70	0.488	2.41
UIP	0.0291	0.0203	1.43	0.160	9.66
Expl	-1.173	0.458	-2.56	0.014	8.77

Regression Equation

Nugget Dia   =   98.9 - 46.6 V - 10.97 I + 0.00635 P - 0.0684 R - 0.0203 Stabil + 0.0291 UIP
                 - 1.173 Expl

Fits and Diagnostics for Unusual Observations

Obs	Nugget Dia	Fit	Resid	Std Resid	
5	6.590	6.122	0.468	2.23	R
16	6.220	6.222	-0.002	-0.01	X
46	5.280	5.246	0.034	0.23	X
50	5.200	5.234	-0.034	-0.23	X

R Large residual
X Unusual X

Residual Plots for Nugget Dia
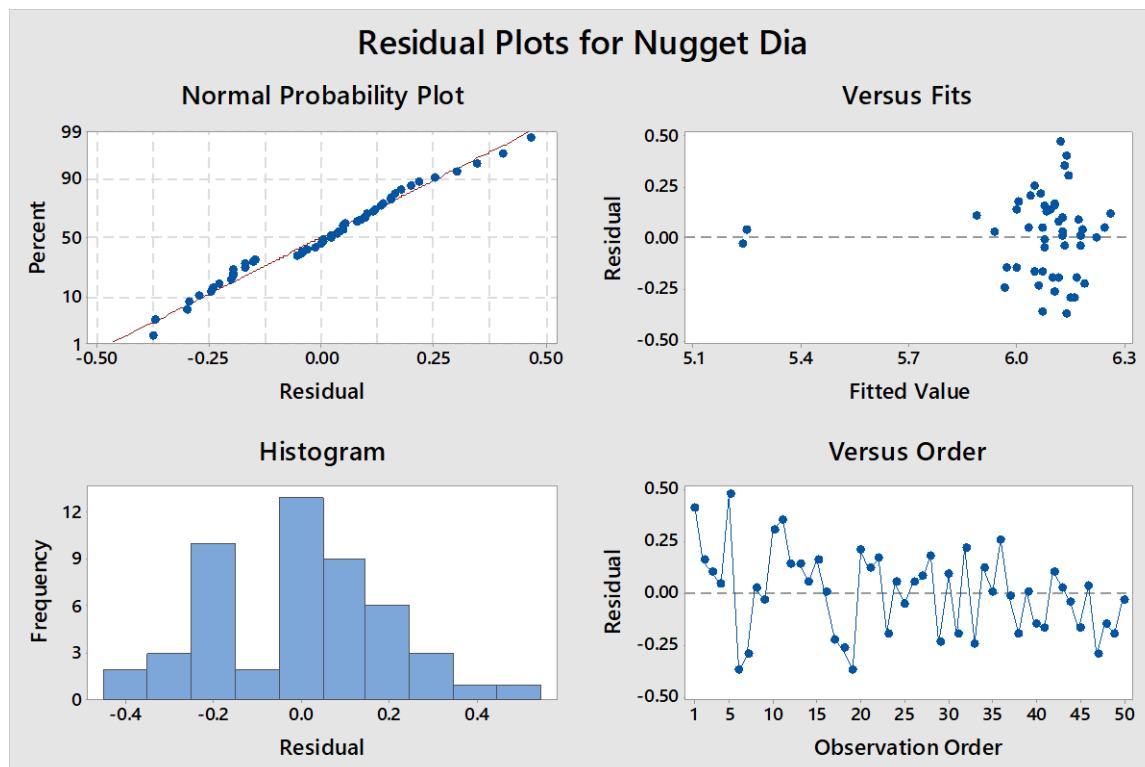
Regression Analysis: Nugget Dia versus V, I, P, R, Stabil, UIP, Expl

The following terms cannot be estimated and were removed:
Expl*Expl, V*P, I*P, I*Expl, P*Expl, R*Expl, Stabil*Expl, UIP*Expl, V*V*V, I*I*I, P*P*P, R*R*R, V*V*I, V*V*P, V*V*R, V*V*Stabil, V*V*UIP, V*V*Expl, V*I*I, V*I*P, V*I*R, V*I*Stabil, V*I*UIP, V*I*Expl, V*P*P, V*P*R, V*P*Stabil, V*P*UIP, V*P*Expl, V*R*R, V*R*Stabil, V*R*UIP, V*R*Expl, V*Stabil*Stabil, V*Stabil*UIP, V*Stabil*Expl, V*UIP*UIP, V*UIP*Expl, V*Expl*Expl, I*I*P, I*I*R, I*I*Stabil, I*I*UIP, I*I*Expl, I*P*P, I*P*R, I*P*Stabil, I*P*UIP, I*P*Expl, I*R*R, I*R*Stabil, I*R*UIP, I*R*Expl, I*Stabil*Stabil, I*Stabil*UIP, I*Stabil*Expl, I*UIP*UIP, I*UIP*Expl, P*P*R, P*P*Stabil, P*P*UIP, P*P*Expl, P*R*R, P*R*Stabil, P*R*UIP, P*R*Expl, P*Stabil*Stabil, P*Stabil*UIP, P*Stabil*Expl, P*UIP*Expl, R*R*Stabil, R*R*UIP, R*R*Expl, R*Stabil*Stabil, R*Stabil*UIP, R*Stabil*Expl, R*UIP*UIP, R*UIP*Expl, Stabil*Stabil*Expl, Stabil*UIP*UIP, Stabil*UIP*Expl, UIP*UIP*Expl

Backward Elimination of Terms

α to remove = 0.1

Analysis of Variance

Source	DF	Adj SS	Adj MS	F-Value	P-Value
Regression	24	2.60338	0.108474	2.68	0.009
V	1	0.21429	0.214287	5.30	0.030
I	1	0.21113	0.211134	5.22	0.031
P	1	0.06748	0.067482	1.67	0.208
R	1	0.30153	0.301535	7.46	0.011
Stabil	1	0.22717	0.227172	5.62	0.026
UIP	1	0.27958	0.279579	6.92	0.014
Expl	1	0.33104	0.331041	8.19	0.008
Stabil*Stabil	1	0.37818	0.378184	9.36	0.005
UIP*UIP	1	0.40209	0.402089	9.95	0.004
V*R	1	0.31218	0.312176	7.72	0.010
V*Stabil	1	0.49309	0.493094	12.20	0.002
V*UIP	1	0.43308	0.433084	10.72	0.003
V*Expl	1	0.33148	0.331484	8.20	0.008
I*R	1	0.32657	0.326567	8.08	0.009
I*Stabil	1	0.47290	0.472904	11.70	0.002
I*UIP	1	0.44350	0.443501	10.97	0.003
P*R	1	0.33654	0.336544	8.33	0.008
P*Stabil	1	0.47304	0.473042	11.70	0.002

Term	DF	Adj SS	Adj MS	F-Value	P-Value
P*UIP	1	0.00008	0.000084	0.00	0.964
Stabil*UIP	1	0.37125	0.371247	9.19	0.006
Stabil*Stabil*Stabil	1	0.33844	0.338442	8.37	0.008
UIP*UIP*UIP	1	0.43333	0.433327	10.72	0.003
P*UIP*UIP	1	0.18013	0.180132	4.46	0.045
Stabil*Stabil*UIP	1	0.37291	0.372913	9.23	0.006
Error	25	1.01034	0.040414		
Total	49	3.61372			

Model Summary

S	R-sq	R-sq(adj)	R-sq(pred)
0.201032	72.04%	45.20%	*

Coefficients

Term	Coef	SE Coef	T-Value	P-Value	VIF
Constant	-4526	13608	-0.33	0.742	
V	22330	9698	2.30	0.030	65043567.81
I	4375	1914	2.29	0.031	36934856.53
P	-1.52	1.17	-1.29	0.208	49678179.79
R	-223.8	81.9	-2.73	0.011	1.91403E+08
Stabil	-772	325	-2.37	0.026	3.43668E+08
UIP	432	164	2.63	0.014	7.19400E+08
Expl	1269	443	2.86	0.008	9332882.65
Stabil*Stabil	10.46	3.42	3.06	0.005	1.39121E+09
UIP*UIP	-2.425	0.769	-3.15	0.004	6.64897E+08
V*R	158.2	56.9	2.78	0.010	4.90405E+08
V*Stabil	-337.1	96.5	-3.49	0.002	83396624.06
V*UIP	-188.1	57.5	-3.27	0.003	3.20890E+08
V*Expl	-900	314	-2.86	0.008	8605213.74
I*R	31.6	11.1	2.84	0.009	95938700.11
I*Stabil	-67.3	19.7	-3.42	0.002	1.13007E+08
I*UIP	-36.8	11.1	-3.31	0.003	1.42918E+08
P*R	-0.02230	0.00773	-2.89	0.008	3.49530E+08

P*Stabil	0.0462	0.0135	3.42	0.002	95018515.10
P*UIP	-0.0005	0.0118	-0.05	0.964	6.18764E+08
Stabil*UIP	5.12	1.69	3.03	0.006	6.25461E+08
Stabil*Stabil*Stabil	-0.02666	0.00921	-2.89	0.008	2.08291E+08
UIP*UIP*UIP	0.00336	0.00103	3.27	0.003	28535926.89
P*UIP*UIP	0.000122	0.000058	2.11	0.045	5.12729E+08
Stabil*Stabil*UIP	-0.02705	0.00891	-3.04	0.006	1.96185E+08

Regression Equation

Nugget Dia = -4526 + 22330 V + 4375 I - 1.52 P - 223.8 R - 772 Stabil + 432 UIP + 1269 Expl
+ 10.46 Stabil*Stabil - 2.425 UIP*UIP + 158.2 V*R - 337.1 V*Stabil - 188.1 V*UIP
- 900 V*Expl + 31.6 I*R - 67.3 I*Stabil - 36.8 I*UIP - 0.02230 P*R
+ 0.0462 P*Stabil - 0.0005 P*UIP + 5.12 Stabil*UIP
- 0.02666 Stabil*Stabil*Stabil + 0.00336 UIP*UIP*UIP + 0.000122 P*UIP*UIP
- 0.02705 Stabil*Stabil*UIP

Fits and Diagnostics for Unusual Observations

Obs	Nugget Dia	Fit	Resid	Std Resid	
16	6.220	6.202	0.018	0.97	X
19	5.700	6.062	-0.362	-2.08	R
46	5.280	5.280	0.000	*	X
50	5.200	5.200	0.000	*	X

R Large residual
X Unusual X

131

Residual Plots for Nugget Dia